Electronic correlation and magnetism in multi-band Kondo lattice model

Application to real materials

DISSERTATION

zur Erlangung des akademischen Grades
doctor rerum naturalium
(Dr. rer. nat.)
im Fach Physik

eingereicht an der
Mathematisch-Naturwissenschaftlichen
Fakultät I
Humboldt-Universität zu Berlin

von
Herr MSc. Anand Sharma

Präsident der Humboldt-Universität zu Berlin:
Prof. Dr. Christoph Markschies

Dekan der Mathematisch-Naturwissenschaftlichen
Fakultät I:
Prof. Dr. Christian Limberg

Gutachter:

1. Prof. Dr. Wolfgang Nolting
2. Prof. Dr. Wladyslaw Borgiel
3. Prof. Dr. Recardo Manzke

eingereicht am: 12. Oktober 2007
Tag der mündlichen Prüfung: 20. Dezember 2007

Abstract

This dissertation deals with a combination of many- body evaluation of a spin exchange interaction between the itinerant electrons and localized 4f moments on a periodic lattice, i.e. within the so- called multi- band Kondo lattice model (KLM), and the T=0 first principles calculations in order to study the electronic correlation effects in real materials like Europium Sulphide (EuS) and Gadolinium Nitride (GdN). The single- particle ground state energy or hopping integral acting as an input in the many- body part is obtained using tight binding linear muffin- tin orbital within atomic sphere approximation (TB-LMTO- ASA) program and is a matrix in general.

The physical properties of interest like the quasi- particle spectral density and quasi- particle density of states are calculated within the Green function theory and the equation of motion method. In order to do so the required multi- band self- energy of the band electrons is taken as an ansatz, i.e. the so- called interpolating self- energy approach (ISA), which reproduces one of the exactly solvable non- trivial limiting case of the multi- band KLM, namely the ferromagnetically saturated semiconductor. The electronic excitation spectrum gets a striking temperature dependence by its exchange coupling to the localized spin system. In case of ferromagnetic semiconductor EuS, the temperature dependent quasi- particle bandstructure is obtained for both the 5d conduction as well as 3p valence bands while in GdN only the conduction bands are studied. We observe very strong temperature dependent electronic correlation effects in GdN and the calculated red- shift of the lower conduction band is in close comparison with experiment.

In order to determine the pure f- spin correlations, we develop the multi-band modified RKKY theory. The central idea of this theory being to average out the itinerant electron degrees of freedom from the spin- exchange interaction and map the latter on to an effective Heisenberg model. As an input for the evaluation of the effective exchange integrals, we utilize the multi-band self- energy (ISA) ansatz. Using this procedure, we determine the magnetic properties of the system like Curie temperature (within Random Phase Approximation) while calculating the chemical potential and magnetization within a self consistent scheme for various configurations of system parameters. The results are discussed in detail and the model is also considered in order to study the role of itinerant charge carriers for stabilizing ferromagnetism in GdN.

Zusammenfassung

Die vorliegende Arbeit untersucht elektronische Korrelationseffekte in Realsubstanzen wie Europium- Sulphid (EuS) und Gadolinium- Nitrid (GdN). Es wird dazu eine Kombination von vielteilchentheoretischen Analysen der Spin- Austauschwechselwirkung zwischen itineranten Bandelektronen und lokalisierten 4f- Momenten, durchgefuehrt im Rahmen eines Mehr- Band- Kondo- Gitter-Modells (KLM), mit first- principles (T=0) Bandstrukturrechnungen vorgeschlagen. Die Ein- Teilchen- Energien (hopping- Integrale), die als Energie-Matrix in den Mehr- Band- Hamilton- Operator eingehen, werden einer TB-LMTO- ASA entnommen.

Die interessierenden physikalischen Eigenschaften wie die Quasiteilchen-Spektraldichte und die Quasiteilchen- Zustandsdichte werden mit der Bewegungsgleichungs- Methode Greencher Funktionen berechnet. Dazu wird fuer die gesuchte Mehr- Band- Selbstenergie der itineranten Ladungstraeger als Verallgemeinerung des sogenannten Interpolating Selfenergy Approach (ISA) ein Ansatz vorgeschlagen, der einen wichtigen, nicht- trivialen Grenzfall des Mehr-Band- Kondo- Gitter- Modells, naemlich den des ferromagnetisch gesaettigten Halbleiters, korrekt reproduziert. Es stellt sich heraus, dass das elektronische Anregungsspektrum durch die Austausch- Kopplung an das lokalisierte Momenten- System eine spektakulaere Temperaturabhaengigkeit aufweist, in Uebereinstimmung mit vorliegenden experimentellen Beobachtungen. Im Fall von EuS wird die temperaturabhaengige Quasiteilchen- Bandstruktur sowohl fuer die leeren 5d- Leitungsband als auch fuer die voll- besetzten 3p- Valenzbaender bestimmt. Stark temperaturbestimmte Korrelationseffekte werden registriert, z.B. eine mit fallender Temperatur in der ferromagnetischen Phase auftretende Rotverschiebung der unteren Leitungsbandkante in guter Uebereinstimmung mit experimentellen Daten.

Um die reinen f- Spin- Korrelationen zu beschreiben, wird eine modifizierte RKKY- Theorie fuer Mehr- Band- Systeme entwickelt, wobei durch Ausmitteln der elektronischen Freiheitsgrade das Mehr- Band KLM auf ein effektives Heisenberg- Modell abgebildet wird. Mit einer RPA- Theorie wird das effektive Heisenberg- Modell auf Aussagen zu zentralen magnetischen Eigenschaften wie Curie- Temperatur und Magnetisierungskurve analysiert. Durch gezielte Variation der Systemparameter wird die Brauchbarkeit des Modells getestet und dadurch die Rolle der itineranten Ladungstraeger fuer die Stabilitaet des Ferromagnetismus in GdN untersucht.

To My Family

Contents

Chapter 1

Introduction

The ability to reduce everything to simple fundamental laws does not imply the ability to start from those laws and reconstruct the universe.

- P.W.Anderson, Nobel Prize in Physics, 1977

1.1 The many body problem

Condensed Matter Physics is the study of materials in solid and liquid phases. It encompasses the study of ordered crystalline phases of solids, as well as disordered phases such as the amorphous and glassy. Solid state has the quite remarkable property that, due to the large number of particles involved, the behavior of the materials may be qualitatively distinct from those of the individual constituents. In order to study its constitution, there is only one correct approach and that is to consider it as a many body problem with as many constituents as the number of particles in the actual piece of matter. The behavior of the incredibly large number of particles is governed by (quantum) statistics which, through the chaotically complicated motion of the particles, produces new types of order. These emergent phenomena are best exemplified in phenomenon such as magnetism or superconductivity where the collective behavior results in transitions to new phases. The development of solid- state theory has been, since the advent of quantum mechanics, primarily a search for methods of approximation that would enable one to gain some insight into the behavior of the solutions to this basically unmanageable problem.

A good starting point for a discussion of the many body problem in physics might be the question of how many bodies are actually required before we can define it as a problem ? If one is interested in exact solution, then it can be answered by taking a look at the history. In eighteenth- century Newtonian mechanics, the three- body problem was insoluble. With the birth of general relativity around 1910 and quantum electrodynamics in 1930, the two- and one- body problems became insoluble. And within modern quantum field theory, the problem of zero bodies (vacuum) is insoluble. So, if we are out for exact solutions, no bodies at all is already too many. We are certainly not

really interested in the exact solutions, so let us look around for a better statement of the problem.

The calculation of the motion of one particle is, under classical or quantum mechanics, a well- defined problem with a well- defined solution. If one takes into account two or three particles, then one may regard the problem to be soluble on considering whether they have mutual interaction or not. Once the realm of large number of particles is reached, sheer computational difficulty prevents a solution. The only exception is the case of *noninteracting* set of particles for then the total Hamiltonian splits into independent single- particle Hamiltonians. Once the *interaction* term is turned on, however weak, the situation must change. The motion of any particle now becomes a function of all other particles so that the very concepts of single- particle motion and properties become much less useful. This leads us to the following definition which is graphically as depicted below;

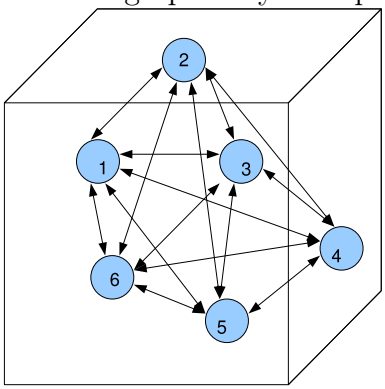

The many body problem is the study of the effects of interactions between particles on the behavior of a many particle system.

Now let us focus on the problem if we are ought to study the physics of a solid body in terms of a collection of interacting particles and methods to solve them.

A solid consists of an array of atoms in close proximity. In surveying the properties of materials it is convenient to separate them according to two disparate time scales. One time scale is a slow time scale which governs the structural dynamics, and a faster time scale that governs the electronic motion. The large difference between the time scales is due to the large ratio of the nuclear masses to the electronic mass. The long- ranged electromagnetic force binds these two constituents of different masses into electrically neutral material. The slow moving nuclear masses can be considered to be quasi- static, and are responsible for defining the structure of matter. In this approximation, the fast moving electrons equilibrate in the quasi- static potential produced by the nuclei.

The difference in the relevant time scales for electronic and nuclear motion allows one to make the Born- Oppenheimer Approximation [1]. In this approximation, firstly it is noted that in order to determine the electronic energy levels we may consider the nuclei fixed at their empirically known equilibrium positions. However, when treating the slow motions of the nuclei, the electrons are considered as adapting instantaneously to the potential of the charged nuclei, thereby minimizing the electronic energies. Thus, the nuclei charges are dressed by a cloud of electrons forming ionic or atomic- like aggregates. Sec-

ondly, a qualitative estimate of the relative energies of nuclear versus electronic motion can be obtained, i.e. we may be able to divide the atomic electrons into those belonging to closed shells, whose excitation potentials are too high, and the relatively loosely bound valence electrons; the effect of the closed shells (the "core") upon the valence electrons will then consist of a static potential.

When we come to treat the valence electrons, the problems become severe. We are faced here by a system comprising an immense number of particles (of the order of one valence electron per atom); the charateristic energies are all the same, while their mutual (Coulomb) interactions are by no means weak. We may consider four conceivable approaches on the problem :

1. Ignoring the interaction between the electrons. Such a procedure is absurd if we are after numerical results, but may be useful for qualitative insight.

2. Solving the problem with self- consistent fields; that is, consider each electron as moving in the average potential due to all the others. This is called *Hartree* method.

3. Same as second approach, but with an additional provison that the wave function be not just a product, but an antisymmetrized product of one electron functions. This is called the *Hartree- Fock* method.

4. Really solve the problem. This approach, which has no special name, is in practice impossible because of the incredibly intricate motions of the particles in an interacting system and thus justifies why we are not actually interested in exact solution.

Before discussing the methods in order to accomplish these four approaches, it may be useful to introduce some nomenclatures which are often found in the literature. The difference between the methods 3. and 2. is said to be due to *exchange* while the difference in any quantity between what would be calculated by approaches 4. and 3. is said to be due to *correlation* i.e. interaction effects beyond static mean fied theories (Hartree- Fock). According to Vollhardt, there are a few more explanations of the term *correlation* [2] but throughout the thesis we restrict ourselves to the above mentioned simple definition. Note that *correlation* and *exchange* are not physical phenomena, but names of mathematical patching procedures. Imagine that if the electron energy were correctly calculated (method 4.), then there would be no way of identifying which part of it is *correlation* energy, or which part is *exchange* energy.

With the knowledge of these definitions, the next step is to explore the basic theoretical tools in order to solve the many body problem. Out of the several approximate methods, one of the most successful and the one which is still used extensively today, is the *canonical transformation* technique. This involves transforming the Schrödinger equation to a new set of co- ordinates in which the interaction term becomes small. The problem of strongly coupled many body system is transformed into a set of approximately (or exactly,

in the simple cases) independent fictitous bodies which can be viewed based on the concepts of *elementary excitations*. They are generally divided into two categories: quasi- particles and collective excitations Examples of quasi-particle are *quasi- electron*[1], *polaron*, etc.. while that of elementary collective excitations are *phonons*, *plasmons*, *magnons*, etc.. The principal drawback with this technique is that it is not as systematic as one would like, and this sometimes makes it difficult to apply.

But its study provided the necessary background for understanding the significance of a modern useful tool, *quantum field theory*. With its success in elementary particle physics, it was shown to provide a powerful and unified way of attacking the many body problem. In this thesis, we shall be mainly concerned with the field theoretic technique known as the *propagator* or *Green Function Theory* (GFT). This is based on the idea that in order to find the important physical properties of a system it is not necessary to know the detailed behaviour of each particle but, rather, just the average behaviour of one or two typical particles. The quantities which describe this average behaviour are called the *single particle propagator* and *two particle propagator*, respectively. In Appendix A, we present a short description of this theory while in chapter 2 we utilise it (in the form of the so- called double- time retarded single particle Green function method) to solve the many body problem in hand.

The other tool which we will make use of is the so- called *Density Functional Theory* (DFT) which is briefly introduced in Appendix C. It is used to calculate the ground state properties of the system like single particle energies, electronic bandstructures, density of states, etc...

The basic aim of the thesis is to combine the many body theoretical technique (GFT) along with ground state single particle energies (DFT) to predict the temperature dependent electronic correlation effects of real materials like the rare earth chalcogenides and pnictides which are magnetic semiconductors or semi- metals and can be well described within many body Hamiltonian (Kondo lattice model). We also try to understand the basic nature of magnetism in these materials and thereby evaluate some of their magnetic properties.

The next section describes in short the motivation in order to study these magnetic semiconductors.

1.2 Spintronics

Basic research in the physical sciences, especially condensed matter physics, can result in important developments in applied physics and engineering. In the last century, there have been various examples of rapid transition from

[1] an electron in an electron gas with a uniform positive charge background repels other electron, thus getting surrounded by a positive screening cloud. The electron plus screening cloud constitutes quasi- electron.

discovery to commercialization. For instance, the transistor action in Ge semiconductor was observed at Bell labs in 1947 by W.Shockley, J.Bardeen and W.Brattain. They were honored for their work with 1956 Nobel Prize in Physics. And less than five years since the initial discovery, the transistors were commercially available for use and has been ultimately developed into solid state electronics industry. The other very recent being that of spin polarized electronic transport which developed into magnetic information and data storage.

Spintronics[2] (also known as magnetoelectronics) is an emergent technology which exploits the charge states of electrons as in semiconductors as well as the quantum spin states as used in data storage technology. The discovery of Giant Magnetoresistance (GMR) in multilayers of iron and chromium by Albert Fert [3] along with its simultaneous and independent discovery by Peter Grünberg [4] is considered as the birth of spintronics. For their path- breaking research they have been recently honored by 2007 Nobel Prize in Physics.

In order to make a spintronic device, the primary requirement is to have a system that can generate a current of spin polarized electrons, and a system that is sensitive to the spin polarization of the electrons. Such devices are used in the field of mass- storage and the most successful spintronic device to date is the spin valve, a GMR device. This device utilizes a layered structure of thin films of magnetic materials, which changes electrical resistance depending on applied magnetic field direction. In a spin valve, one of the ferromagnetic layers is "pinned" so its magnetization direction remains fixed and the other ferromagnetic layer is "free" to rotate with the application of a magnetic field.

When the magnetic field aligns the free and the pinned layer magnetization vectors parallel to each other then the electrical resistance of the device is at its minimum. When the magnetic field causes the free layer magnetization vector to rotate in a direction antiparallel to the pinned layer magnetization vector, the electrical resistance of the device increases due to spin dependent scattering. The magnitude of the change in resistance i.e. the difference between the antiparallel and parallel resistance upon the parallel resistance is called the GMR ratio. Spin valves can be designed with magnetically soft free layers which have a sensitive response to very weak fields (such as those originating from tiny magnetic bits on a computer disk), and have replaced anisotropic magnetoresistance sensors in computer hard disk drive heads since the late 1990s.

Today's spintronics research involves virtually all- material families. However, the interest in semiconductor- based spintronics has greatly stimulated studies of magnetic semiconductors [5], both from the fundamental physics and device application point of view. Though one of the earliest known ferromagnetic semiconductors (so- called 1^{st} generation materials) like the rare earth monochalcogenides [Europium Oxide (EuO), Europium Sulphide (EuS)] were discovered in early 1960s [6, 7] but due to their low Curie temperature, far below the room temperature, they were not ready for any practical purpose. Since then there have been a long and unyielding search for semiconductors

[2]The term spintronics was put forward by S.A.Wolf.

exhibiting magnetism at or above 300 K. Though recently there have been a lot of progress[3] in order to achieve this task by doping a host semiconductor material with transition metal ferromagnetic atoms producing diluted magnetic semiconductors (DMS, so- called 2^{nd} and 3^{rd} generation materials) with Curie temperature as high as 173 K [10] but due to the complication in growth and measurement techniques and because of approximate theories there is still a lack of complete understanding which has hindered the commercialization of this technology.

In this respect, it is very encouraging to first understand the concentrated ferromagnetic semiconductors which eventually also form the types of materials of our study. In general, they come under an important class of materials called *strongly correlated electron systems*. These are a wide class of materials which exhibit unusual (often technologically useful) electronic and magnetic properties, such as metal- insulator transitions or half- metallicity. Many, if not most, transition metal oxides belong into this class which may be subdivided according to their behavior, e.g. high Tc superconductors, spintronic materials, Mott insulators, spin Peierls materials, heavy fermion materials, quasi low- dimensional materials etc. The single most intensively studied effect is probably high temperature superconductivity in doped cuprates, e.g. $La_{1-x}Sr_xCuO4$. Other ordering or magnetic phenomena and temperature induced phase transitions in many transition metal oxides are also gathered under the term strongly correlated materials. Typically, strongly correlated materials have incompletely filled d or f electron shells with narrow bands. One can no longer consider any electron in the material as being in a 'sea' of the averaged motion of the others. Each single electron has a complex influence on it's neighbours.

The term "strong correlation" refers to behavior of electrons in solids that is not well- described by simple one- electron theories such as the Local Density Approximation (LDA) of DFT. For instance, the seemingly simple material NiO has a partially filled $3d$- band (the Ni atom has 8 of 10 possible $3d$- electrons) and therefore would be expected to be a good conductor. However, strong Coulomb repulsion (a correlation effect) between d- electrons makes NiO instead a wide band gap insulator. Thus, strongly correlated materials have electronic structures that are neither simply free- electron like nor completely ionic, but a mixture of both.

Future applications may include a spin- based transistor which requires the development of magnetic semiconductors exhibiting room temperature ferromagnetism. The operation of MRAM or magnetic random access memory is also based on spintronic principles. Multiferroics which have properties of being able to change internal molecular geometry under electrostatic or electromagnetic influence is lately a hotbed of research while applications in the field of bioinformatics may bring in a revolution in the field of medicine and healthcare.

[3] see review articles like [8, 9] on Mn- doped II- VI and III- V semiconductors and references therein. An extensive database is created at http://unix12.fzu.cz/ms.

1.3 Outline

The organization of the thesis is as follows. In chapter 2, we first introduce the Kondo problem (intra- atomic exchange between single localized impurity with that of sea of fermions in a metal) and then we present its lattice counterpart namely the Kondo lattice model (KLM). Within a single band theory (for the itinerant electrons) we try to evaluate the temperature dependent physical properties of the sytem like quasi- particle density of states for a given quantum spin and width of the itinerant electron band but for different strength of the intra- atomic exchange. We further extend our theory to a multi- band case and determine the similar physical properties for a two band situation with an additional parameter being the strength of hybridization between the bands. In chapter 3, we perform the perform the T=0 first principles calculations using the TB- LMTO- ASA program in order to obtain the ground state energies which we combine along with our many body theory so as to study the temperature dependent correlation effects in the conduction and valence bands of real materials like EuS and GdN. In chapter 4 we derive the multiband analogue of the modified RKKY theory and evaluate it for two band situation. Using the multi- band modified RKKY theory we try to explain the role of charge carriers in stabilizing the ferromagnetism in GdN. Finally in chapter 5, we summarize our findings and conclude the thesis with an outlook. In order to keep the content of the thesis in a self- contained manner, we briefly describe the method of Green function theory, Density Functional Theory, commutation relations due to spin operators and anti- commutation of the fermionic creation and annihilation operators, basic spectroscopic techniques and some technical aspects as a part of appendix. We have also used elaborative analytical formulation and explanations wherever required so as to keep continuity in the text and making it enjoyable to read.

Chapter 2

Multi- band Kondo lattice model

Individuality is only possible if it unfolds from wholeness.

- D. Bohm.

2.1 The Kondo Problem

Already in the 1930's it was found that *the resistance curve of the gold wires measured (not very pure) has a minimum at low temperatures* [11]. It was later realized that it contained transition metal impurities and can be characterized as dilute magnetic alloys. Their properties are basically determined by the exchange interaction between the conduction electrons of the metal and the single impurity magnetic moment. A conventional description of this interaction is based on the so- called *s- d exchange* or *Kondo* model where the conduction electrons are due to the s- orbital while the impurity is represented by the localized partially filled d- shell magnetic moment $\mathbf{S} = (\mathrm{S}_x, \mathrm{S}_y, \mathrm{S}_z)$. Though this model was theoretically described in the early 1950s [12] but was not well understood until 1964 when Jun Kondo [13] applied perturbation theory to this model and explained the logarithmic growth of the resistivity at low temperatures. His paper gave rise to an enormous amount of theoretical and experimental activity in this area.

The Hamiltonian of the s- d exchange model is [13],

$$H = \sum_{\mathbf{k},\sigma} \epsilon(\mathbf{k}) c^{\dagger}_{\mathbf{k}\sigma} c_{\mathbf{k}\sigma} - J \sum_{\substack{\mathbf{k},\mathbf{k}' \\ \sigma,\sigma'}} c^{\dagger}_{\mathbf{k}\sigma} \boldsymbol{\sigma}_{\sigma\sigma'} c_{\mathbf{k}\sigma} \mathbf{S} \tag{2.1}$$

where $c^{\dagger}_{\mathbf{k}\sigma}$, $c_{\mathbf{k}\sigma}$ are the creation and annihilation operators of the conduction electron, $\epsilon_{\mathbf{k}}$ is the electron's kinetic energy and $\boldsymbol{\sigma}$ is the Pauli matrix. J is the spin exchange interaction between the conduction electrons and the localized moment which can be ferromagnetic (> 0) or anti- ferromagnetic (< 0). Kondo observed that the effective amplitude due to spin- flip scattering, $I(T)$,

as computed within the second order perturbation theory, rises with decrease in the energy and temperature. It was in contrast to the phonon part of the amplitude which rapidly decreases. Hence the total, phonon- and impurity- induced, amplitude should have a minimum. The resistivity due to the magnetic impurity, R_i, is proportional to square of the scattering amplitude [13]

$$R_i \sim cI^2(T) \sim c[J + \rho J^2\, ln\frac{D}{k_B T} + O(\rho^2 J^3)]^2 \tag{2.2}$$

where c is the concentration of the impurity ions and D is bandwidth of the conduction electrons and $\rho = \rho(E_F)$. When the temperature is of the order of Kondo temperature,

$$k_B T_K \sim D\, exp\left(\frac{-1}{\rho \mid J \mid}\right) \tag{2.3}$$

all the terms in the perturbation expansion are of the same order in magnitude and despite the weak bare coupling, perturbation theory breaks down. This is the so- called *Kondo* problem.

There have been several attempts to go beyond perturbation theory but however inevitably due to uncontrolled approximations, they resulted in wrong results. For details on the introduction of this subject one can refer to *theory of dilute magnetic alloys* [14] and references therein while the different techniques and methods applied to meet this challenge can be found in [15, 16]. Finally, in order to grasp the lastest development in this field, one can follow Ref [17].

Before describing our approach to the s- d or Kondo model Hamiltonian i.e. Eq. 2.1, we would like to mention another very interesting model which also deals with problem on dilute magnetic alloys and is known as single impurity Anderson model [18]. Its development started with two questions: "Under what circumstances does a localized moment exist in a metal?" and "What are the consequences of the interaction between a localized moment and the conduction electrons?". Apart from the usual kinetic energy term, the model Hamiltonian also includes a hybridization (admixture) of impurity d level and the conduction electron band states which can lead to delocalization of the impurity electron states and thus can destroy its magnetic moment. In this model, it is also supposed that no more than two electrons can occupy the impurity level making it a non- degenerate model. An extensive study on the similar problem was first initiated by Friedel [19] and collaborators around 1958.

The above problem of dilute alloys fall into class of systems with strong electron correlations while the other being the cuprates and high temperature superconductors, charge- and spin- ordering and fluctuations, manganites and colossal magnetoresistance, low- dimensional systems and transport, Mott-Hubbard transition and the quantum Hall effect [20].

2.2 Single band model

We reconsider the single impurity s- d exchange model and regard its periodic lattice analogue, i.e. at each site of a given lattice structure we take into

account the spin exchange interaction between the itinerant electron and localized moment, in order to obtain the so- called Kondo lattice model (KLM). Probably the most interesting aspect in the Kondo lattice problem is the possible interplay of the long range magnetic order and the Kondo effect. A preliminary study of the critical properties of such kind of systems was initiated by Doniach et al, on a 1- d analog of the Kondo lattice, giving rise to the "Kondo necklace" [21].

Apart from it, other theoretical studies on this model concentrated a great deal on various properties of real materials like heavy fermion systems [16], magnetic semiconductors [22], manganese- based pervoskite oxides [23], thin films of europium chalcogenides [24], the rare- earth metals [25] and their films [26] and recently also on the dilute magnetic semiconductors [27, 28].In some cases, the exchange coupling between the itinerant conduction electrons and the localized moments was taken to be positive rendering the so- called *ferromagnetic Kondo lattice model* i.e. FKLM as shown in Figure 2.1. It also

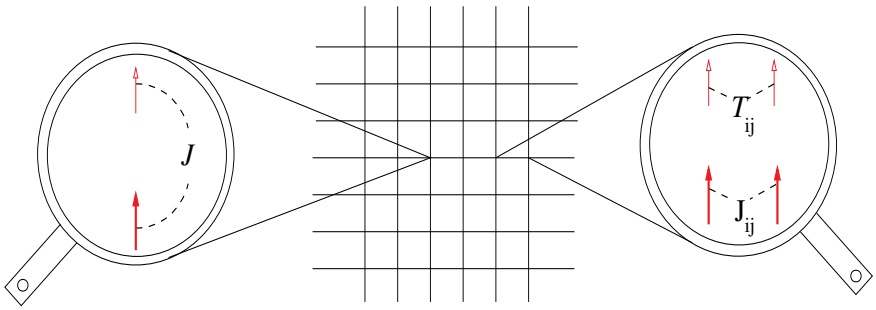

Figure 2.1: The Kondo lattice model. J is the ferromagnetic s- d interaction, $T_{\rm ij}$ is the site- to- site itinerant electron (shown as thin red arrow) hopping and $\rm J_{ij}$ is the direct ferromagnetic exchange interaction between two localized moments (depicted as thick red arrow) which we do not consider in our model.

forms the basic model of our study and henceforth, throughout the thesis we shall call it as only KLM.

Considering the wide range of applicability of the KLM, let us study the single band Kondo lattice Hamiltonian written in the second quantized form,

$$H = \sum_{ij\sigma} T_{ij} c^{\dagger}_{i\sigma} c_{j\sigma} - \frac{J}{2} \sum_{i\sigma} (z_\sigma S^z_i c^{\dagger}_{i\sigma} c_{i\sigma} + S^{\sigma}_i c^{\dagger}_{i-\sigma} c_{i\sigma}) \tag{2.4}$$

with $c^{\dagger}_{i\sigma}$ and $c_{i\sigma}$ being the fermionic creation and annihilation operators, respectively, at lattice site $\rm R_i$.The latin indices, i and j, denote the lattice sites and σ is the spin index. There is a localized spin on each site of the lattice. Conduction electrons are hopping site to site by the nearest neighbour transfer interaction, known as kinetic energy which is given by the first term in Eq. (2.4) while their interaction with the localized spin is denoted by the second term in the above equation. It is further split into two subterms. The first describes the Ising type interaction between the z- component of the localized and itinerant carrier spins while the other comprises spin exchange processes which

are responsible for many of the KLM properties. J is the exchange coupling strength which we assume to be **k**- independent and S_i^σ refers to the localized spin at site R_i

$$S_i^\sigma = S_i^x + iz_\sigma S_i^y \ ; \ \ z_\uparrow = +1, z_\downarrow = -1 \tag{2.5}$$

The Hamiltonian in Eq.(2.4) provokes a nontrivial many body problem that cannot be solved exactly. We proceed to solve the problem using the equation of motion method for the double- time retarded Green function as briefly introduced in Appendix A[4],

$$G_{lm\sigma}(E) = \langle\langle c_{l\sigma}; c^\dagger_{m\sigma}\rangle\rangle_E \tag{2.6}$$

The equation of motion reads as follows,

$$EG_{lm\sigma}(E) = \langle [c_{l\sigma}, c^\dagger_{m\sigma}]\rangle + \langle\langle [c_{l\sigma}, H]_-; c^\dagger_{m\sigma}\rangle\rangle \tag{2.7}$$

or in a more elaborated form as,

$$EG_{lm\sigma}(E) = \delta_{lm} + \sum_j T_{lj}G_{jm\sigma}(E) - \frac{J}{2}\Big[z_\sigma \Gamma_{llm\sigma}(E) + F_{llm\sigma}(E)\Big] \tag{2.8}$$

where we use the following notations, written in a more generalized form as

$$\Gamma_{klm\sigma}(E) = \langle\langle S_k^z c_{l\sigma}; c^\dagger_{m\sigma}\rangle\rangle_E \tag{2.9a}$$

$$F_{klm\sigma}(E) = \langle\langle S_k^{-\sigma} c_{l-\sigma}; c^\dagger_{m\sigma}\rangle\rangle_E \tag{2.9b}$$

We find that Eq.(2.9a) and Eq.(2.9b) are higher order Green functions blocking the direct solution of the equation of motion as they can't be decoupled into the forms of the original Green function. Approximations must be considered in the similar form as given in the Appendix A. But a rather formal solution can be stated as

$$G_{\mathbf{k}\sigma}(E) = [(E + i0^+) - \epsilon(\mathbf{k}) - \Sigma_{\mathbf{k}\sigma}(E)]^{-1} \tag{2.10}$$

where we have used the following Fourier- transform,

$$G_{\mathbf{k}\sigma}(E) = \frac{1}{N}\sum_{ij} G_{lm\sigma}(E) \ e^{-i\mathbf{k}\cdot(\mathbf{R}_l - \mathbf{R}_m)} \tag{2.11}$$

In Eq.(2.10), $\epsilon(\mathbf{k})$ is the hopping term in Bloch representation and 0^+ is a small quantity added to have complex energies so as to analytically continue the function $G_{lm\sigma}(E)$ in a complex plane[5]. The self- energy, $\Sigma_{\mathbf{k}\sigma}$(E), containing all the influences being of fundamental importance, can be understood using site representation :

$$\langle\langle [c_{l\sigma}, H_{int}]; c^\dagger_{m\sigma}\rangle\rangle = \sum_p \Sigma_{lp\sigma}(E) G_{pm\sigma}(E) \tag{2.12}$$

[4]Throughout the thesis, we drop the superscript (r) for simplicity.

[5]While utilizing Eq. (2.10) for numerical calculation, one has to optimize the value of 0^+ so as to get reasonable results. This point is elaborately discussed in Appendix E.

where H_{int} is the second term in Eq.(2.4).

Thus one can imagine of a single particle moving through the system, surrounded by a cloud of other particles that are being pushed out of the way or dragged along by its motion, so that the entire entity moves along somewhat like a free particle. Such a particle is known as a quasi- particle. It is one of the most important concept in condensed matter physics, because it is one of the few known ways of simplifying the quantum mechanical many- body problem and is applicable to an extremely wide range of many- body systems.

So, now we are left with a problem of finding a self- energy ansatz in order to compute the Green function and thereby calculate the quasi- particle physical quantities of interest like the spectral density (SD)

$$\boxed{S_{\mathbf{k}\sigma}(E) = -\frac{1}{\pi} Im(G_{\mathbf{k}\sigma}(E))} \tag{2.13}$$

and the quasi- particle density of states (Q- DOS)

$$\boxed{\rho_{\sigma}(E) = \frac{1}{N}\sum_{\mathbf{k}} S_{\mathbf{k}\sigma}(E)} \tag{2.14}$$

The unavoidable approximations to the not exactly solvable many body problem of the KLM have been extensively studied by Nolting and coworkers during the last two decades. But before we mention the well developed methods, it is important to highlight couple of exactly solvable limiting cases of the model which eventually will be treated as guidelines while testing the approximations which are being used.

1. *Zero-bandwith limit*: Let us assume that the arbitrarily filled conduction band is shrunk to an N- fold degenerate level, $\epsilon(\mathbf{k}) \longrightarrow T_0 \,\forall\, \mathbf{k}$. Nevertheless, we consider the f- spin system as collectively ordered for $T < T_c$ (Curie temperature) by any direct or indirect exchange interaction. In this case, the hierarchy of equations of motion decouples exactly and can rigorously be solved resulting in four energy levels of the system along with corresponding spectral weights [29].

2. *Ferromagnetically saturated semiconductor*: It concerns the situation of a single electron in an otherwise empty conduction band at $T = 0$, when the local moment system is ferromagnetically saturated [22]. In the next section, we will also analytically prove this case for the multi- band KLM.

As far as approximate solutions to the KLM are concerned, we mention some of the approaches in the following text while the details can be found in the corresponding references. A very fruitful comparison between four different methods namely dynamical mean field theory (DMFT) [30], the second- order perturbation theory (SOPT), self- consistent coherent potential approximation (CPA) and moment conserving decoupling approximation (MCDA) [31] was done by Meyer et al, [32]. But it is a known [33] fact that the methods of DMFT can not be directly applied to the Kondo lattice model. One exception

is the case of the classical spin limit, thus removing the quantum nature of the spins. While there is another possibility to derive a DMFT for Kondo lattice model, based on the fermionization of the localized spin operators as suggested in [34], but it is limited to S=$\frac{1}{2}$ and a similar approach was followed by Meyer et al, An altogether different approach was taken by T.Hickel in his doctral thesis [35, 36] whereby he developed the Mori's projection- operator formalism for KLM.

In this thesis, we will make use of an self- energy ansatz known as interpolating self- energy approach (ISA) which was initially developed for low-carrier densities [37] and lateron extended for the complete range of carrier concentration [38]. The aim to construct such an approximate expression for the electronic self- energy was to fulfill not only the above two limiting cases, but also to reproduce the correct strong coupling (high energy series expansion) and weak coupling (SOPT) behavior. The ansatz is given as [37] :

$$\Sigma_\sigma(E) = -\frac{J}{2}M_\sigma + \frac{J^2}{4}a_\sigma G_\sigma\left(E - \frac{J}{2}M_\sigma\right)\left[1 - \frac{J}{2}G_\sigma\left(E - \frac{J}{2}M_\sigma\right)\right]^{-1} \quad (2.15)$$

where

$$M_\sigma = z_\sigma\langle S^z\rangle;\;\; a_\sigma = S(S+1) - M_\sigma(M_\sigma+1). \quad (2.16)$$

and the non- interacting (free) Green function matrix is defined as :

$$G_\sigma(E) = \frac{1}{N}\sum_{\mathbf{k}}\Big[(E + i0^+) - \epsilon(\mathbf{k})\Big]^{-1}$$

As seen in Eq.(2.15), the form of local self- energy can also be understood as

$$\Sigma_\sigma(E) = \frac{1}{N}\sum_{\mathbf{k}}\Sigma_{\mathbf{k}\sigma}(E)$$

The wave- vector dependence of the self- energy is mainly due to the magnon energies $\omega(\mathbf{k})$ appearing at finite temperature. But in our analysis *we neglect a direct Heisenberg exchange between the localized spins* since we are only interested in the influence of inter- band exchange on the conduction band states in order to study the electronic correlations and currently not aimed at calculating the magnetic properties via self consistent calculation of localized magnetizations. This can be interpreted as the $\omega(\mathbf{k}) \rightarrow 0$ limit. The localized magnetization $\langle S^z\rangle$ shall be considered as an external parameter being responsible for the induced temperature dependence of the band states.

Considering our electronic self- energy ansatz, we proceed to perform a model calculation on a simple cubic (sc) lattice where the hopping term, $\epsilon(\mathbf{k})$, is taken using the sc Bloch representation in the tight binding approximation [39]. We assume the bandwidth (W) of the band to be 1.0 eV and S=3.5 ($4f$ systems) as the quantum spin. The variables in our calculation are the strength of the intra- atomic exchange coupling, J and magnetization, $\langle S^z\rangle$.

Figure 2.2 describes the temperature dependent quasi- particle density of states (DOS) of a sc lattice for the parameters : J=0.1, 0.3 and 0.6 eV and for different values of magnetization, $\frac{\langle S^z\rangle}{S}$=1.0, 0.5 and 0.0 which are represented

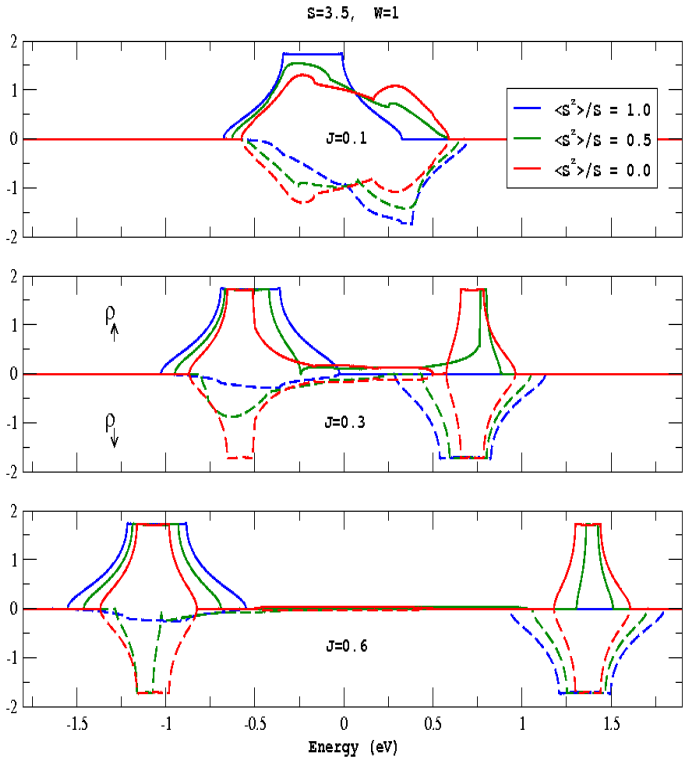

Figure 2.2: Temperature dependent quasi- particle density of states for a sc lattice with different values of exchange coupling strength: J=0.1, 0.3 and 0.6 eV. The bandwidth is taken to be 1.0 eV and spin value is S=3.5

in blue, green and red respectively. The spin- $\uparrow$ is denoted by full lines and broken lines is for spin- $\downarrow$ case. The exact solution, ferromagnetically saturated semiconductor, coincides with the results of $\frac{\langle S^z \rangle}{S}$=1.0.

In order to study the electronic correlations, one examines the effect of a test electron by creating (or annihilating) it in an empty (or filled) band. In our case, we create an electron in a completely empty band. Thus, addition of $\uparrow(\downarrow)$ electron will give a useful insight into the system. The correlation effects are studied by calculating the electronic self- energy. But apart from electronic sub- system, we also have the magnetic sub- system. The exchange coupling between the itinerant electron and localized spins adds up to the correlation effects as they produce spin- flip transitions and Ising like interactions[6] in addition to the kinetic energy.

At T=0 K and fully empty bands, the addition of a $\uparrow$ electron produces a stable single particle excitations (quasi- particles) since the $\uparrow$ electron has no chance to flip its spin with the ferromagnetically saturated spin ($\Uparrow$) subsystem. The imaginary part of the self- energy vanishes indicating infinite lifetimes. The situation is different for the addition of a $\downarrow$ electron as the $\downarrow$ electron can exchange its spin with the ferromagnetically saturated spin subsystem and have finite lifetime. It can emit a magnon and become a $\uparrow$ elec-

[6]in a magnetically ordered case it corresponds to shifting of the energy scale for the up and down spin spectrum as compared to the paramagnetic situation

tron provided there exist ↑ electron states which can be occupied after spin-flip process. These are the 'scattering states' which occupy the same energy regions as of the ↑ spectrum. The scattering states become more distinct with increasing coupling strength as seen in the lower part of Figure 2.2 with J=0.3 and 0.6 eV exhibiting the intermediate and strong coupling limit. The other possibility for the ↓ electron to exchange its spin could be by repeated emission and absorption of magnons, resulting in a 'dressed' particle (quasi- particle) propagating through the lattice accompanied by a virtual cloud of magnons and is termed as magnetic polaron [40].

However, at finite temperatures, the spin sub- system is no longer perfectly aligned. There are magnons in the system that can be absorbed by the itinerant ↑ charge carriers. As seen in Figure 2.2, at finite temperatures the spectral weight gets redistributed due to spin flip term in the exchange interaction with deformations in the density of states. In the limit $T \to T_c$ ($\langle S^z \rangle \to 0$) the induced spin asymmetry is removed.

Now before turning our attention to real materials, we extend the above model Hamiltonian for the case of two hybridized bands and try to study its consequence on the density of states and thereby on other properties of the system.

2.3 Two band analysis

The single band calculations are certainly not sufficient in order to understand the electronic structure of real materials. One has to take into account the band degeneracy with corresponding interband interactions. The multi- band models are also of growing interest for their wide range of phenomena like novel electronic phases, magnetism and superconductivity [41]. For instance, it was found out using a two- band Hubbard model , that there was a possibility of existence of ferromagnetism around half- filling in contrast to antiferromagnetism in single band model [42]. The numerical studies on ground state properties of multi- band periodic Anderson model revealed the minor role played by the competition between RKKY and Kondo interactions again in contrast to the single band case [43]. With this motivation, we try to understand the interplay of the kinetic and potential energy within a multi- band Kondo lattice model.

Let us consider the following Hamiltonian;

$$H = H_{kin} + H_{int} \tag{2.17}$$

where

$$H_{kin} = \sum_{ij\alpha\beta\sigma} T_{ij}^{\alpha\beta} c_{i\alpha\sigma}^{\dagger} c_{j\beta\sigma} \tag{2.18}$$

and

$$H_{int} = -\frac{J}{2} \sum_{i\alpha\sigma} (z_\sigma S_i^z c_{i\alpha\sigma}^{\dagger} c_{i\alpha\sigma} + S_i^{\sigma} c_{i\alpha-\sigma}^{\dagger} c_{i\alpha\sigma}) \tag{2.19}$$

The term H_{kin} denotes the usual kinetic energy of the system. The latin letters (i,j,...) symbolize the crystal lattice cites while the band indices are

depicted in Greek letters (α,β,..) and the spin is denoted as $\sigma(=\uparrow,\downarrow)$. So, the new feature as compared to the analysis in the previous section 2.2 are the band indices and the aim is to study its effect onto the system. The multi-band hopping term, $T_{ij}^{\alpha\beta}$ in general will be obtained from an LDA calculation as shown in Chapter 3 incorporating in a realistic manner the influences of all those interactions which are not directly accounted for by our model Hamiltonian. But in this chapter we will be mainly interested in a model calculation in order to test the theory by considering that at each lattice site there are two Bloch- like non- degenerate bands with a finite hybridization between them. The real space hopping, $T_{ij}^{\alpha\beta}$, can be Fourier transformed to the **k**- space free Bloch energies using the relation, $\epsilon^{\alpha\beta}(\mathbf{k})$,

$$\epsilon^{\alpha\beta}(\mathbf{k}) = \frac{1}{N}\sum_{ij} T_{ij}^{\alpha\beta}\, e^{-i\mathbf{k}\cdot(\mathbf{R}_i-\mathbf{R}_j)} \tag{2.20}$$

H_{int} is the usual intra- atomic exchange interaction but with an assumption that itinerant electron in each band is coupled to the localized moment by the same coupling strength, J. The total Hamiltonian will be solved in the similar fashion as shown in the previous section and so, the Green function under consideration is,

$$G_{lm\sigma}^{\mu\nu}(E) = \langle\langle c_{l\mu\sigma}; c_{m\nu\sigma}^{\dagger}\rangle\rangle_E \tag{2.21}$$

where l,m and μ,ν are the lattice and band indices, respectively, and the equation of motion is given as

$$EG_{lm\sigma}^{\mu\nu}(E) = \delta_{lm}\delta_{\mu\nu} + \sum_{j\beta} T_{lj}^{\mu\beta} G_{jm\sigma}^{\beta\nu}(E) - \frac{J}{2}[z_\sigma \Gamma_{llm\sigma}^{\mu\nu}(E) + F_{llm\sigma}^{\mu\nu}(E)] \tag{2.22}$$

with the following notations written in more general form as used in the previous section,

$$\Gamma_{klm\sigma}^{\mu\nu}(E) = \langle\langle S_k^z c_{l\mu\sigma}; c_{m\nu\sigma}^{\dagger}\rangle\rangle_E \tag{2.23a}$$

$$F_{klm\sigma}^{\mu\nu}(E) = \langle\langle S_k^{-\sigma} c_{l\mu-\sigma}; c_{m\nu\sigma}^{\dagger}\rangle\rangle_E \tag{2.23b}$$

And the required solution is,

$$\widehat{G}_{\mathbf{k}\sigma}(E) = [(E+i0^+)\widehat{I} - \widehat{\epsilon}(\mathbf{k}) - \widehat{\Sigma}_{\mathbf{k}\sigma}(E)]^{-1} \tag{2.24}$$

where we exclude the band indices by representing the terms in a generalized matrix form on symbolizing a hat over it.

The terms in Eq. (2.24) can be explained as follows : $\hat{I}$ is an identity matrix, 0^+ is a small quantity as explained earlier and $\hat{\epsilon}(\mathbf{k})$ is a hopping matrix with the diagonal terms of the matrix denoting the intra- band hopping and the off-diagonal terms being the inter- band hopping. The self- energy, $\widehat{\Sigma}_{\mathbf{k}\sigma}$(E), can be written as :

$$\langle\langle [c_{l\mu\sigma}, H_{int}]; c_{m\nu\sigma}^{\dagger}\rangle\rangle = \sum_{p\gamma} \Sigma_{lp\sigma}^{\mu\gamma}(E) G_{pm\sigma}^{\gamma\nu}(E) \tag{2.25}$$

So, we again fall upon the identical problem of finding a multi- band self-energy ansatz in order to compute the Green function matrix and thereby

calculate the physical quantities of interest like the quasi- particle spectral density (SD) by taking a trace over the band indices,

$$\boxed{S_{\mathbf{k}\sigma}(E) = -\frac{1}{\pi} ImTr(\widehat{G}_{\mathbf{k}\sigma}(E))} \tag{2.26}$$

and the quasi- particle density of states (Q- DOS)

$$\boxed{\rho_\sigma(E) = \frac{1}{N}\sum_{\mathbf{k}} S_{\mathbf{k}\sigma}(E)} \tag{2.27}$$

In order to get the nature of the self- energy ansatz for the multi- band KLM, we try to analytically formulate one of its limiting case, namely the ferromagnetically saturated semiconductor. This will not only help us to obtain the multi- band self- energy ansatz thereby allowing its comparison with that of the single band case, Eq. (2.15), but will also guarantee its applicability.

What we are interested in is to find a solution for the model at T=0 with ferromagnetically saturated spin sub- system ($\langle S^z\rangle$ = S) and for fully empty bands. In such situation, the Ising- like higher order Green function Eq. (2.23a) for spin σ becomes;

$$\Gamma^{\mu\nu}_{klm\sigma}(E) = SG^{\mu\nu}_{lm\sigma}(E) \tag{2.28}$$

Now let us consider : a) $\sigma = \uparrow$ and b) $\sigma = \downarrow$ and try to evaluate the spin-flip function Eq. (2.23b) in both the cases and thereby the self- energy.

a) For $\sigma = \uparrow$, the spin- flip function

$$\begin{aligned} F^{\mu\nu}_{klm\sigma}(E) &= \langle\langle S^{-\sigma}_k c_{l\mu-\sigma}; c^\dagger_{m\nu\sigma}\rangle\rangle_E \\ &= \langle\langle S^-_k c_{l\mu\downarrow}; c^\dagger_{m\nu\uparrow}\rangle\rangle_E = 0 \end{aligned}$$

vanishes since neither annihilation of any particle is possible for empty bands nor raising of the localized spin at T=0. Hence the equation of motion for the Green function, i.e. Eq. (2.22) reduces to,

$$\left(E + \frac{JS}{2}\right) G^{\mu\nu}_{lm\uparrow}(E) = \delta_{lm}\delta_{\mu\nu} + \sum_{p\gamma} T^{\mu\gamma}_{lp} G^{\gamma\nu}_{pm\uparrow}(E)$$

And upon taking Fourier transform (see Appendix B) we have,

$$\left(E + \frac{JS}{2}\right) G^{\mu\nu}_{\mathbf{k}\uparrow}(E) = \delta_{\mu\nu} + \sum_{\gamma} \epsilon^{\mu\gamma}(\mathbf{k}) G^{\gamma\nu}_{\mathbf{k}\uparrow}(E)$$

which can be written in matrix form

$$\widehat{G}_{\mathbf{k}\uparrow}(E) = \left[\left(E + \frac{JS}{2} + i0^+\right)\widehat{I} - \widehat{\epsilon}(\mathbf{k})\right]^{-1} \tag{2.29}$$

which implies that poles are shifted by a constant amount $\frac{JS}{2}$. Thus, in this case the self- energy becomes;

$$\widehat{\Sigma}_\uparrow(E) = -\frac{JS}{2}\widehat{I} \tag{2.30}$$

b) For $\sigma = \downarrow$, the function

$$\begin{aligned} F^{\mu\nu}_{klm\sigma}(E) &= \langle\langle S^{-\sigma}_k c_{l\mu-\sigma}; c^\dagger_{m\nu\sigma}\rangle\rangle_E \\ &= \langle\langle S^{+}_k c_{l\mu\uparrow}; c^\dagger_{m\nu\downarrow}\rangle\rangle_E \neq 0 \end{aligned}$$

is more complicated due to spin- flip processes. It is non- zero since a $\downarrow$ electron created in an empty band can flip its spin with the ferromagnetically saturated spin sub- system and thus can have finite lifetime. Now if we try to derive its equation of motion then we have,

$$EF^{\mu\nu}_{klm\downarrow}(E) = \langle\langle [S^+_k c_{l\mu\uparrow}, H]; c^\dagger_{m\nu\downarrow}\rangle\rangle_E$$

which takes the form as given below yielding higher order Green functions,

$$\begin{aligned} EF^{\mu\nu}_{klm\downarrow}(E) = \sum_{p\gamma} T^{\mu\gamma}_{lp}\langle\langle S^+_k c_{p\gamma\uparrow}; c^\dagger_{m\nu\downarrow}\rangle\rangle_E - \frac{J}{2}\Bigg[&\langle\langle S^+_k S^z_l c_{l\mu\uparrow}; c^\dagger_{m\nu\downarrow}\rangle\rangle_E \\ &- \sum_\lambda \Bigg(\sum_\sigma z_\sigma \langle\langle S^+_k c^\dagger_{k\lambda\sigma} c_{k\lambda\sigma} c_{l\mu\uparrow}; c^\dagger_{m\nu\downarrow}\rangle\rangle_E \\ &- 2\langle\langle S^z_k c^\dagger_{k\lambda\uparrow} c_{k\lambda\downarrow} c_{l\mu\uparrow}; c^\dagger_{m\nu\downarrow}\rangle\rangle_E \Bigg) + \langle\langle S^+_k S^-_l c_{l\mu\downarrow}; c^\dagger_{m\nu\downarrow}\rangle\rangle_E \Bigg] \end{aligned} \tag{2.31}$$

The higher order Green functions resulting from the spin- flip equation of motion can be evaluated exactly for the case of fully empty bands (n=0) and at ferromagnetic saturation,

$$\begin{aligned} \langle\langle S^+_k S^z_l c_{l\mu\uparrow}; c^\dagger_{m\nu\downarrow}\rangle\rangle_E &= \langle\langle (S^z_l S^+_k - S^+_k \delta_{kl}) c_{l\mu\uparrow}; c^\dagger_{m\nu\downarrow}\rangle\rangle_E \\ &= (S - \delta_{kl}) F^{\mu\nu}_{klm\downarrow}(E) \end{aligned} \tag{2.32a}$$

$$\langle\langle S^+_k (c^\dagger_{k\lambda\uparrow} c_{k\lambda\uparrow} - c^\dagger_{k\lambda\downarrow} c_{k\lambda\downarrow}) c_{l\mu\uparrow}; c^\dagger_{m\nu\downarrow}\rangle\rangle_E \overset{n=0}{=} 0 \tag{2.32b}$$

$$\langle\langle S^z_k c^\dagger_{k\lambda\uparrow} c_{k\lambda\downarrow} c_{l\mu\uparrow}; c^\dagger_{m\nu\downarrow}\rangle\rangle_E \overset{n=0}{=} 0 \tag{2.32c}$$

$$\begin{aligned} \langle\langle S^+_k S^-_l c_{l\mu\downarrow}; c^\dagger_{m\nu\downarrow}\rangle\rangle_E &= \langle\langle (S^-_l S^+_k + 2S^z_k \delta_{kl}) c_{l\mu\downarrow}; c^\dagger_{m\nu\downarrow}\rangle\rangle_E \\ &= 2S\delta_{kl} G^{\mu\nu}_{lm\downarrow}(E) \end{aligned} \tag{2.32d}$$

On substituting the Eq.(2.32) in the spin- flip equation of motion we get,

$$EF^{\mu\nu}_{klm\downarrow}(E) = \sum_{p\gamma} T^{\mu\gamma}_{lp} F^{\gamma\nu}_{kpm\downarrow}(E) - \frac{J}{2}\Big[(S - \delta_{kl}) F^{\mu\nu}_{klm\downarrow}(E) + 2S\delta_{kl} G^{\mu\nu}_{lm\downarrow}(E)\Big] \tag{2.33}$$

and upon re- arranging the terms and taking its Fourier transform (see Appendix B) we obtain;

$$\begin{aligned} \left(E + \frac{JS}{2}\right) F^{\mu\nu}_{\mathbf{k},\mathbf{k-q},\mathbf{q}\downarrow}(E) = \sum_\gamma \epsilon^{\mu\gamma}(\mathbf{k-q}) F^{\gamma\nu}_{\mathbf{k},\mathbf{k-q},\mathbf{q}\downarrow}(E) + \frac{J}{2N}\sum_{\mathbf{t}} F^{\mu\nu}_{\mathbf{k},\mathbf{k-t},\mathbf{t}\downarrow}(E) \\ - \frac{JS}{\sqrt{N}} G^{\mu\nu}_{\mathbf{k}\downarrow}(E) \end{aligned} \tag{2.34}$$

while in the matrix form, it can be written as follows

$$\left[\left(E+\frac{JS}{2}\right)\widehat{I}-\widehat{\epsilon}(\mathbf{k\text{-}q})\right]\widehat{F}_{\mathbf{k},\mathbf{k\text{-}q},\mathbf{q}\downarrow}(E)=\frac{J}{2N}\sum_{\mathbf{t}}\widehat{F}_{\mathbf{k},\mathbf{k\text{-}t},\mathbf{t}\downarrow}(E)-\frac{JS}{\sqrt{N}}\widehat{G}_{\mathbf{k}\downarrow}(E)$$

Let us now define the "effective" Green function,

$$\widehat{G}^{\text{eff}}_{\downarrow}\left(E+\frac{JS}{2}\right)=\frac{1}{N}\sum_{\mathbf{q}}\left[\left(E+\frac{JS}{2}\right)\widehat{I}-\widehat{\epsilon}(\mathbf{k\text{-}q})\right]^{-1}$$

which upon substituting in the matrix form of the spin-flip equation of motion and performing $\mathbf{q}$ summation on both sides implies,

$$\frac{1}{\sqrt{N}}\sum_{\mathbf{q}}\widehat{F}_{\mathbf{k},\mathbf{k\text{-}q},\mathbf{q}\downarrow}(E)=-JS\widehat{G}^{\text{eff}}_{\downarrow}\left(E+\frac{JS}{2}\right)\left[\widehat{I}-\frac{J}{2}\widehat{G}^{\text{eff}}_{\downarrow}\left(E+\frac{JS}{2}\right)\right]^{-1}\widehat{G}_{\mathbf{k}\downarrow}(E) \tag{2.35}$$

Now if we consider the Fourier transform of Eq. (2.22) and substitute Eq. (2.35) and Eq. (2.28) in it , we get the result for the Green function as

$$\left[\left(E-\frac{JS}{2}\right)\widehat{I}-\widehat{\epsilon}(\mathbf{k})\right]\widehat{G}_{\mathbf{k}\downarrow}(E)=\widehat{I}$$
$$+\frac{J^2S}{2}\widehat{G}^{\text{eff}}_{\downarrow}\left(E+\frac{JS}{2}\right)\left[\widehat{I}-\frac{J}{2}\widehat{G}^{\text{eff}}_{\downarrow}\left(E+\frac{JS}{2}\right)\right]^{-1}\widehat{G}_{\mathbf{k}\downarrow}(E)$$

i.e.

$$\widehat{G}_{\mathbf{k}\downarrow}(E)=$$
$$\left[(E+i0^{+})\widehat{I}-\widehat{\epsilon}(\mathbf{k})-\frac{JS}{2}\widehat{I}-\frac{J^2S}{2}\widehat{G}^{\text{eff}}_{\downarrow}\left(E+\frac{JS}{2}\right)\left[\widehat{I}-\frac{J}{2}\widehat{G}^{\text{eff}}_{\downarrow}\left(E+\frac{JS}{2}\right)\right]^{-1}\right]^{-1}$$

If we compare Eq. (2.24) with the above equation, we get the self-energy ansatz as

$$\widehat{\Sigma}_{\downarrow}(E)=\frac{JS}{2}\widehat{I}+\frac{J^2S}{2}\widehat{G}^{\text{eff}}_{\downarrow}\left(E+\frac{JS}{2}\right)\left[\widehat{I}-\frac{J}{2}\widehat{G}^{\text{eff}}_{\downarrow}\left(E+\frac{JS}{2}\right)\right]^{-1} \tag{2.36}$$

As seen, Eq. (2.36) and Eq. (2.30) give the spin- dependent form of the self-energy which for the case of fully empty bands and ferromagnetically saturated spin sub- system can be written down as follows;

$$\widehat{\Sigma}_{\sigma}(E)=-\frac{JSz_{\sigma}}{2}\widehat{I}-\frac{J^2S(z_{\sigma}-1)}{4}\widehat{G}^{\text{eff}}_{\sigma}\left(E-\frac{JSz_{\sigma}}{2}\right)\left[\widehat{I}-\frac{J}{2}\widehat{G}^{\text{eff}}_{\sigma}\left(E-\frac{JSz_{\sigma}}{2}\right)\right]^{-1} \tag{2.37}$$

On comparing Eq. (2.15) and Eq. (2.37), we obtain the temperature dependent[7] multi- band self- energy ansatz as

$$\widehat{\Sigma}_\sigma(E) = -\frac{J}{2}M_\sigma\widehat{I} + \frac{J^2}{4}a_\sigma\widehat{G}_\sigma\left(E - \frac{J}{2}M_\sigma\right)\left[\widehat{I} - \frac{J}{2}\widehat{G}_\sigma\left(E - \frac{J}{2}M_\sigma\right)\right]^{-1} \quad (2.38)$$

where

$$M_\sigma = z_\sigma\langle S^z\rangle;\;\; a_\sigma = S(S+1) - M_\sigma(M_\sigma+1). \quad (2.39)$$

and the bare Green function matrix is defined as :

$$\widehat{G}_\sigma(E) = \frac{1}{N}\sum_{\mathbf{k}}\left[(E+i0^+)\widehat{I} - \widehat{\epsilon}(\mathbf{k})\right]^{-1} \quad (2.40)$$

Such an analysis was also carried out for the case of two fully occupied bands and similar structure of multi-band self- energy ansatz was obtained in that situation [44].

Now we consider two weakly hybridized empty bands on a simple cubic (sc)

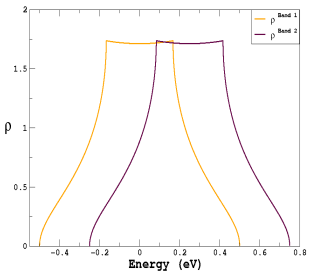

Figure 2.3: The density of states of a sc lattice for a two band model. The separation between the center of gravities of both the bands is 0.25 eV while each has a bandwidth of 1.0 eV

lattice where the terms in the (2 x 2) hopping matrix, $\widehat{\epsilon}(\mathbf{k}) = \begin{bmatrix} \epsilon^1(\mathbf{k}) & \epsilon^3(\mathbf{k}) \\ \epsilon^3(\mathbf{k}) & \epsilon^2(\mathbf{k}) \end{bmatrix}$ are $\epsilon^1(\mathbf{k}) = E_0^1 - \frac{W^1}{6}(cos(k_x a) + cos(k_y a) + cos(k_z a))$, $\epsilon^3(\mathbf{k}) = \mathrm{V}$ and $\epsilon^2(\mathbf{k}) = E_0^2 - \frac{W^2}{6}(cos(k_x a) + cos(k_y a) + cos(k_z a))$. We assume the bandwidth (W) of both the bands $W^1 = W^2$, i.e. intra- band transfer energy to be 1.0 eV. The center of gravity of one of the free Bloch band E_0^1 is chosen to be energy zero while for the other, E_0^2, it is taken as 0.25 eV as shown in above Figure 2.3. The inter- band transfer (hybridization) term, V, is assumed to be dispersionless parameter while one can also consider it having a finite dispersion.

Using the above hopping matrix as an input in Eq. (2.40), we calculate the multi- band self- energy (2.38) and thereby each element of the single particle Green function matrix as given in Eq. (2.24) which enables us to calculate the total density of states according to Eq. (2.27) for different values of hybridization V and exchange coupling strength, J but for a fixed spin, S. We are interested in studying the interplay of hybridization, exchange coupling and temperature which are our basic model parameters.

Figure 2.4 shows the result for the weak coupling behavior, J=0.1 and for hybridization, V=0.0, 0.1 and 0.2. Though the V=0.0 and 0.1 spectrum for both the spins are nearly indistinguishable, apart from certain distinct features, but even in the weak coupling regime it is seen that V=0.2 produces

[7] which arises due to temperature- dependent magnetization, $\langle S^z\rangle$.

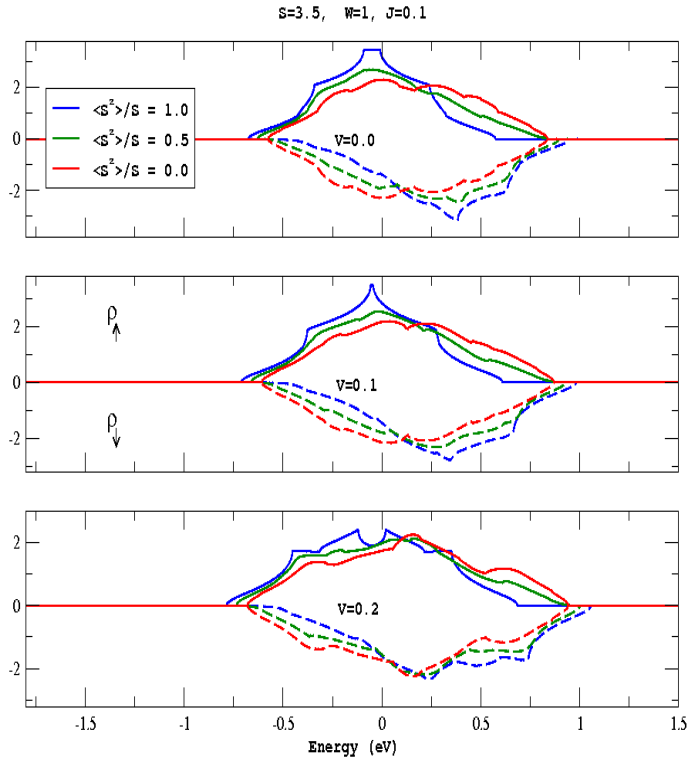

Figure 2.4: Temperature dependent quasi- particle density of states of two band KLM for a sc lattice with different values of hybridization: V=0.0, 0.1 and 0.2 eV. The bandwidth of each band is taken to be 1.0 eV, spin S=3.5 and weak exchange coupling, J=0.1 eV

a drastic change in the density of states which is responsible for changes in the electronic properties of the system. It is observed that at T=0 K upon increasing the strength of hybridization, the energy bandwidth for both the spins gets widened as the bands starts merging with each other.

If we move to intermediate and strong coupling regime, as shown in Figure 2.5 and Figure 2.6 respectively, the 'scattering states' start becoming very distinct at T=0 K for spin-$\downarrow$ and are absent for spin- $\uparrow$ while the physical reason remains the same as explained earlier. And for higher temperatures, strong correlation effects are clearly visible and the scattering states begin to appear also in the spin- $\uparrow$ spectrum which is eventually a signature of spin-flip transitions. As it was observed in Figure 2.2 that at the paramagnetic temperature the effect of increasing J was to obtain two separate peak structures (spectral weight distribution) but in two band situation this effect is caused due to an additional increase in the strength of hybridization. This suggests that at the limit of strong hybridization and exchange coupling, the multi-band model is a straight forward extension of the single band case and that strong hybridization brings about localization. This point will be further discusssed in chapter 4 where the effect of electron concentration on the Curie temperature is studied. Another interesting aspect could be the variation of bandwidth (i.e. change in kinetic energy) in order to study the competition

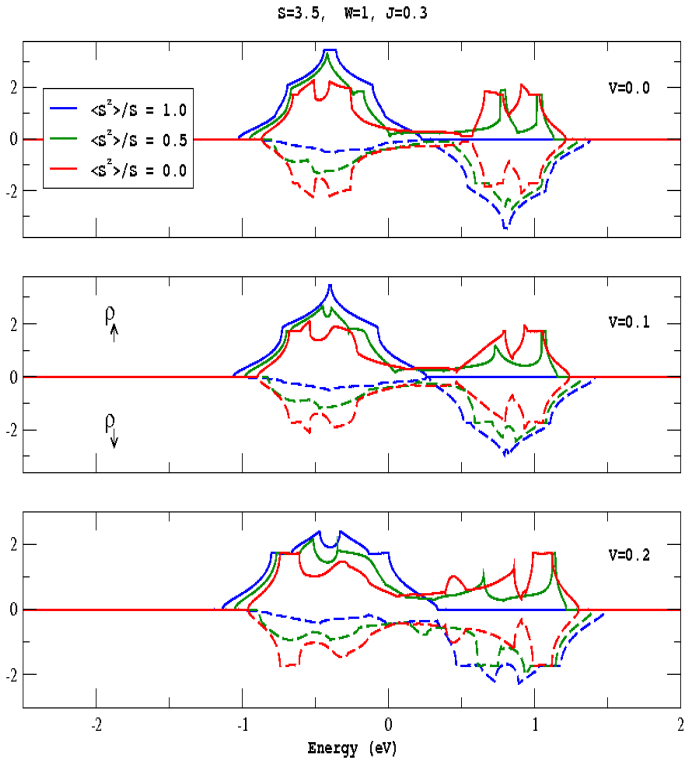

Figure 2.5: The same as in Figure 2.4 but for intermediate exchange coupling, J=0.3 eV

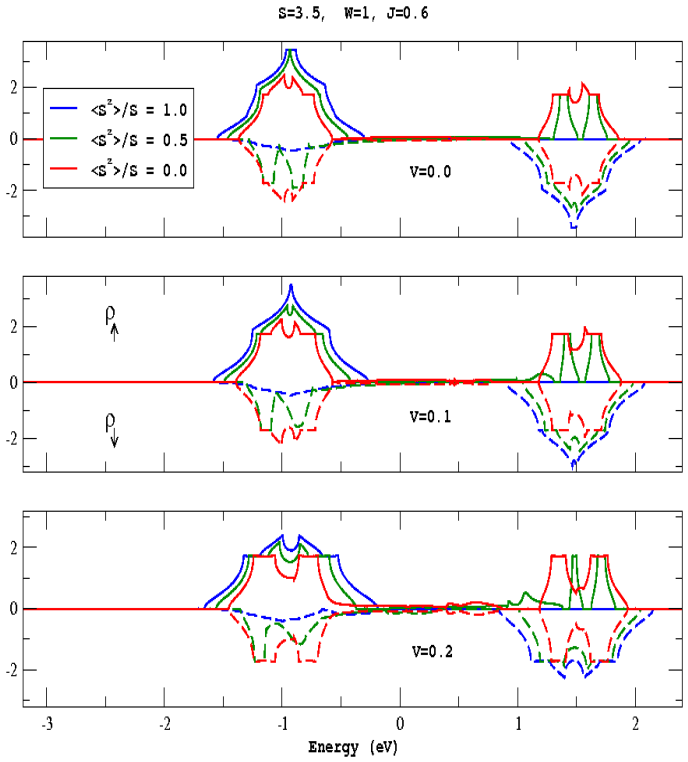

Figure 2.6: The same as in Figure 2.4 but for strong exchange coupling, J=0.6 eV

between the kinetic and exchange potential energy for different hybridization strength. A similar analysis for single and multi- band KLM can be carried out for a face centered cubic (fcc) lattice.

In the next chapter, we briefly discuss how we obtain ground state single particle energies of real materials within density functional theory and then how we combine it with the theory developed in this chapter to study the temperature dependent electronic correlation effects in those substances.

Chapter 3

Electronic structure of real materials

"Dr. Linus Pauling is the man for me.
He makes violent changes in my chemistry.
Oh, fie, when he rolls his eyes
All my atoms ionize."

- Song from "The Road to Stockholm." 1954.

One of the central issues of basic and applied physics is to understand the relation between the electronic structure or composition of a given material and its different electronic, transport and magnetic properties. The methods that are applied may be either experimental or theoretical, but ultimately only through a combination of both these approaches one can achieve a detail understanding of such a relationship. In experimental situation the specific class of materials are studied within precise measurements of their various physical properties while the same is calculated in theory based on model Hamiltonian by making use of the parameters which are in close proximity to the experimental ones.

The advantage of such theoretical studies as compared to the experimental ones is that the systems are well defined. Therefore, the results are not doubtful because of unwanted effects like impurities, inhomogeneities, etc. Furthermore, in certain cases the theoretical studies provide much more information beyond the reach of experiments. On the other hand, the biggest drawback is that in almost all cases one has to study idealized systems which has less relation with reality. Since in some cases the above mentioned unwanted effects are very much desirable but due to their complexity it is quite difficult to treat them theoretically. Therefore, an interconnection between experiments and theory is quite important to get a thorough understanding of the new or existing materials.

In the field of applied solid state theory, out of the various physical properties the calculation of quasi- particle bandstructure of bulk, thin films and surfaces of real substances have always been of great interest since they can be directly compared with experimental studies (for details refer to Appendix D)

and can provide a lot of physical insight into the underlying basic mechanism concerning electronic correlation. But for the derivation of the electronic structure one must have already an idea of a relative arrangement of energy levels.

In the case of relatively ionic compounds e.g., members of rare earth chalcogenides and pnictides like Europium Sulphide (EuS) or Gadolinium Nitride (GdN), a treatment using atomic energy level diagram is more adequate than derivations using the plane waves since one of the decisive factor in such rare earth compounds is the position of the localized $4f^7$ states. Also in these materials, one may take advantage of tight binding scheme assuming complete charge transfer between cation and anion.

Generally in an energy level diagram one always displays energy states in a (N-1) configuration plus an electron for a system of N electrons. It means that the energy difference which one reads in the diagram represents the energy which one has to supply to the system in order to make this transition. And in case of above materials, it means that such excitations can go from occupied anion valence p- bands to cation $5d$- or $6s$- bands or from $4f^7$ states to the $5d$-$6s$ conduction bands. An energy level diagram based on such considerations have been proposed for the Eu chalcogenides by Wachter [45], Kasuya [46] and Kaldis and Wachter [47] making use of the thermochemical Haber- Born process.

Figure 3.1 shows the energy level scheme for EuS and GdN using the

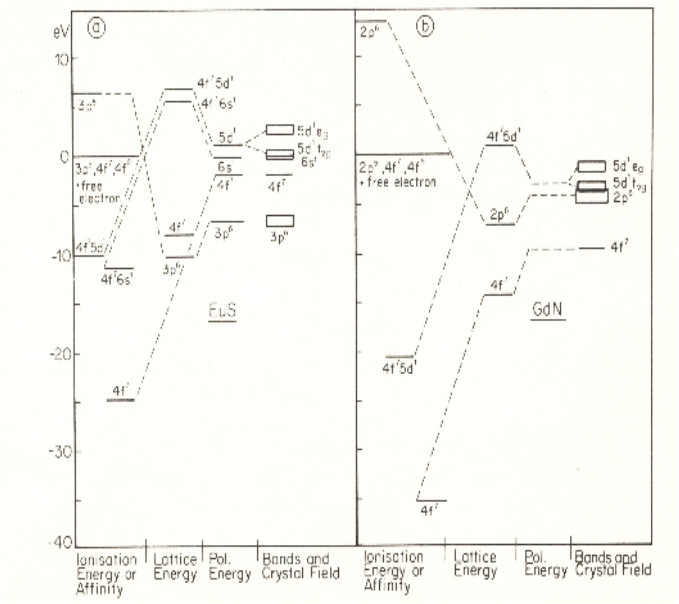

Figure 3.1: Energy level diagram for (a) EuS and (b) GdN as obtained from Refs. [47, 48].

above process and as given in Refs. [47, 48]. According to those authors, "*on comparing the energy level diagrams of EuS and GdN one realizes some important differences. The $4f^7$ level in EuS is about 1-2 eV below the 5d band and above the valence p band. Between the p and d bands there is an energy gap of several eV. In GdN, the $4f^7$ level is about 7 eV below the 5d band and also*

appreciably below the valence p band. Between the p and the 5d bands there is hardly an energy gap and overlap at certain points in the Brillouin zone can be expected."

Keeping this relative energy level scheme in mind we proceed further to calculate the ground state energies of EuS and GdN using available experimental input parameters namely the symmetry of the crystal, lattice constant, positions of the atoms, etc ... and thereby combine it with the many body theory in order to determine some of their temperature dependent physical properties.

3.1 Theoretical techniques

In chapter 2, for the non- interacting kinetic part of our model Hamiltonian, we used a particular form of dispersion within the tight- binding Bloch representation for the case of a single and also two non- degenerate bands. But while calculating the properties of real substances one normally deals with a multi- band system for instance, the six $3p$ valence bands of EuS or ten $5d$ conduction bands of GdN. In such a situation, the ground state kinetic energies are the eigenenergies acquired using the ground state wavefunctions which are obtained exactly from the determinant of the single particle bands. Thus, even to calculate the ground state kinetic energies is a great computational effort.

A considerable amount of obstacle is removed using the formulation of density functional theory (DFT). It is a method to solve the quantum many body problem in order to get the ground state kinetic energies. The main objective of density functional theory is to replace the many body electronic wavefunction with the electronic density as the basic quantity. Although its history goes back to the early 1930s [49], but it has been formally established in 1964 by two theorems due to Hohenberg and Kohn [50] as stated in the Appendix C. Later on, the work by Kohn- Sham [51] opened the gates for its practical application. Their approach was to reduce the many body problem of interacting electrons in a static potential into a fictitious non- interacting system. Thus enabling the non- interacting electrons to move in an effective potential which included the external potential and the effects of the Coulomb interactions between the electrons, e.g. the exchange and correlation interactions. Modeling the latter two interactions becomes the difficulty within Kohn- Sham DFT. The simplest approximation is the local density approximation (LDA) which has been successfully applied to various real systems so as to study their ground state properties.

The next step would be to combine such ground state energies along with many body perturbative or non- perturbative approaches in order to include the correlation which the above mentioned approximate scheme has neglected. Though there are a lot of extensions to the LDA within the DFT like LDA+U (where U is the Coulomb interaction), Generalized Gradient Approximation (GGA), Self- Interaction Correction (SIC) but on the other hand, there have also been proposals to use the simple LDA input into those existing many body theories. In the following we mention some of the paths which have been

taken along this direction:

- LDA+DMFT : In this approach, the band structure input due to LDA and inclusion of the electronic correlation by dynamical mean field theory (DMFT) are solved within a self- consistent scheme to yield the ground state density [52, 53]. In general, the DMFT solution results in a change of the occupation of the different bands involved. This changes the electron density and thus results in a new LDA Hamiltonian since it depends on density. At the same time there is also a change in the Coulomb interaction U since its calculation depends on the second derivative of the LDA ground state energy w.r.t density [52] and thus, U needs to be determined by a new constraint LDA calculation. In a self- consistent LDA+DMFT scheme, the LDA Hamiltonian and U would define a new Hamiltonian which again needs to be solved within DMFT until convergence is reached.

- LDA+GW : The GW approximation (G is the Green function and W is the screened Coulomb interaction) was proposed by Hedin [54] in 1965 (infact earlier than LDA as proposed by Kohn- Sham [51]). But a big step forward was put by Hybersten and Louie [55] when they employed the LDA eigenfunctions to generate the GW self- energy, $\Sigma = iGW$ and showed that fundamental gaps were considerably improved over the LDA. Since then a lot of review on GW theory [56, 57] and extensions [58] to it (quasi- particle self- consistent GW theory) have been proposed.

- LDA+MCDA : Within the method of Green function theory, the elements of electronic self- energy are explicitly calculated by using self-consistent self- energy approach and a moment conserving technique for all higher order Green functions which appear in the equations of motion of lowest order Green function. Using this self- energy along with the ground state energies due to LDA as an input, one obtains the required physical properties [59]. The drawback of this method is in the way that it deals with the decomposition of the multi- band system into single non-degenerate subbands. Though we employ a similar idea of combining the LDA output along with multi- band self- energy but our approach differs in the following two aspects. First of all, we make the direct use of the ground state energies in the matrix form while retaining the multi- band character of the system. The numerical details are explained in the next section. Secondly we have another formulation of the self- energy i.e. ISA as described in the previous chapter and this results in some marked differences between the two approaches as will be discussed in section 3.3.

3.2 Computational details

The ground state calculations are performed using the freely available *The Stuttgart TB- LMTO code* [60]. For the introduction to the tight binding linear muffin- tin atomic sphere approximation (TB- LMTO- ASA) method please refer to Refs. [61, 62, 63]. In this section, we will discuss in a very brief manner the numerical details concerning *TB- LMTO* program for GdN while the details of the codes can be found in Ref. [60].

Figure 3.2 is an example of the so- called control "CTRL" file for GdN as

```
HEADER    GdN, cubic face-centred
VERS      TB+U: v47
IO        VERBOS=97 HELP=f WKP=f IACTIV=f ERRTOL=2 OUTPUT=LM ERR=*
SYMGRP    NGEN=3 GENGRP=I R4X R3D
          SPCGRP=Fm-3m USESYM=f
STRUC     ALAT=9.447
          PLAT=0.0 0.5 0.5
               0.5 0.0 0.5
               0.5 0.5 0.0 FIXLAT=t
DIM       NBAS=2 NCLASS=2 NL=4 LDIM=5 IDIM=17 NSYMOP=48 NKP=11921
OPTIONS   NSPIN=2 REL=t CCOR=t NONLOC=f NRXC=1 NRMIX=2 CORDRD=f
          NITATOM=30 CHARGE=f FATBAND=f AFM=f SEWALD=f FS=f
          CARTESIAN=t WRIBAS=f Q=----- COHP=f RMES=f GAMMA=f
CLASS     ATOM=N   Z= 7 R=2.2450172 LMX=2 CONF=3 2 3 4 IDXDN=2 3 2
                 IDMOD=0 0 0
          ATOM=Gd Z=64 R=3.2342428 LMX=3 CONF=6 6 5 5 IDXDN=2 2 1 2
                 IDMOD=0 0 0 0
SITE      ATOM=N  POS=0.5 0.5 0.5
          ATOM=Gd POS=0.0 0.0 0.0
SCALE     SCLWSR=t OMMAX1=.16 .18 .20 OMMAX2=.40 .45 .50
STR       KAPPA2=0 RMAXS=3.2 NDIMIN=350 NOCALC=f IALPHA=0
          DOWATS=f DELTR=.1 LMAXW=8
          ATOM=N  SIGMA=.7 .7 .7
          ATOM=Gd SIGMA=.7 .7 .7 .7
START     NIT=1 BROY=f WC=-1 NMIX=1 BETA=0
          FREE=f CNVG=.000001 CNVGET=.000001 BEGMOM=t CNTROL=t
          EFERMI=.37698099 VMTZ=-.64448967
          ATOM=N  P=3.02044605 2.80604234 3.18968171
                    3.02609327 2.82799692 3.19242029
                  Q=0.00435169 0.00000000 0.00001181
                    1.60760998 -.01853517 0.00602617
                    0.00430559 0.00000000 0.00000830
                    0.00581734 0.00000000 0.00001897
                    1.93054119 -.02264598 0.00670944
                    0.00559334 0.00000000 0.00001279
              enu   =-0.24185010 -0.22487231 -0.21270059
                     -0.23434834 -0.21358156 -0.19485466
              c     =-1.58903407 -0.12316631  3.09609236
                     -1.70548717 -0.15814235  3.06680642
              sqrdel=-0.47049115  0.18819461  0.24857584
                     -0.49728027  0.18623552  0.24757771
              p     = 0.33374455  0.22745912  0.00757567
                      0.33723987  0.24324801  0.00774793
              gamma = 0.19561399  0.02673265  0.01557437
                      0.18590340  0.02554446  0.01551353
          ATOM=Gd P=6.47896925 6.19230534 5.39456396 4.17470615
                    6.44557504 6.17319595 5.36656548 4.14161447
                  Q=0.14094663 0.00000000 0.00022572
                    0.21346514 0.00000000 0.00037424
                    0.54132749 0.01182508 0.00303046
                    0.48799348 0.00000000 0.00103620
                    0.14433048 0.00000000 0.00027714
                    0.23382540 0.00000000 0.00049884
                    0.53650938 0.01025307 0.00403764
                    0.14338288 0.00000000 0.00043840
              enu   =-0.30650757 -0.20795070 -0.23406733 -0.21781416
                     -0.30055662 -0.19396781 -0.22551107 -0.19823777
              c     = 0.07042932  1.35846167  0.35403064 -0.09499602
                      0.12525847  1.66630658  0.43678432  0.76055940
              sqrdel=-0.41564265  0.54772323  0.29270383  0.05937374
                     -0.41963295  0.63540806  0.30688455  0.21873614
              p     = 0.04036786  0.16305145  0.18724677 10.12319520
                      0.03938455  0.24693723  0.15611168  0.80882526
              gamma = 0.49258433  0.22068154  0.06455243 -0.00582072
```

Figure 3.2: CTRL file for GdN obtained after convergence of the program.

obtained after convergence. The basic idea is to execute the main program file called "lm.run" which uses the data from an initial "INIT" file containing the input parameters like the spacegroup symmetry, lattice constant and position

of atoms. For GdN, these data are in the form of highlighted text in Figure 3.2. The leftmost column exhibits the names of the subprograms (sections) whose internal files are edited as per the requirements. The numbers against the text (both in blue) are the final values of the corresponding parameters used to obtain the converged results.

The standard protocol is to execute the files in the following sequence: lminit.run, lmhart.run, lmovl.run, change (VER=50) in the CTRL, lm.run, change (CONF, IDXDN values, VER=40, BROY=f, NSPIN=2 for spin polarized calculations) in the CTRL, REL=f, NKABC=80 80 80 (number of divisions along each **k** direction), lmprep.run, lm.run, lmstr.run, change VER=97, lmprep.run and finally lm.run to obtain converged results. Though details for each of the nomenclatures can be found in Ref. [60] but in the following we mention a few important ones.

The CONF for an atom (in the CLASS section) signifies the valence orbitals. In GdN, CONF=6 6 5 5 for Gd atom means $6s$, $6p$, $5d$ and $5f$ orbitals and all lower orbitals are part of core. This suggests that in order to circumvent the typical difficulties arising in LDA due to the strongly localized character of the $4f$ electrons in europium and gadolinium compounds, we consider them as core electrons. The motivation to do so is because our main interest is focused on the reaction of the empty conduction or full valence bands on the magnetic state of the localized moments. For our purpose the half- filled $4f$ level appear only as localized spins which can be described within an effective Heisenberg model. In case of EuS too, we treat the $4f$ electrons as core. The IDXDN for an atom (in the CLASS section) takes on the values from 0 to 3 where for the corresponding orbitals 1 : means it fully mixes with other electrons, 2 : means it only mixes with electrons of certain energies, 3 : means no mixing at all and 0 : means program decides how to mix them. With this knowledge, one can proceed further to calculate the electronic bandstructure and density of states for both the compounds. Though in case of EuS, we could obtain the complete scenario i.e. correct placement of both the conduction and valence bands but for GdN we encountered some numerical difficulties in getting the correct behaviour of the valence bands. The concerned problems and their solution (converged result as in Figure 3.2) are as explained below.

It has been known from the litterature that GdN show an intricate conducting character. Despite several theoretical and experimental efforts[8] since last decade or so it is still not clear whether its electronic ground state is half-metallic or semiconducting.

On theoretical side based on bandstructure calculations, there have been two long standing problems which have hindered the progress. One of them being the usual band gap problem while the other being the placement and treatment of the strongly localized half- filled $4f$ states. Using different computational methods in order to deal with problems in hand, GdN is predicted to be a semiconductor [64, 65, 66], half- metal [67, 68, 69] or a semiconductor in the paramagnetic and a semimetal in the ferromagnetic case using quasi-particle self energy corrections [70]. In the latter, it is assumed that the $4f$

[8]For details please refer to subsection 3.3.2.

level is a part of core states.

We also performed the ground state spin- polarized electronic bandstructure

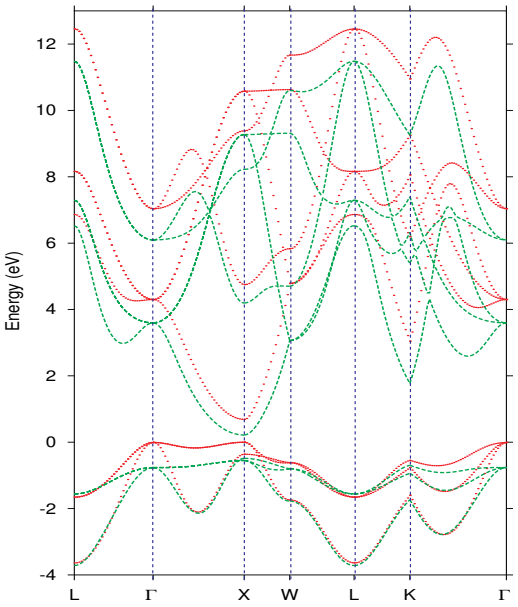

Figure 3.3: Spin- dependent (broken green lines up- spin, dotted red lines down- spin) bandstructure of Gd $5d$ conduction bands of bulk GdN calculated for equilibrium lattice constant a=4.99 Å. The $4f$ levels which are treated as core states are not shown while energy zero conincides with the Fermi energy.

calculation of bulk GdN with the result as shown in Figure 3.3. It is obtained from the *TB- LMTO* program for equilibrium lattice constant of a=4.99 Å. The broken green lines is for up- spin while dotted red line shows the down-spin part.

According to the recent photoemission spectrum [71] the occupied $4f$ level lie within the N $2p$ bands. Though this information was used by other groups [65, 66] in order to fix the $4f$ level but unfortunately we could not get converged results in our calculations and so had to treat them as core states. But the problem in this case is that the $4f$ level just act as a spin dependent exchange correlation potential and thus do not actually interact explicitly with the N $2p$ states while one of the important consequence of this interaction results in the spin reversal of the valence bands as compared to the conduction bands which can be understood as follows. The majority spin f bands (say up- spin) push up the N p like valence bands of the same spin because they lie above them while the minority f spin bands (down- spin) push the N p down- spin further down. The net magnetic moment on N p (which is small) turns out to be opposite to the Gd f moment whereas the Gd d moment is in the same direction as the Gd f. In case of N p bands, this results directly from the hopping integrals between nearest neighbour sites but for Gd d since on a given atomic site the d and f orbitals are orthogonal, in principle they do not interact and so the exchange correlation potential set up by the f electrons in this case results in a shift of d electrons of the same spin in the same direction as also correctly

obtained in our calculations.

In this thesis, apart from the treating the $4f$ level as core we also do not

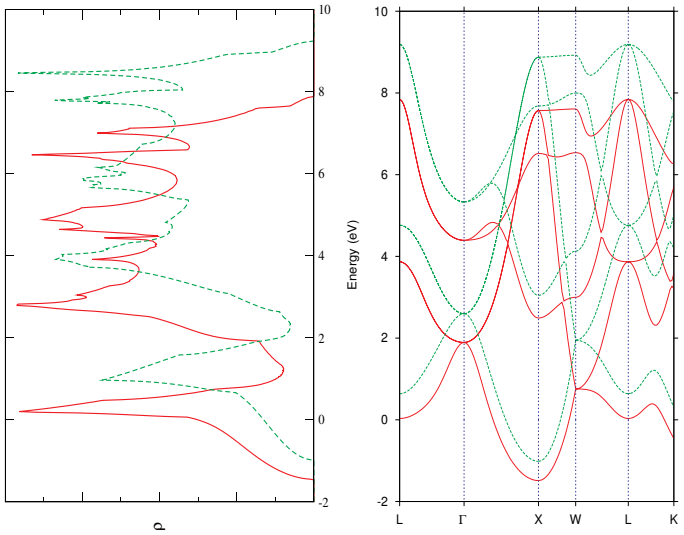

Figure 3.4: Density of states (left panel) and bandstructure (right panel) of Gd $5d$ conduction bands of bulk GdN. Full red lines are up- spin and broken green ones are down- spin.

address the band gap problem (especially for GdN) as far as the ground state energy calculations are concerned. Moreover, since we are mainly concerned in overall temperature dependent electronic correlation effects, the extreme details of the bandstructure are surely not so important and so, we just consider the empty Gd $5d$ conduction bands (ignoring the valence bands) as shown in Figure 3.4. The Fermi energy is fixed at -2.0 eV (with a band gap of 0.3 eV as predicted by Lambrecht [65]) thus assuming the ground state of bulk GdN to be semiconducting.

Figure 3.5 shows the orbital l- projected conduction band density of states of bulk GdN. Though the major contribution stems from the Gd $5d$ bands but its hybridization with other orbitals is equally seen. This suggests that the single particle output contains this mixing and can not be separated out. Actually, the single particle output is in the form of $\mathbf{k}$- resolved Hamiltonian and overlap matrices posing a generalized eigenvalue problem to be solved. One can factorize the original $\mathbf{k}$- resolved Hamiltonian matrices so as to obtain new Hamiltonian matrices via the overlap matrices which can be used directly as hopping integrals, $\widehat{\epsilon}(\mathbf{k})$ as explained below.

The Schrödinger equation for the band structure problem reads,

$$\sum_{\nu} \left(H^{\mu\nu}_{\mathbf{k}} - E_{\mathbf{k}} O^{\mu\nu}_{\mathbf{k}} \right) u_{\nu}(\mathbf{k}) = 0 \tag{3.1}$$

where μ,ν are the band indices and $u_{\nu}(\mathbf{k})$ being the eigenfunctions to the eigenvalue $E_{\mathbf{k}}$. They are related to the Bloch functions $\phi_{\nu}(\mathbf{k})$ via coefficients $c_{\mu\nu}(\mathbf{k})$,

$$u_{\nu}(\mathbf{k}) = \sum_{\mu} c_{\mu\nu}(\mathbf{k}) \phi_{\mu}(\mathbf{k}) \tag{3.2}$$

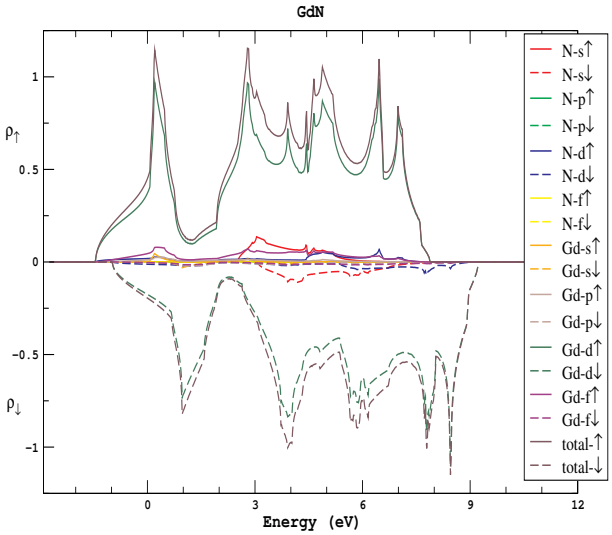

Figure 3.5: The orbital l- projected conduction band density of states of bulk GdN.

where

$$\phi_\mu(\mathbf{k}) = \frac{1}{\sqrt{N}} \sum_{\mathbf{R}} e^{i\mathbf{k}\cdot\mathbf{R}} \phi_\mu(\mathbf{r} - \mathbf{R}) \tag{3.3}$$

and $\phi_\mu(\mathbf{r} - \mathbf{R})$ are the muffin- tin orbitals of the atom at position $\mathbf{R}$. The $H_{\mathbf{k}}^{\mu\nu}$ represents the matrix elements of the Hamiltonian operator, H with respect to the basis functions $\phi_\nu(\mathbf{k})$,

$$H_{\mathbf{k}}^{\mu\nu} = \langle \phi_\mu(\mathbf{k}) | \mathrm{H} | \phi_\nu(\mathbf{k}) \rangle \tag{3.4}$$

and the overlap matrix $O_{\mathbf{k}}^{\mu\nu}$ is given as,

$$O_{\mathbf{k}}^{\mu\nu} = \langle \phi_\mu(\mathbf{k}) | \phi_\nu(\mathbf{k}) \rangle \tag{3.5}$$

In order to use such matrices as an input for the many body calculations, one can perform a Cholesky decomposition so as to reduce the generalized problem to an eigenvalue problem with,

$$O_{\mathbf{k}}^{\mu\nu} = \sum_{\gamma} L_{\mathbf{k}}^{\mu\gamma} \left(L_{\mathbf{k}}^{\dagger} \right)^{\gamma\nu} \tag{3.6}$$

and which upon subsituting in Eq. (3.1) transforms it to new Hamiltonian matrices with respect to an orthogonal set of basis function,

$$\sum_{\nu} \left[\left(H_{\mathbf{k}}^{'} \right)^{\mu\nu} - E_{\mathbf{k}} \right] u_\nu^{'}(\mathbf{k}) = 0 \tag{3.7}$$

where,

$$\left(H_{\mathbf{k}}^{'} \right)^{\mu\nu} = \sum_{\gamma} \left(L_{\mathbf{k}}^{\mu\gamma} \right)^{-1} H_{\mathbf{k}}^{\mu\nu} \left(\left(L_{\mathbf{k}}^{\dagger} \right)^{\gamma\nu} \right)^{-1} \tag{3.8}$$

and

$$u'_{\nu}(\mathbf{k}) = \sum_{\gamma} \left(L^{\dagger}_{\mathbf{k}}\right)^{\gamma\nu} u_{\nu}(\mathbf{k}) \tag{3.9}$$

And as a result, we can directly use the **k**- resolved new Hamiltonian matrices, $\left(H'_{\mathbf{k}}\right)^{\mu\nu}$, as the required hopping integrals $\widehat{\epsilon}(\mathbf{k})$. We note that the advantage of the such factorization and direct use of Hamiltonian matrices is that it circumvents the problem of the somewhat ambiguous decomposition of the conduction band [25, 72, 73] into single non- degenerate subbands. Finally, we compute the single particle Green function to calculate the spectral densities and densities of states of the real substances as discussed in the next section.

3.3 Bandstructure and Density of States

The rare earth monopnictides and monochalcogenides form a very facinating group of materials. They show a rich variety of anomalous physical properties attracting a considerable attention for basic and applied research. Among the rare earth alloys, the isomorphic compounds like $Gd^{3+}X_p^{3-}$, where X_p = N,P,As,Sb,Bi and $Eu^{2+}X_c^{2-}$, where X_c = O,S,Se,Te can be compared since they are isoelectronic in nature. If pure ionic bonding is considered then they are expected to be insulators or semiconductors. The divalent rare earth monochalcogenides are indeed insulators or semiconductors [74, 75] but the trivalent rare earth monopnictides, especially the rare earth nitride GdN, exhibit a complex conducting behavior. But these materials are particularly interesting since they combine a number of features of ideal ferromagnet, such as simple cyrstal structure (NaCl) and localized, spin- only moment for the magnetic ions.

3.3.1 EuS : Europium Sulphide

The rare earth chalcogenide, EuS, was under a lot of experimental and theoretical investigation regarding its magnetic and electronic properties, starting from early 1960s which reported nuclear magnetic resonance [76] till the latest being on spin- polarization in EuS [77] while the list remains extensive.

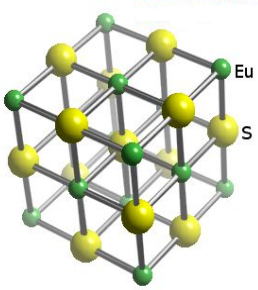

Figure 3.6: The crystal structure of EuS. The small green spheres are Eu atoms while big yellow ones are S atoms.

EuS crystallizes in a rocksalt structure as shown in Figure 3.6 with lattice constant, a=5.95 Å. Each Eu^{2+} ion has twelve nearest and six next nearest

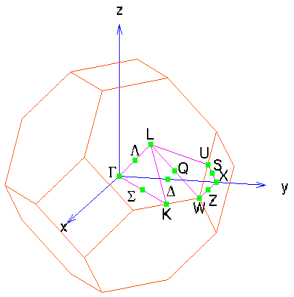

Figure 3.7: Some important symmetry points on the first Brillouin zone of a fcc crystal.

Eu- neighbors and they occupy lattice sites of a fcc structure whose first Brillouin zone is as given in Figure 3.7.

The magnetism in EuS is due to the half- filled $4f$ shell of Eu^{2+} and its magnetic properties are well described using the Heisenberg model with the ferromagnetic transition temperature, T_c=16.54 K. In this material, the nearest neighbor exchange interaction is ferromagnetic while the next nearest neighbor is anti- ferromagnetic. But throughout this section, the magnetization will be treated as an external parameter.

In order to have the single particle excitation energies, i.e. the hopping matrices, for EuS we perform the bandstructure calculations using the *TB-LMTO* program [60] as described in the previous section 3.2.

Figure 3.8 describes spin- polarized bandstructure of bulk EuS calculated

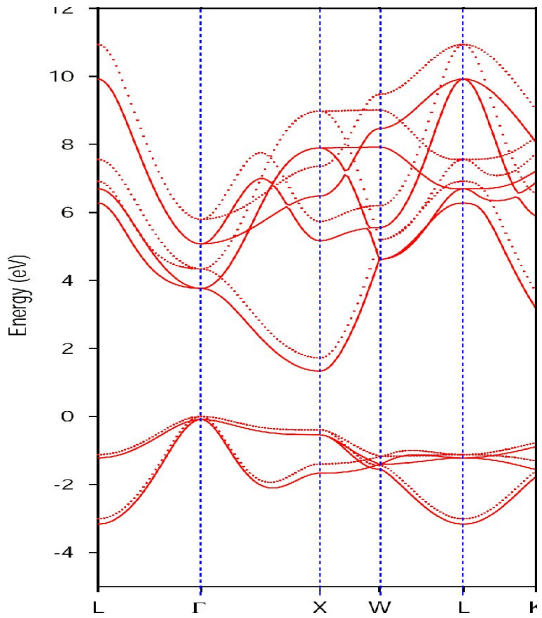

Figure 3.8: Spin- dependent (full lines up- spin, dotted lines down- spin) bandstructure of bulk EuS calculated for equilibrium lattice constant a=5.95 Å. The $4f$ levels which are treated as core states are not shown while energy zero conincides with the Fermi energy.

for equilibrium lattice constant a=5.95 Å. In order to study the temperature dependent correlation effects in EuS, we will first consider only the fully occupied valence bands since until now it has not been studied. Lateron we

proceed further by also considering its empty conduction bands and compare the results with other theoretical methods. Finally, on combining the conduction and valence bands we obtain the temperature dependent quasi- particle bandstructure of bulk EuS.

Figure 3.9 shows the spin- dependent bandstructure (LSDA) of the $3p$

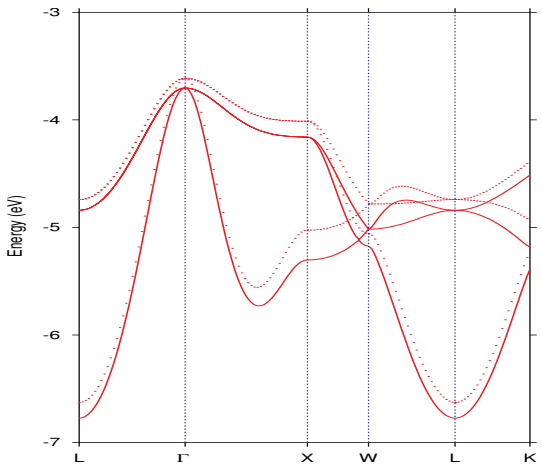

Figure 3.9: LDA bandstructure of $3p$ valence bands of EuS. Full lines are up-spin and dotted ones are down- spin.

valence bands of EuS with full lines representing the spin ↑ and dotted ones the spin ↓ part. The total bandwidth of around 3.0 eV is in good agreemeent with the energy distribution curves (EDCs) as reported for the paramagnetic EuS [78], which is the only reported experiment on the valence bands of EuS.

These $3p$ bands also contain the contribution from other orbitals which is

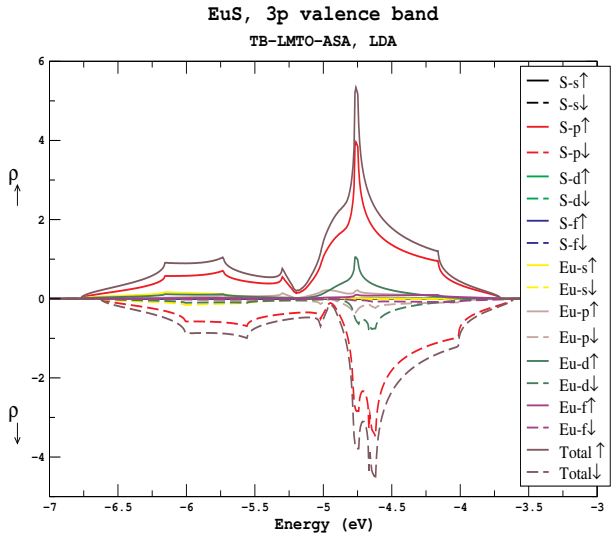

Figure 3.10: The orbital l- projected valence band density of states of EuS.

shown in Figure 3.10 in the form of orbital l- projected valence band density of states of bulk EuS. One can see the hybridization effects due to other orbitals though the major contribution arises from the S $3p$ bands. Thus as an output

from LDA calculations we take on the full Hamiltonian matrix.

In Figure 3.11, we consider the total density of states (as obtained from

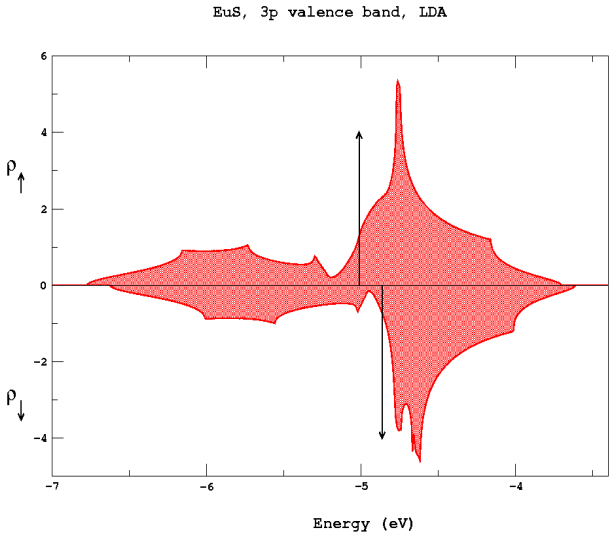

Figure 3.11: Spin- dependent density of states of $3p$ bands of EuS. Using the center of gravity of the bands, the exchange splitting amounts to ΔE=0.1512 eV.

Figure 3.10) exhibiting a distinct exchange splitting which can be used to fix the interband exchange coupling J. Assuming that the LDA treatment of the ferromagnetism is quite compatible with the Stoner (mean field) picture, as stated by several authors [79, 80], the T=0 splitting should amount to ΔE=JS. On taking the centers of gravity of the DOS for both the spins and along with the above assumption, the exchange splitting amounts to ΔE=0.1512 eV which results in the value for the exchange coupling strength as J=0.0432 eV where the spin value, S=3.5. One can also calculate the exchange coupling by taking the energy difference of the upper edge shift between both the spins which gives J=0.0253 eV. It was found that the coupling strength obtained by center of gravity approach, reflects more correlation effects as was shown in the previous work [59] for the conduction bands of EuS.

It is worthwhile to mention the often discussed *double counting problem* in relation to KLM and LDA. It is observed that the interband exchange interaction enters twice in the numerical evaluations, once explicitly by the interaction Hamiltonian, H_{int}, and secondly through H_{kin} by LDA procedure since it is not possible to switch off the interaction in the LDA code. This problem needs a special treatment which is described at a later stage.

. Utilizing the multi- band self energy ansatz for completely full valence bands [44] we compute the Green function Eq. (2.21) and thereby calculate the spectral densities Eq. (2.26) and densities of states Eq. (2.27).

In order to get a first impression of correlation effects in the valence bands of EuS we evaluate our theory for T=0 K ($\langle S^z \rangle$ = S). The quasi- particle density of states is shown in Figure 3.12. Since at T=0 K and fully occupied bands, the *removal* of a $\downarrow$ electron (i.e. creation of a $\uparrow$ hole) produces

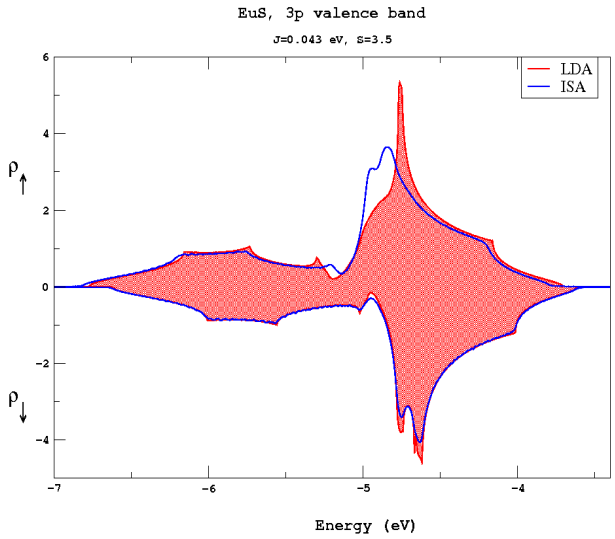

Figure 3.12: Spin- dependent density of states of $3p$ bands of EuS. Using the center of gravity of the bands, the exchange splitting amounts to ΔE=0.1512 eV.

a stable quasi- particle since the total spin of the itinerant sub- system ($\uparrow$) has no chance to flip its spin with the ferromagnetically saturated localized spin sub- system ($\Uparrow$). The removed $\downarrow$ electron carries the information of the itinerant sub- system. Due to absence of any spin flip process, its spectrum is unaffected by the usual value of J and thus coincides with the respective LDA curve. Here, we have compensated for the unimportant rigid shift ($-\frac{JS}{2}$) and so our approach fulfills the exact (T=0 K, $\sigma = \downarrow$) limit. The slight deviations seen in the middle part of Figure 3.12 are exclusively due to the numerical rounding procedure. This demonstrates that our method for implementing the LDA input into the many body theory calculation definately circumvents the earlier discussed *double counting problem*. The reason for this success lies in the fact that for the special case of ferromagnetically saturated semiconductor the $\downarrow$ spectrum is free of correlation effects which is due to the intra-atomic exchange Hamiltonian.

The upper half of Figure 3.12 demonstrates that correlation effects do appear even at T=0 K. The reason being that the removal of $\uparrow$ electron from a completely filled system leaves the total spin of the itinerant sub- system to be $\downarrow$ which can exchange its spin with the ferromagnetically saturated spin subsystem ($\Uparrow$) and have finite lifetime. Besides a slight band narrowing (due to small value of J), the density of states calculated within our many body theory provoke deformations and shifts with respect to the LDA result.

But our main focus is on the temperature dependent correlation effects which is exhibited in the plot of quasi- particle density of states (Q- DOS) in Figure 3.13. Due to weaker exchange coupling, the appearance of polaronlike quasi- particle branches are less likely in the real material calculation as compared to the model calculations in chapter 2. The temperature influence on the spectrum is seen in terms of deformations, mostly at the center (which

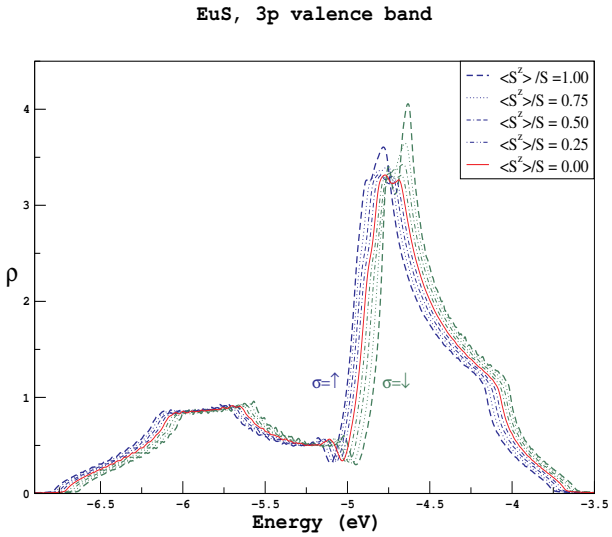

Figure 3.13: Quasi- particle density of states (Q- DOS) as a function of energy of the $3p$ valence bands of EuS.

will be more clearly seen in the quasi- particle bandstructure), and in terms of shifts.

Figure 3.14 represents the quasi- particle band- structure for some high-symmetry directions in the first Brillouin zone. The red area signifies zero magnitude while the dark blue gives the maximum value of the spectral function signifying infinte lifetimes for the quasi- particle. So on going downwards from blue (as represented through the color bar which is placed adjacent to the figure), correlation effects tend to increase. Within this definition, one can clearly see the correlation effects along many parts especially along the center of the valence band. As observed in the $\uparrow$ spectrum even at T=0 K ($\frac{\langle S^z \rangle}{S}$=1), few parts of the dispersions are washed out showing lifetime effects due to correlation in terms of magnon emission and re- absorption with simultaneous spin- flips as explained in section 2.2. But at the same temperature, the $\downarrow$ spectrum shows sharp peak- like structures (the dark blue points) indicating infinite lifetime as expected. At finite temperature ($\frac{\langle S^z \rangle}{S}$=0.5), the finite lifetimes appear in case of both the spin spectra as the ferromagnetically saturated spin system is not perfectly aligned giving rise to magnons which can be absorbed by the itinerant charge carriers. At transition temperature ($\frac{\langle S^z \rangle}{S}$=0.0), the spin asymmetry is removed. Strong temperature dependent correlation effects are seen mainly along the W- L directions.

In order to have a closer look at the correlations, the spin and **k**- dependent spectral densities are plotted at some high- symmetry points (W,L,X) in the first Brillouin zone. It can be compared with the angle- resolved photoemission experiments (for more details please refer to Appendix D).

As seen in Figure 3.15, well defined quasi- particle peaks appear with an additional spin split below T_c. The exchange splitting collapses for $T \rightarrow T_c$. The correlations are clearly observed at the W- point. With increasing temperature, there's a strong damping as seen along the high energy spectrum.

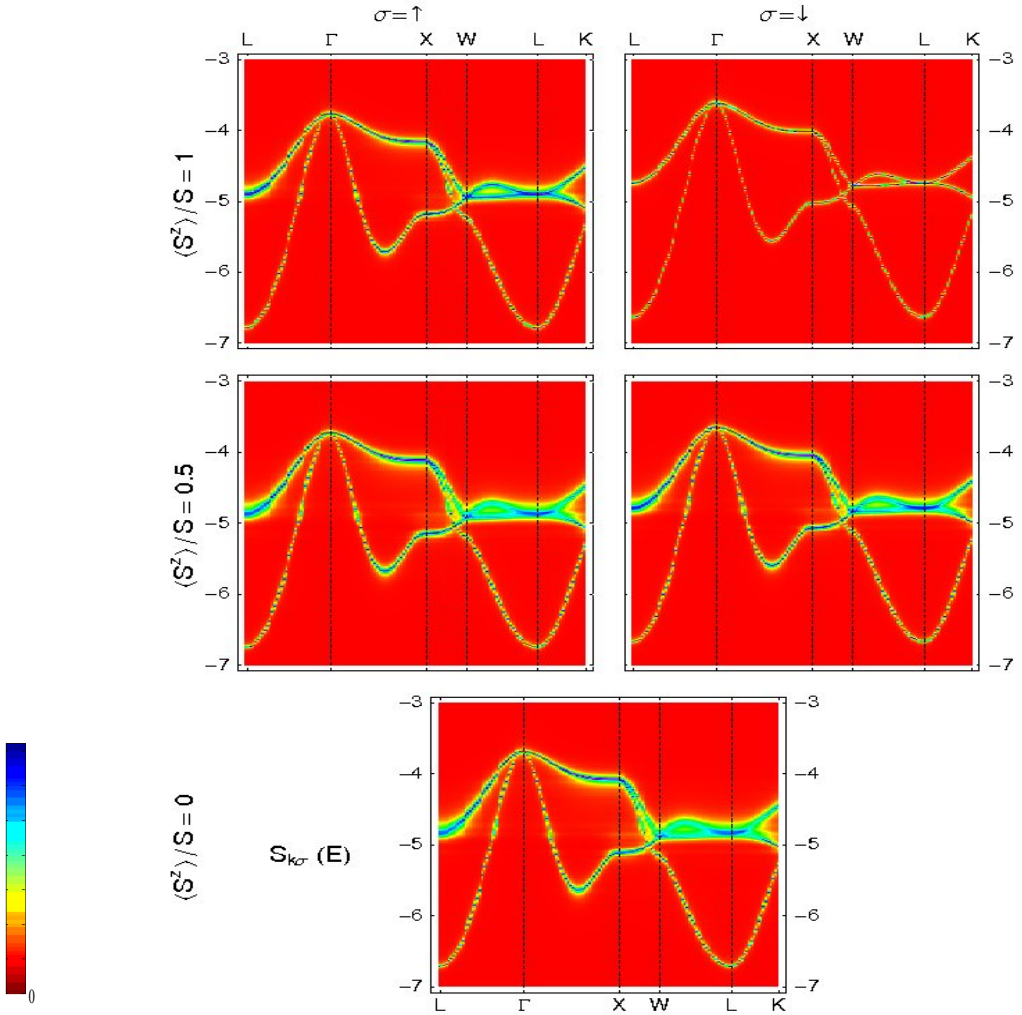

Figure 3.14: Spin- dependent quasi- particle bandstructure of $3p$ valence bands of EuS for different values of magnetization $\frac{\langle S^z \rangle}{S}$.

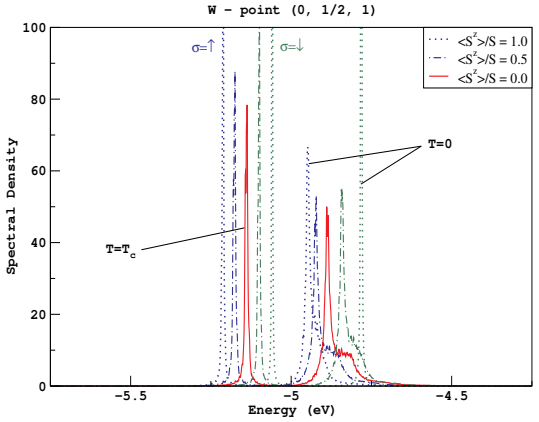

Figure 3.15: Spectral density at W - point.

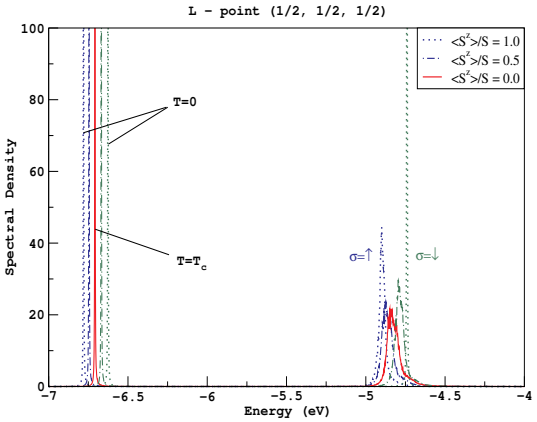

Figure 3.16: Spectral density at L - point.

Interestingly, the same W- point remains the point of discussion in case of the conduction band calculations of EuS [59]. Similar explanations hold for the other high- symmetry point Figure 3.16. While the **k**- dependent spectral densities refers to the angle resolved photoemission, the quasi- particle density of states as shown in Figure 3.13 can be considered as the angle integrated part.

The above anaylysis can also be carried out for the conduction bands of EuS. We can obtain the hopping matrices and the exchange coupling of only the conduction bands in the same way as we obtained the valence bands. From the T=0 bandstructure 3.8, it is evident that the strength of the exchange coupling is greater in case of conduction band as compared to the valence band due to large exchange splitting in the former. For our calculations we take J=0.23 eV for the conduction band, the same as obtained previously by Müller et al [59] who studied the conduction bands of EuS within the LDA+MCDA method as discussed in section 3.2. This also forms another motivation for studying the conduction bands of EuS as we can compare our results with that in Ref. [59].

Figure 3.17 compares the spin- resolved quasi- particle density of states of

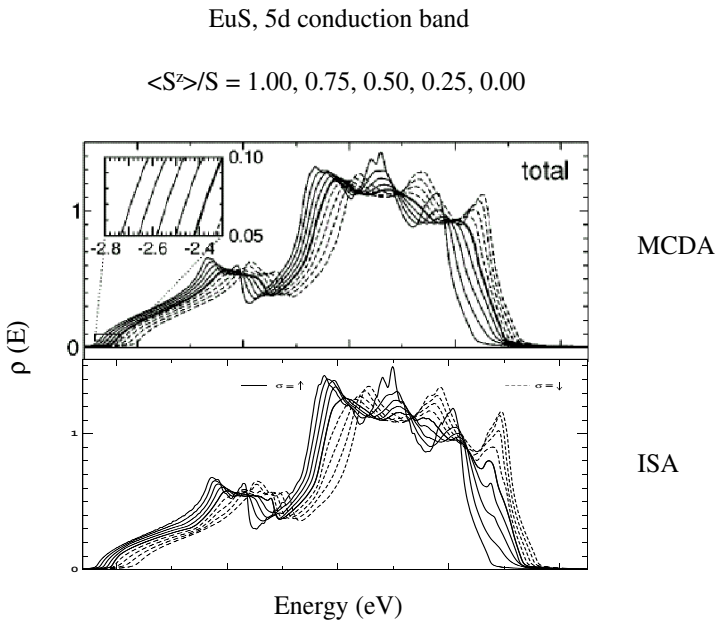

Figure 3.17: Spin- dependent quasi- particle density of states of $5d$ conduction bands of EuS calculated for exchange coupling J=0.23 eV and different $4f$ magnetizations $\langle S^z \rangle$/S. In the upper panel calculations have been performed using MCDA self- energy as taken from Ref. [59] while in the lower using ISA self- energy.

$5d$ conduction bands of EuS as a function of energy. The upper part exhibits the result calculated within the moment conserving decoupling approximation (MCDA) self energy while the lower with that of our interpolating self- energy approach (ISA) self- energy. Though the overall features almost remain the

same, like the shift in the lower band edge with temperature giving the the measure of the ferromagnetic red- shift of the optical gap, but some of the features are quite distinct. For instance, in the high energy region (near the end of the spectrum) within our method the emergence of the peak can be clearly seen with lowering temperature and more correlation effects are highlighted as compared to the LDA+MCDA. The reason for this discrepancy seems to lie in different ways of using the single particle input which in our case is in the matrix form. It is less likely due to different forms of self- energies as in low carrier regime, which is true in case of EuS, calculations performed using both the self- energies yield identical results.

Since the conduction and valence bands of EuS can be studied individu-

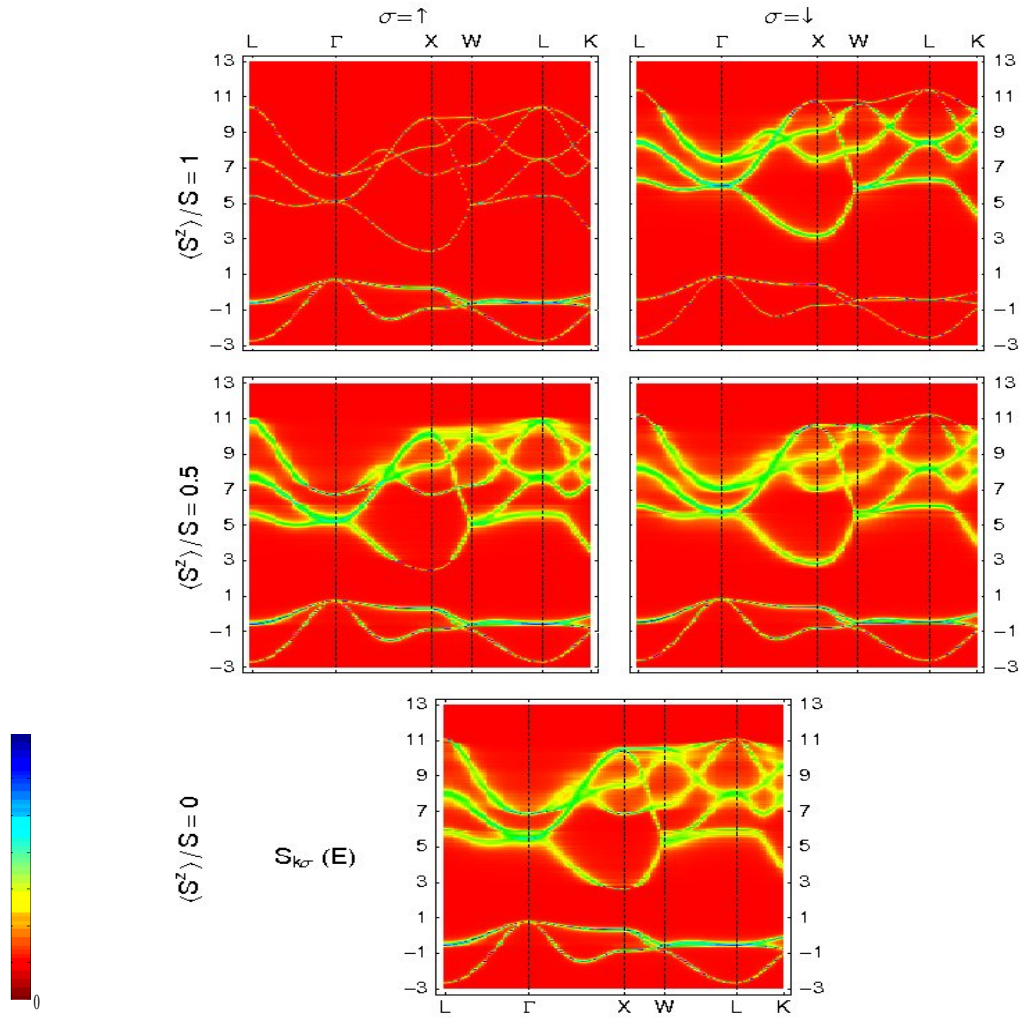

Figure 3.18: The temperature dependent quasi- particle bandstructure of bulk EuS.

ally, it would be even very interesting to see the complete picture. Figure 3.18 shows the temperature dependent quasi- particle bandstructure of bulk EuS. As far as the author is concerned, it is the first picture of its kind where quasi-particle bandstructure is exhibited both for the conduction as well as valence

bands. In Figure 3.18, strong temperature dependent correlation effects are seen in the conduction band as compared to the valence band due to the greater strength of exchange coupling in case of conduction band as compared to the valence band.

3.3.2 GdN : Gadolinium Nitride

The rare earth monopnictide, GdN, is a strongly correlated electron system. These are a wide class of materials that show unusual (often technologically useful) electronic and magnetic properties, such as metal- insulator transitions or half- metallicity. Typically, strongly correlated materials have incompletely filled d or f electron shells with narrow bands.

According to experimental results, bulk GdN was demonstrated to be a low carrier semimetallic [81] or the thin films to be insulating [82]. But there have been recent claims [83] of semiconducting ground state of stoichiometric GdN thin films based on resistivity values measured at low temperatures which were found to be typical features of semiconductor.

Historically, the first self- consistent electronic bandstructures of GdN for the paramagnetic case was calculated by the Hasegawa et.al, [64] using augmented plane wave (APW) method. Their calculations employed one- electron potential instead of local spin density (LSD) functional theory. Later on Lambrecht [65] addressed the problem by estimating the gap corrections beyond local density approximation (LDA) while Ghosh [66] performed self consistent spin polarized calculations using full potential linear muffin- tin orbital (FP-LMTO) but with rigid shifts in the $5d$ and $4f$ states in order to fit the experimental X- ray photoemission spectroscopy (XPS) and X- ray Bremsstrahlung Isochromat spectroscopy (BIS) results. The other methods, within the so-called Self Interaction Corrected local spin density (SIC- LSD) calculations by Aerts et.al, [67] and augmented spherical wave (ASW) within LDA and generalized gradient approximations (GGA) by Eyert [68] rendered half- metallic nature to GdN. This latter property has led to some interest in GdN as a possible candidate for spin- dependent transport device [84, 85].There has also been an interesting investigation on the electronic structure and magnetic properties of GdN by Duan et.al, [69] based on "first principles" calculations as a function of unit cell volume. Upon changing the equilibrium lattice constant one eventually changes the effective bandwidths of the bands which is similar to shifting the $5d$ rigidly in order to fix the band gap problem. They eventually found that GdN transforms first from half- metallic to semi- metallic and then finally to a semiconductor upon applying stress. These features reveal a strong lattice constant dependence on the electronic structure of GdN. Lastly, in a very recent calculation using the quasi- particle self- consistent GW (QSGW) method, Chantis et al [86] predicted GdN to be very near to a critical point of a metal- insulator transition.

We combine our many body analysis of the multi- band Kondo lattice model along with the first principles TB- LMTO spin- polarized bandstructure calcu-

lations to investigate the temperature dependent electronic correlation effects in the conduction bands of GdN [87]. We wish to emphasize that upon using bandstructure calculations we are not aiming to find the nature of the electronic ground state of GdN but rather take its output as the starting point (input) for our many body theory and compare the results for the temperature dependence with that of the experimental ones (redshift phenomenon). Very recently a similar study has been reported [88] but using a different approach for determining the self- energy [89] and also for the input in the many body part.

In order to have the single particle excitation energies i.e. the hopping matrices and the exchange coupling strength we also performed the TB- LMTO [61, 63] bandstructure calculations within LDA. It is known that GdN crystallizes in a rocksalt structure, which is same as shown in Figure 3.6 but with Gd atoms sitting in place of Eu and N in that of S. It has an experimental lattice constant of 4.99 Å and symmetry group Fm- 3m which we used as an input for our *TB- LMTO* program and as shown in Figure 3.2. So, it is known that each Gd^{3+} ion has twelve nearest and six next nearest Gd- neighbours.

Figure 3.19 indicates the calculated spin- dependent $5d$ conduction bands

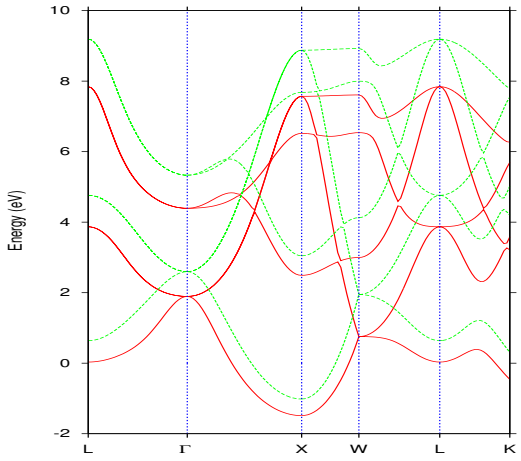

Figure 3.19: LDA bandstructure of $5d$ conduction bands of GdN. Full (red) lines are spin ↑ and broken (green) ones are spin ↓.

of GdN. Our evaluation is restricted only to $5d$ bands while considering GdN to be a semiconductor in accordance with Refs. [64, 65, 66] and the $4f$ electrons as core electrons as explained in section 3.2.

In Figure 3.20 the LDA- density of states is displayed. A distinct exchange splitting is visible as compared to valence bands of EuS. It can be used to fix the interband exchange coupling constant J in Eq. (2.19). Considering the same assumption as made previously that the LDA treatment of the ferromagnetism is quite compatible with the Stoner (mean field) picture, the T=0 splitting amounts to ΔE=JS. On taking the center of gravity of both the

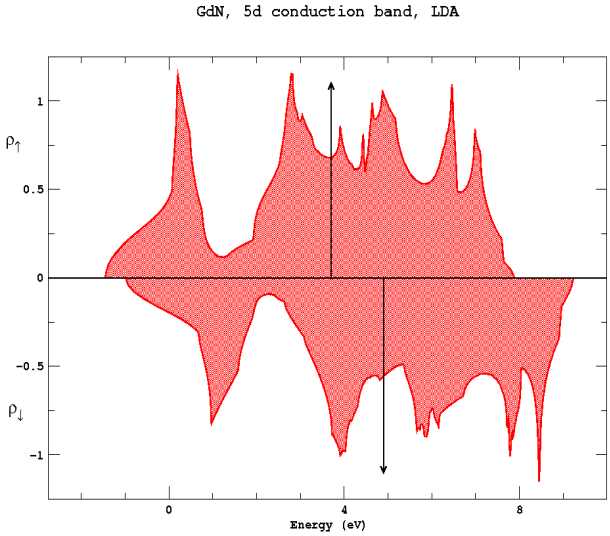

Figure 3.20: Spin- dependent density of states of $5d$ bands of GdN. Using the center of gravity of the bands, the exchange splitting amounts to $\Delta E = 1.237$ eV.

bands[9] and along with the above assumption we obtain:

$$\Delta E = 1.237 \text{ eV} \qquad \Rightarrow \qquad J = 0.35 \text{ eV} \tag{3.10}$$

It is understood that in the bandstructure calculations, one cannot switch off the inter- band exchange interaction (Eq. (2.19)) in the LDA code, but one can speculate from the exact T=0 result for empty conduction band [37] that such an interaction leads only to a rigid shift in the ↑ spectrum while the ↓ spectrum is remarkably deformed by correlation effects due to spin exchange processes between the delocalized and localized states. So we take from the LDA calculation, which holds by definition for T=0, the ↑ part as the single-particle input in Eq. (2.18). Therewith, it is guaranteed that all other interactions which do not explicitly come into our Hamiltonian are implicitly taken into account by the LDA single particle Hamiltonian. On the other hand, a double counting of any decisive interaction is avoided *since in the ↑- spectrum the inter- band exchange (Eq.* (2.19)*) only shifts the energy zero.* Note that in case of valence bands of EuS, it was the down part which was correlation free and acted as an input for the many body theory.

In order to get a first impression of the correlation effects we have evaluated our theory for T=0 K and the results are presented in Figure 3.21. The ↑ spectrum is unaffected by the actual value of J and coincides with the respective LDA curve, after a compensation of the unimportant rigid shift ($\frac{JS}{2}$) which is positive in this case. The slight deviations, seen in the upper part of Figure 3.21 are again exclusively due to numerical procedures. The above procedure confirms yet again that our theoretical method in order to implement the LDA input into the many body theory satisfies the exact limit (T=0, σ =

[9]We do not consider the other way of obtaining exchange coupling by taking the energy difference of the lower edge shift between both the spins

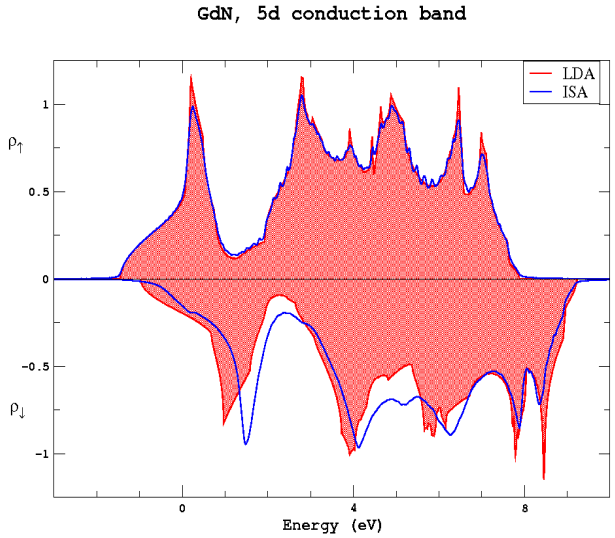

Figure 3.21: The same as in Figure 3.20 with additional T=0 results of our combined many body and first principles theory for exchange coupling J = 0.35 eV, shown in broken lines.

↑). The lower half, ↓ spectrum, of Figure 3.21 demonstrates that correlation effects do appear even at T=0 K. Apart from a considerable band narrowing[10], they provoke strong deformations and shifts with respect to the LDA result.

The quasi- particle density of states (Q- DOS) are calculated for J=0.35 eV and plotted in Figure 3.22 for various values of $4f$ magnetizations i.e. different temperature. As observed (from the inset of Figure 3.22), the lower edge of spin - ↑ Q- DOS performs a shift to lower energies upon cooling from T=T_c down to T=0 K which explains the redshift effect of the optical absorption edge for an electronic transition. We find a redshift of 0.34 eV. *Here, one should note that a simple mean field treatment with J=0.35 eV and S=3.5 would result in a redshift of 0.6125 eV. Obviously, the correlation effects drastically reduce this value.* A similar redshift phenomenon was discussed by Lambrecht [65] with a calculated value of 0.30 eV and was also reported experimentally having a value of 0.40 eV by Leuenberger [90] and very recently by Trodahl [91] also obtained the same value of 0.40 eV. Leuenberger observed this effect as a shift of the L_2 edge on a relative comparison between absoprtion spectra measured on a 2000 Å GdN film at T > T_c and T < T_c in X- ray magnetic circular dichroism (XMCD) experiment. The L_2 absorption spectra is sensitive to the polarization of t_{2g} states. Trodahl observed the signatures of the direct optical gap with an absorption edge seen as a rapid loss of transmitted intensity as the photon energy rises through the edge. In Ref.[88], the redshift of 0.483 eV was obtained using J for the lowest band of the bulk GdN and was found to be overestimated.

Figure 3.23 represents the quasi- particle bandstructure for some high-symmetry directions in the first Brillouin zone. The magnitude of the spectral

[10]in case of valence bands of EuS it was not a prominent feature due to small value of exchange coupling

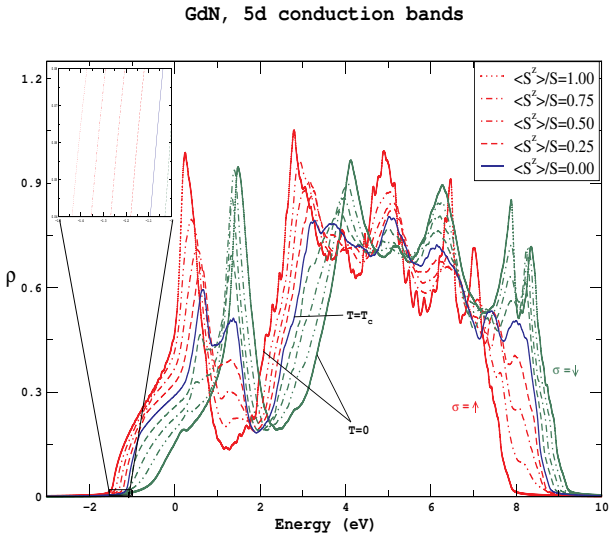

Figure 3.22: Quasi- particle density of states (Q- DOS) of the $5d$ conduction bands of GdN for various temperatures (different $4f$ magnetizations). The outermost curves belong to T=0 K ($\frac{\langle S^z \rangle}{S}$=1).On increasing the temperature they approach each other. The inset shows on an enlarged scale the temperature shift of the lower edge for the case of $\uparrow$.

function is indicated using color bar with red as value zero. As observed in the $\downarrow$ spectrum even at T=0 K ($\frac{\langle S^z \rangle}{S}$=1), parts of the dispersions are washed out showing lifetime effects due to very strong correlation.

At T=0 K and empty bands, the addition of a $\uparrow$ electron produces a stable quasi- particle since the $\uparrow$ electron has no chance to flip its spin with the ferromagnetically saturated spin ($\Uparrow$) sub- system. The imaginary part of the self- energy vanishes indicating infinite lifetimes. And since the $\downarrow$ electron can exchange its spin with the ferromagnetically saturated spin sub- system, it can have finite lifetime. Actually, it can emit a magnon and become a $\uparrow$ electron provided there exist $\uparrow$ electron states (scattering states) which can be occupied after spin- flip process. The other possibility for the $\downarrow$ electron to exchange its spin could be by repeated emission and absorption of magnons, thus forming a quasi- particle called magnetic polaron. For strong coupling, the above mentioned elementary processes can even lead to correlation- caused splitting of the dispersion. This is clearly visible at certain parts in Figure 3.23.

For finite temperatures, the spin sub- system is no longer perfectly aligned. There are magnons in the system that can be absorbed by the itinerant charge carriers provoking quasi- particle damping in the $\uparrow$ spectrum too. The spectral weight gets redistributed due to spin flip term in the exchange interaction with deformations in the density of states. The overall exchange splitting reduces with increasing temperature, until in the limit $T \rightarrow T_c$ ($\langle S^z \rangle \rightarrow 0$) , the vanishing $4f$ magnetization removes the induced spin asymmetry.

In order to have a closer look at the correlations, the spin and **k**- dependent spectral densities are plotted at some high- symmetry points (W, K, X) in the first Brillouin zone and for different temperatures. As discussed earlier, it can

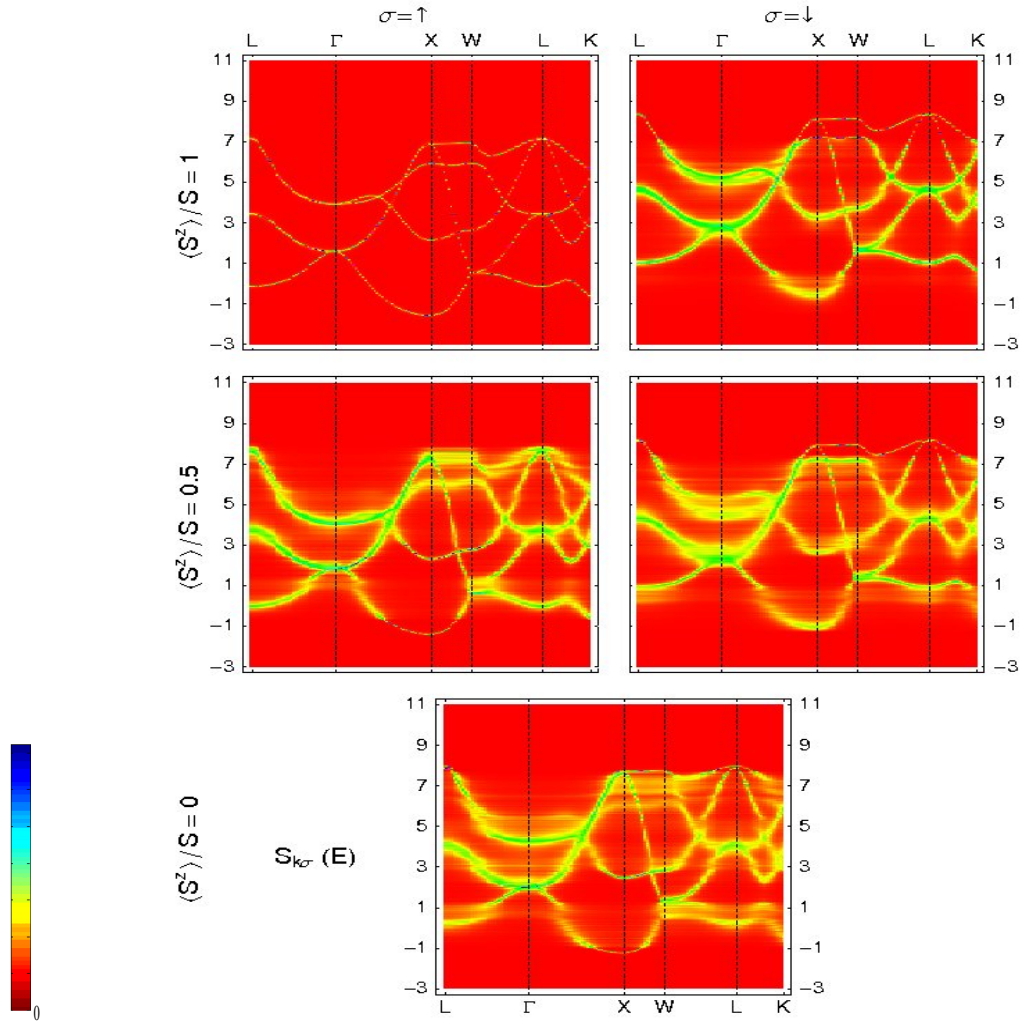

Figure 3.23: Spin- dependent quasi- particle bandstructure of $5d$ conduction bands of GdN for different values of magnetization $\frac{\langle S^z \rangle}{S}$.

directly be compared with spin and angle resolved inverse photoemission experiments.

In accordance with the quasi- particle bandstructure, it is observed in Fig-

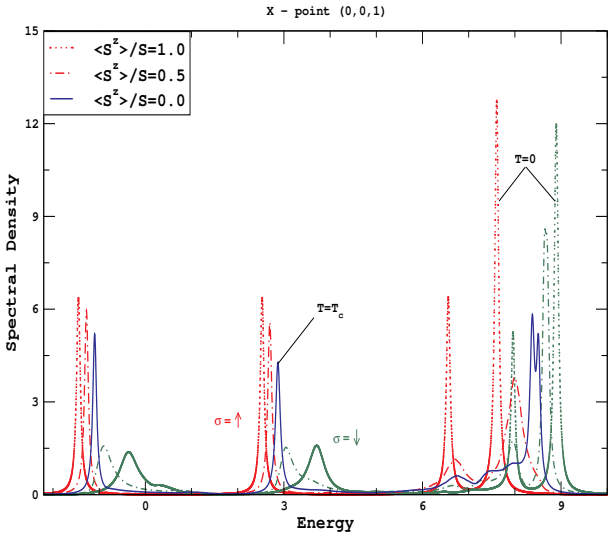

Figure 3.24: Spectral density at X - point. The case of $\frac{\langle S^z \rangle}{S} = 1.0$ is shown by dotted lines, while $\frac{\langle S^z \rangle}{S} = 0.50$ is denoted as broken lines and the full lines represent $\frac{\langle S^z \rangle}{S} = 0.0$

ure 3.24 that four sharp peaks appear at T=0 K for ↑ spectrum and though already strongly damped (at lower energies), the same peak sequence comes out in the ↓ spectrum. The exchange splitting collapses for $T \rightarrow T_c$ and the quasi- particle damping increases with increasing temperature. For $T=T_c$ (full lines), the spectrum is cleansed at higher energies exhibiting extreme strong correlation effects.

Similar explanations hold for the other high- symmetry points (Figure 3.25 and Figure 3.26). There's a strong damping as seen along the entire energy spectrum. And some of the peaks (lower energy peaks in Figure 3.25) are so strongly damped that they may not be visible in the inverse photoemission experiment. Altogether, the 5d spectral densities exhibit drastic temperature dependencies, what concerns the positions and the widths of quasi- particle peaks. For this reason, it would be highly encouraging to perform inverse photoemission spectroscopy of the conduction bands of GdN.

On observing such strong electronic correlations in GdN, it would be highly motivating to study the nature of exchange mechanism in this compound which eventually is an unsolved problem as discussed in the following chapter. But first we will discuss the general behvaior of direct and indirect exchange phenomenon and then formulate the modified RKKY mechanism for the multiband KLM.

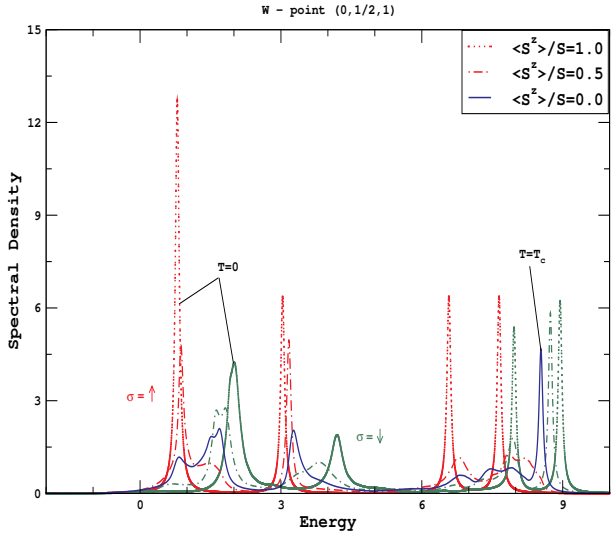

Figure 3.25: The same as in Figure 3.24 but for W - point.

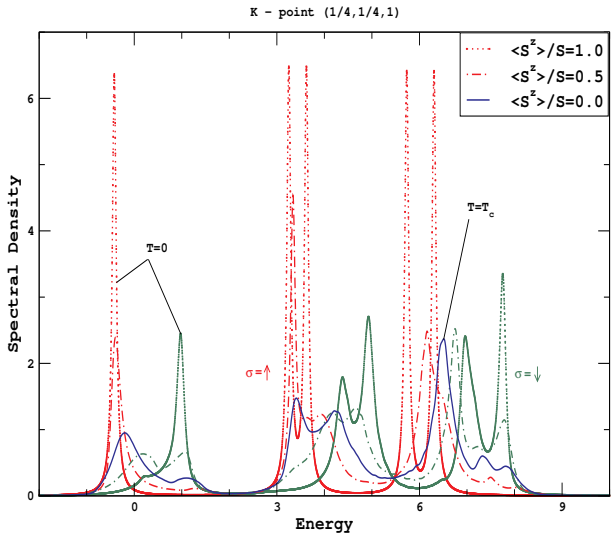

Figure 3.26: The same as in Figure 3.24 but for K - point.

Chapter 4

Exchange Phenomenon

.. : we applied much prolonged labour on investigating the magnetical forces ; so wonderful indeed are they, compared with the forces of all other minerals, surpassing even the virtues of all other bodies about us.

- William Gilbert, Preface to *On the Magnet* (1600 AD).

4.1 Direct and Indirect mechanisms

The exchange interactions represents a characteristic quantum effect having no analog in classical mechanics and its main goal being in determining the spontaneous magnetization for a system having permanent magnetic moments. This phenomenon of collective magnetism [92] is a part of one of the oldest and basic problems in solid state physics. Due to the lack of its complete understanding, it is currently one of the very hot topic in fundamental research. The main weakness being the absence of a unified theory which would be able to explain the rich diversity of the subject within the framework of one and the same theoretical model. The different types of magnetic materials (metals, non- metals) fulfills different models descriptions, each of them having a fairly restricted regime. Thus, while studying their magnetic properties one should specify the model under consideration.

The simplest model of magnetism in solids is the following : electrons in well localized magnetic d or f states interact with one another via a Heisenberg nearest neighbor exchange mechanism [93]. The direct overlap of wave functions belonging to neighboring spins leads to a magnetic interaction which can be of either sign- ferromagnetic or antiferromagnetic. But in many metals or non- metals calculations suggest that the direct exchange between the nearest neighbors in a localized spin model is itself not responsible for ferromagnetism because the distance between the nearest neighbors is too great for there to be appreciable overlap of the wave functions.

The general idea of the exchange interaction have therefore been extended by the concept of "indirect exchange" which was first suggested by Kramers [94].

The principle involved in this interaction is that exchange between two magnetic ions does not occur directly but it is maintained via an intermediatory diamagnetic ion. In the simplest terms exchange alignment occurs between an electron on the magnetic ion and one on the diamagnetic ion and the latter then interacts with the next magnetic ion so producing a further alignment. The net effect is therefore an exchange coupling between the two magnetic ions.

When applied to non-metals it is termed as *superexchange* [95] by Anderson. In his treatment he assumes that the d states of the magnetic ions will be modified by the presence of the nearby diamagnetic p states so that they will have some p admixture. The new wave functions of the magnetic ions will have much more overlap than did the original simple d functions because now they each have some of the p character of the diamagnetic ions. He then calculates the direct exchange between two magnetic ions using the modified wave functions. Such calculations as have been made suggest that this is a satisfactory approach to the problem of the exchange mechanism in insulators.

The same principle from that of Kramer's has been extended by Zener [96] to conductors within the so-called *double exchange* phenomenon. He proposed that the interaction between the localized $3d$ or $4f$ electrons on different ions arose by means of a coupling via the conduction electrons instead of via the diamagnetic ions as was discussed earlier.

And an equivalent treatment exist for metals where the exchange interaction results in oscillatory function as a consequence of the sharp Fermi surface. In such systems there is an important contribution to the spin- spin interaction due to the polarization of the itinerant electrons and their interaction with localized spins. Originally ascribed to Ruderman and Kittel [97], the interaction was proposed as a means of explaining unusually broad nuclear spin resonance lines that had been observed in natural metallic silver. It was long ranged and decreased only as the inverse cube of the distance at large separation. Kasuya [98] later proposed that a similar indirect exchange coupling could be applied to localized d electron spins interacting via conduction electrons. A subsequent modification by Yosida [99] even further increased the range and thereafter this indirect mechanism is termed as the *RKKY interaction.*

Bloembergen and Rowland [100] adapted the same concept to nonmetals and found qualitatively the same oscillatory behavior but a range reduced by "tunneling".

Apart from the above explained exchange interactions there are a multitude of possible other interactions like *triple exchange* [101],*biquadratic superexchange* [102], some explaining exchange mechanisms in magnetic semiconductors [103, 104, 105] while others in diluted magnetic semiconductors [106, 107]. A point which has to be stressed out is that *in any particular material these indirect exchange couplings may or may not be comparable in energy to the direct coupling and the two mechanisms doubtless can coexist in the same substance.*

In the next section, we try to formulate one of the indirect exchange mechanisms for the case of multi- band Kondo lattice model.

4.2 Multiband Modified RKKY Theory

In Chapter 2, we did not consider a direct exchange interaction between the localized f spins and the magnetization was treated as a parameter so as to determine the electronic properties due to the itinerant electrons. But if one

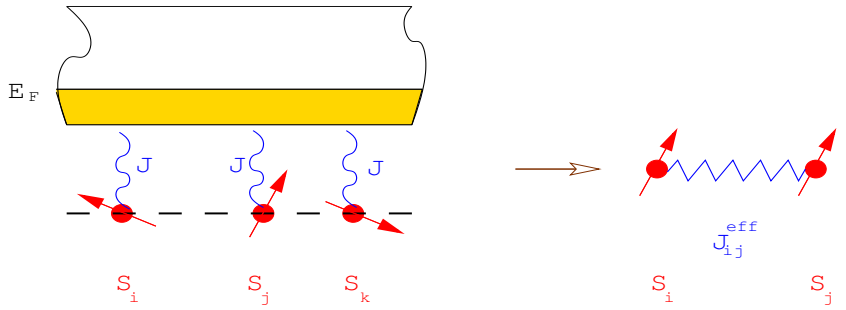

Figure 4.1: An effective indirect exchange, J_{ij}^{eff}, between localized f spins (red arrows) mediated by intra-atomic exchange, J, due to itinerant electrons. E_F denotes the Fermi edge.

is interested in determining the magnetic properties of multi- band Kondo lattice model then both the sub- systems (localized as well as itinerant) should be solved within a self consistent scheme. Therefore, we would like to take into account an effective indirect coupling, J_{ij}^{eff}, between the localized f spins and the itinerant electrons within the modified RKKY formalism as shown in Figure 4.1.

Consider the multi- band Kondo lattice Hamiltonian which can be written in the following equivalent form,

$$\begin{aligned} H &= H_{kin} + H_{int} \\ &= \sum_{\mathbf{k}\alpha\beta\sigma} \epsilon^{\alpha\beta}(\mathbf{k}) c^{\dagger}_{\mathbf{k}\alpha\sigma} c_{\mathbf{k}\beta\sigma} \\ &- \frac{J}{2N} \sum_{i\alpha\sigma'\sigma} \sum_{\mathbf{kq}} e^{-i\mathbf{q}\cdot\mathbf{R}_i} (\mathbf{S}_i \cdot \boldsymbol{\sigma})_{\sigma'\sigma} c^{\dagger}_{\mathbf{k+q}\alpha\sigma'} c_{\mathbf{k}\alpha\sigma} \end{aligned} \tag{4.1}$$

where all the terminologies remain the same as explained in Chapter 2. The components of the band electron spin operator $\boldsymbol{\sigma}$ are the Pauli spin matrices.

The main idea of the modified RKKY theory is to transform the above Kondo- like exchange Hamiltonian of the conduction electrons into an effective Heisenberg- like spin- spin exchange Hamiltonian of the f spins by averaging H_{int} in the subspace of the conduction electrons ($\langle \quad \rangle$):

$$\begin{aligned} \langle H_{int} \rangle &= H_f \\ &= -\frac{J}{2N} \sum_{i\alpha\sigma'\sigma} \sum_{\mathbf{kq}} e^{-i\mathbf{q}\cdot\mathbf{R}_i} (\mathbf{S}_i \cdot \boldsymbol{\sigma})_{\sigma'\sigma} \langle c^{\dagger}_{\mathbf{k+q}\alpha\sigma'} c_{\mathbf{k}\alpha\sigma} \rangle \end{aligned} \tag{4.2}$$

This is achieved by closely following the treatment as given in Ref. [31]. For averaging procedure the f spin operators are to be considered as c numbers. The expectation values $\langle \quad \rangle$ in Eq. (4.2) may still have operator properties in the f spin subspace and therefore do not vanish for $q \neq 0$ and $\sigma \neq \sigma'$. We would like to obtain $\langle \quad \rangle$ via the spectral theorem with the help of appropriate Green function as given below :

$$G^{\alpha\beta\sigma\sigma'}_{\mathbf{k},\mathbf{k+q}}(E) = \langle\langle c_{\mathbf{k}\alpha\sigma}; c^{\dagger}_{\mathbf{k+q}\beta\sigma'}\rangle\rangle_E \tag{4.3}$$

Its equation of motion can be obtained in the usual way as discussed in Appendix A and is given as

$$\begin{aligned} EG^{\alpha\beta\sigma\sigma'}_{\mathbf{k},\mathbf{k+q}}(E) &= \delta_{\mathbf{k},\mathbf{k+q}}\delta_{\alpha\beta}\delta_{\sigma\sigma'} + \sum_{\gamma}\epsilon^{\alpha\gamma}(\mathbf{k})G^{\gamma\beta\sigma\sigma'}_{\mathbf{k},\mathbf{k+q}}(E) \\ &\quad - \frac{J}{2N}\sum_{i\mathbf{k}'\sigma''} e^{-i(\mathbf{k}-\mathbf{k}')\cdot\mathbf{R}_i}(\mathbf{S}_i\cdot\boldsymbol{\sigma})_{\sigma\sigma''}G^{\alpha\beta\sigma''\sigma'}_{\mathbf{k}',\mathbf{k+q}}(E) \end{aligned} \tag{4.4}$$

The above equation can be iterated up to any desired accuracy producing spin products of the type :

$(\mathbf{S}_i\cdot\boldsymbol{\sigma})_{\sigma\sigma''}, \quad (\mathbf{S}_i\cdot\boldsymbol{\sigma})_{\sigma''\sigma'''}, \quad (\mathbf{S}_i\cdot\boldsymbol{\sigma})_{\sigma'''\sigma''''}$

On excluding the band indices in Eq. (4.4) by representing the terms in a generalized matrix form on symbolizing a hat over it we get

$$\begin{aligned} E\widehat{G}^{\sigma\sigma'}_{\mathbf{k},\mathbf{k+q}}(E) &= \delta_{\mathbf{k},\mathbf{k+q}}\delta_{\sigma\sigma'}\widehat{I} + \widehat{\epsilon}(\mathbf{k})\widehat{G}^{\sigma\sigma'}_{\mathbf{k},\mathbf{k+q}}(E) \\ &\quad - \frac{J}{2N}\sum_{i\mathbf{k}'\sigma''} e^{-i(\mathbf{k}-\mathbf{k}')\cdot\mathbf{R}_i}(\mathbf{S}_i\cdot\boldsymbol{\sigma})_{\sigma\sigma''}\widehat{G}^{\sigma''\sigma'}_{\mathbf{k}',\mathbf{k+q}}(E) \end{aligned} \tag{4.5}$$

Rearranging the terms in Eq. (4.5) yields

$$\begin{aligned} \Big[E\widehat{I} - \widehat{\epsilon}(\mathbf{k})\Big]\widehat{G}^{\sigma\sigma'}_{\mathbf{k},\mathbf{k+q}}(E) &= \delta_{\mathbf{k},\mathbf{k+q}}\delta_{\sigma\sigma'}\widehat{I} \\ &\quad -\frac{J}{2N}\sum_{i\mathbf{k}'\sigma''} e^{-i(\mathbf{k}-\mathbf{k}')\cdot\mathbf{R}_i}(\mathbf{S}_i\cdot\boldsymbol{\sigma})_{\sigma\sigma''}\widehat{G}^{\sigma''\sigma'}_{\mathbf{k}',\mathbf{k+q}}(E) \end{aligned} \tag{4.6}$$

For symmetry reasons, we write down the equation of motion for $G^{\alpha\beta\sigma\sigma'}_{\mathbf{k},\mathbf{k+q}}(E)$ in an alternative way where the second operator , $c^{\dagger}_{\mathbf{k+q}\beta\sigma'}$, in Eq. (4.3) is the "active" operator.:

$$\begin{aligned} E\widehat{G}^{\sigma\sigma'}_{\mathbf{k},\mathbf{k+q}}(E) &= \delta_{\mathbf{k},\mathbf{k+q}}\delta_{\sigma\sigma'}\widehat{I} + \widehat{G}^{\sigma\sigma'}_{\mathbf{k},\mathbf{k+q}}(E)\widehat{\epsilon}(\mathbf{k+q}) \\ &\quad - \frac{J}{2N}\sum_{i\mathbf{k}'\sigma''} e^{-i\Big(\mathbf{k}'-(\mathbf{k+q})\Big)\cdot\mathbf{R}_i}(\mathbf{S}_i\cdot\boldsymbol{\sigma})_{\sigma''\sigma'}\widehat{G}^{\sigma\sigma''}_{\mathbf{k},\mathbf{k}'}(E) \end{aligned} \tag{4.7}$$

and again upon rearranging the terms in the above equation we get

$$\begin{aligned} \widehat{G}^{\sigma\sigma'}_{\mathbf{k},\mathbf{k+q}}(E)\Big[E\widehat{I} - \widehat{\epsilon}(\mathbf{k+q})\Big] &= \delta_{\mathbf{k},\mathbf{k+q}}\delta_{\sigma\sigma'}\widehat{I} \\ &\quad -\frac{J}{2N}\sum_{i\mathbf{k}'\sigma''} e^{-i\Big(\mathbf{k}'-(\mathbf{k+q})\Big)\cdot\mathbf{R}_i}(\mathbf{S}_i\cdot\boldsymbol{\sigma})_{\sigma''\sigma'}\widehat{G}^{\sigma\sigma''}_{\mathbf{k},\mathbf{k}'}(E) \end{aligned} \tag{4.8}$$

Now let us define the following Green function of the "free" electron system

$$\left[E\widehat{I}-\widehat{\epsilon}(\mathbf{k})\right]=\left(\widehat{G}^{(0)}_{\mathbf{k}}(E)\right)^{-1} \tag{4.9}$$

$$\left[E\widehat{I}-\widehat{\epsilon}(\mathbf{k+q})\right]=\left(\widehat{G}^{(0)}_{\mathbf{k+q}}(E)\right)^{-1} \tag{4.10}$$

Subsituting Eq. (4.9) in Eq. (4.6) gives

$$\begin{aligned}\left(\widehat{G}^{(0)}_{\mathbf{k}}(E)\right)^{-1}\widehat{G}^{\sigma\sigma'}_{\mathbf{k},\mathbf{k+q}}(E)&=\delta_{\mathbf{k},\mathbf{k+q}}\delta_{\sigma\sigma'}\widehat{I}\\&-\frac{J}{2N}\sum_{i\mathbf{k}'\sigma''}e^{-i(\mathbf{k}-\mathbf{k}')\cdot\mathbf{R}_i}(\mathbf{S}_i\cdot\boldsymbol{\sigma})_{\sigma\sigma''}\widehat{G}^{\sigma''\sigma'}_{\mathbf{k}',\mathbf{k+q}}(E)\end{aligned} \tag{4.11}$$

while substituting Eq. (4.10) in Eq. (4.8) yields

$$\begin{aligned}\widehat{G}^{\sigma\sigma'}_{\mathbf{k},\mathbf{k+q}}(E)\left(\widehat{G}^{(0)}_{\mathbf{k+q}}(E)\right)^{-1}&=\delta_{\mathbf{k},\mathbf{k+q}}\delta_{\sigma\sigma'}\widehat{I}\\&-\frac{J}{2N}\sum_{i\mathbf{k}'\sigma''}e^{-i\left(\mathbf{k}'-(\mathbf{k+q})\right)\cdot\mathbf{R}_i}(\mathbf{S}_i\cdot\boldsymbol{\sigma})_{\sigma''\sigma'}\widehat{G}^{\sigma\sigma''}_{\mathbf{k},\mathbf{k}'}(E)\end{aligned} \tag{4.12}$$

Now upon multiplying $\widehat{G}^{(0)}_{\mathbf{k}}(E)$ from left to Eq. (4.11) we get

$$\begin{aligned}\widehat{G}^{\sigma\sigma'}_{\mathbf{k},\mathbf{k+q}}(E)&=\delta_{\mathbf{k},\mathbf{k+q}}\delta_{\sigma\sigma'}\widehat{G}^{(0)}_{\mathbf{k}}(E)\\&-\frac{J}{2N}\sum_{i\mathbf{k}'\sigma''}e^{-i(\mathbf{k}-\mathbf{k}')\cdot\mathbf{R}_i}(\mathbf{S}_i\cdot\boldsymbol{\sigma})_{\sigma\sigma''}\widehat{G}^{(0)}_{\mathbf{k}}(E)\widehat{G}^{\sigma''\sigma'}_{\mathbf{k}',\mathbf{k+q}}(E)\end{aligned} \tag{4.13}$$

And on multiplying $\widehat{G}^{(0)}_{\mathbf{k+q}}(E)$ from right to Eq. (4.12) we obtain

$$\begin{aligned}\widehat{G}^{\sigma\sigma'}_{\mathbf{k},\mathbf{k+q}}(E)&=\delta_{\mathbf{k},\mathbf{k+q}}\delta_{\sigma\sigma'}\widehat{G}^{(0)}_{\mathbf{k+q}}(E)\\&-\frac{J}{2N}\sum_{i\mathbf{k}'\sigma''}e^{-i\left(\mathbf{k}'-(\mathbf{k+q})\right)\cdot\mathbf{R}_i}(\mathbf{S}_i\cdot\boldsymbol{\sigma})_{\sigma''\sigma'}\widehat{G}^{\sigma\sigma''}_{\mathbf{k},\mathbf{k}'}(E)\widehat{G}^{(0)}_{\mathbf{k+q}}(E)\end{aligned} \tag{4.14}$$

Let us make the following crucial first order approximations for the Green functions

$$\widehat{G}^{\sigma\sigma''}_{\mathbf{k},\mathbf{k}'}(E)\approx\delta_{\sigma\sigma''}\delta_{\mathbf{k},\mathbf{k}'}\widehat{G}_{\mathbf{k}\sigma}(E) \tag{4.15}$$

$$\widehat{G}^{\sigma''\sigma'}_{\mathbf{k}',\mathbf{k+q}}(E)\approx\delta_{\sigma''\sigma'}\delta_{\mathbf{k}',\mathbf{k+q}}\widehat{G}_{\mathbf{k+q}\sigma'}(E) \tag{4.16}$$

where

$$\widehat{G}_{\mathbf{k}\sigma}(E)=\left[E\widehat{I}-\widehat{\epsilon}(\mathbf{k})-\widehat{\Sigma}_{\sigma}(E)\right]^{-1} \tag{4.17}$$

$$\widehat{G}_{\mathbf{k+q}\sigma'}(E)=\left[E\widehat{I}-\widehat{\epsilon}(\mathbf{k+q})-\widehat{\Sigma}_{\sigma'}(E)\right]^{-1} \tag{4.18}$$

The renormalization by the interacting Green functions as performed in Eq. (4.15) and Eq. (4.16) should be a sensible approximation since it is observed that if those interacting Green functions are replaced by the free Green functions,

Eq. (4.9) and Eq. (4.10) respectively, then it leads to the correct low-J (i.e. RKKY) behaviour. Now on substituting Eq. (4.16) in Eq. (4.13) we obtain

$$\begin{aligned}\widehat{G}^{\sigma\sigma'}_{\mathbf{k},\mathbf{k}+\mathbf{q}}(E) &= \delta_{\mathbf{q},0}\delta_{\sigma\sigma'}\widehat{G}^{(0)}_{\mathbf{k}}(E) \\ &\quad - \frac{J}{2N}\sum_i e^{i\mathbf{q}\cdot\mathbf{R}_i}(\mathbf{S}_i\cdot\boldsymbol{\sigma})_{\sigma\sigma'}\widehat{G}^{(0)}_{\mathbf{k}}(E)\widehat{G}_{\mathbf{k}+\mathbf{q}\sigma'}(E) \qquad (4.19)\end{aligned}$$

while substituting Eq. (4.15) in Eq. (4.14) gives

$$\begin{aligned}\widehat{G}^{\sigma\sigma'}_{\mathbf{k},\mathbf{k}+\mathbf{q}}(E) &= \delta_{\mathbf{q},0}\delta_{\sigma\sigma'}\widehat{G}^{(0)}_{\mathbf{k}}(E) \\ &\quad - \frac{J}{2N}\sum_i e^{i\mathbf{q}\cdot\mathbf{R}_i}(\mathbf{S}_i\cdot\boldsymbol{\sigma})_{\sigma\sigma'}\widehat{G}_{\mathbf{k}\sigma}(E)\widehat{G}^{(0)}_{\mathbf{k}+\mathbf{q}}(E) \qquad (4.20)\end{aligned}$$

On adding Eq. (4.19) and Eq. (4.20) we get

$$\begin{aligned}\widehat{G}^{\sigma\sigma'}_{\mathbf{k},\mathbf{k}+\mathbf{q}}(E) &= \delta_{\mathbf{q},0}\delta_{\sigma\sigma'}\widehat{G}^{(0)}_{\mathbf{k}}(E) \\ &\quad - \frac{J}{4N}\sum_i e^{i\mathbf{q}\cdot\mathbf{R}_i}(\mathbf{S}_i\cdot\boldsymbol{\sigma})_{\sigma\sigma'}\widehat{A}^{\sigma\sigma'}_{\mathbf{k},\mathbf{k}+\mathbf{q}}(E) \qquad (4.21)\end{aligned}$$

where

$$\widehat{A}^{\sigma\sigma'}_{\mathbf{k},\mathbf{k}+\mathbf{q}}(E) = \Big(\widehat{G}^{(0)}_{\mathbf{k}}(E)\widehat{G}_{\mathbf{k}+\mathbf{q}\sigma'}(E) + \widehat{G}_{\mathbf{k}\sigma}(E)\widehat{G}^{(0)}_{\mathbf{k}+\mathbf{q}}(E)\Big) \qquad (4.22)$$

For the effective spin Hamiltonian in Eq. (4.2) we need the expectation value $\langle c^\dagger_{\mathbf{k}+\mathbf{q}\alpha\sigma'}c_{\mathbf{k}\alpha\sigma}\rangle$, which we express in terms of the imaginary part of the Green function Eq. (4.21) by exploiting the spectral theorem [108] :

$$\begin{aligned}\frac{1}{N}\sum_{\mathbf{k}}\langle c^\dagger_{\mathbf{k}+\mathbf{q}\alpha\sigma'}c_{\mathbf{k}\alpha\sigma}\rangle &= -\frac{1}{\pi N}ImTr\int_{-\infty}^{\infty}dEf_-(E)\sum_{\mathbf{k}}\widehat{G}^{\sigma\sigma'}_{\mathbf{k},\mathbf{k}+\mathbf{q}}(E) \\ &= \delta_{\mathbf{q},0}\delta_{\sigma\sigma'}\left(\frac{-1}{\pi N}\right)ImTr\int_{-\infty}^{\infty}dEf_-(E)\sum_{\mathbf{k}}\widehat{G}^{(0)}_{\mathbf{k}}(E) \\ +\frac{J}{4\pi N^2}\sum_i\Bigg[e^{i\mathbf{q}\cdot\mathbf{R}_i}&(\mathbf{S}_i\cdot\boldsymbol{\sigma})_{\sigma\sigma'}ImTr\int_{-\infty}^{\infty}dEf_-(E)\sum_{\mathbf{k}}\widehat{A}^{\sigma\sigma'}_{\mathbf{k},\mathbf{k}+\mathbf{q}}(E)\Bigg] \qquad (4.23)\end{aligned}$$

where

$f_-(E) = \dfrac{1}{e^{\frac{E-\mu}{k_BT}}+1}$ and μ being the chemical potential or the Fermi edge.

On substituing Eq. (4.23) in Eq. (4.2) we get

$$\begin{aligned}H_f = \frac{J}{2\pi N}\sum_{i\alpha\sigma\sigma'}\delta_{\sigma\sigma'}(\mathbf{S}_i\cdot\boldsymbol{\sigma})_{\sigma\sigma'}ImTr\int_{-\infty}^{\infty}dEf_-(E)\sum_{\mathbf{k}}\widehat{G}^{(0)}_{\mathbf{k}}(E) \\ -\frac{J^2}{8\pi N^2}\sum_{ij\mathbf{q}\sigma\sigma'}\Bigg[e^{-i\mathbf{q}\cdot\Big(\mathbf{R}_i-\mathbf{R}_j\Big)}(\mathbf{S}_i\cdot\boldsymbol{\sigma})_{\sigma'\sigma}(\mathbf{S}_j\cdot\boldsymbol{\sigma})_{\sigma\sigma'} \\ ImTr\int_{-\infty}^{\infty}dEf_-(E)\sum_{\mathbf{k}}\widehat{A}^{\sigma\sigma'}_{\mathbf{k},\mathbf{k}+\mathbf{q}}(E)\Bigg] \qquad (4.24)\end{aligned}$$

i.e.

$$H_f = -\frac{J}{2}\sum_{i\sigma}(\mathbf{S}_i\cdot\boldsymbol{\sigma})_{\sigma\sigma}\langle n_\sigma^{(0)}\rangle + \frac{J^2}{8N}\sum_{ij\mathbf{q}\sigma\sigma'} e^{-i\mathbf{q}\cdot\left(\mathbf{R}_i-\mathbf{R}_j\right)}(\mathbf{S}_i\cdot\boldsymbol{\sigma})_{\sigma'\sigma}(\mathbf{S}_j\cdot\boldsymbol{\sigma})_{\sigma\sigma'}D_{\mathbf{q}}^{\sigma\sigma'} \tag{4.25}$$

where

$$\langle n_\sigma^{(0)}\rangle = -\frac{1}{\pi}ImTr\int_{-\infty}^{\infty}dEf_-(E)\frac{1}{N}\sum_{\mathbf{k}}\widehat{G}_{\mathbf{k}}^{(0)}(E) \tag{4.26}$$

and

$$D_{\mathbf{q}}^{\sigma\sigma'} = -\frac{1}{\pi}ImTr\int_{-\infty}^{\infty}dEf_-(E)\frac{1}{N}\sum_{\mathbf{k}}\widehat{A}_{\mathbf{k},\mathbf{k}+\mathbf{q}}^{\sigma\sigma'}(E) \tag{4.27}$$

If we perform spin summations on r.h.s of Eq. (4.25) we obtain

$$H_f = -\frac{J}{2}\sum_i\left(\langle n_\uparrow^{(0)}\rangle - \langle n_\downarrow^{(0)}\rangle\right)S_i^z + \frac{J^2}{8N}\sum_{ij\mathbf{q}} e^{-i\mathbf{q}\cdot\left(\mathbf{R}_i-\mathbf{R}_j\right)}\left[D_{\mathbf{q}}^{\uparrow\downarrow}S_i^-S_j^+ + D_{\mathbf{q}}^{\downarrow\uparrow}S_i^+S_j^- + \left(D_{\mathbf{q}}^{\uparrow\uparrow}+D_{\mathbf{q}}^{\downarrow\downarrow}\right)S_i^zS_j^z\right] \tag{4.28}$$

The commutation relations which the spin operators S_i^ζ (ζ = +,-,z) satisfy are given in Appendix B. The first term in the above equation is exactly zero since the free system us unpolarized. This finally yields an effective anisotropic Heisenberg- like spin Hamiltonian which can be written as follows

$$H_f = -\sum_{ij}\left[J_{ij}^{(1)}S_i^-S_j^+ + J_{ij}^{(2)}S_i^+S_j^- + J_{ij}^{(3)}S_i^zS_j^z\right] \tag{4.29}$$

where

$$J_{ij}^{(n)} = \frac{1}{N}\sum_{\mathbf{q}}J^{(n)}(\mathbf{q})\ e^{-i\mathbf{q}\cdot\left(\mathbf{R}_i-\mathbf{R}_j\right)} \qquad \text{(n = 1,2,3)} \tag{4.30}$$

with

$$J^{(1)}(\mathbf{q}) = -\frac{J^2}{8}D_{\mathbf{q}}^{\uparrow\downarrow} \tag{4.31}$$

$$J^{(2)}(\mathbf{q}) = -\frac{J^2}{8}D_{\mathbf{q}}^{\downarrow\uparrow} \tag{4.32}$$

$$J^{(3)}(\mathbf{q}) = -\frac{J^2}{8}\left(D_{\mathbf{q}}^{\uparrow\uparrow}+D_{\mathbf{q}}^{\downarrow\downarrow}\right) \tag{4.33}$$

are the effective exchange integrals which via $G_{\mathbf{k}\sigma}$ are functionals of the conduction electron self-energy thereby getting a temperature and carrier concentration dependence. In order to obtain effective isotropic Heisenberg- like spin Hamiltonian, one has to prove that $D_{\mathbf{q}}^{\uparrow\downarrow} = D_{\mathbf{q}}^{\downarrow\uparrow}$ and $D_{\mathbf{q}}^{\uparrow\uparrow} + D_{\mathbf{q}}^{\downarrow\downarrow} = 2D_{\mathbf{q}}^{\downarrow\uparrow}$ which

will result in $J^{(1)}(\mathbf{q}) = J^{(2)}(\mathbf{q}) = J^{(3)}(\mathbf{q})/2 = J^{\text{eff}}(\mathbf{q})$. For that we proceed as follows :

$$\begin{aligned}
\sum_{\mathbf{k}} \widehat{A}^{\uparrow\downarrow}_{\mathbf{k},\mathbf{k+q}}(E) &= \sum_{\mathbf{k}} \left(\widehat{G}^{(0)}_{\mathbf{k}}(E) \widehat{G}_{\mathbf{k+q}\downarrow}(E) + \widehat{G}_{\mathbf{k}\uparrow}(E) \widehat{G}^{(0)}_{\mathbf{k+q}}(E) \right) \\
&= \sum_{\mathbf{k}} \left(\widehat{G}^{(0)}_{\mathbf{k}}(E) \widehat{G}_{-(\mathbf{k+q})\downarrow}(E) + \widehat{G}_{\mathbf{k}\uparrow}(E) \widehat{G}^{(0)}_{-(\mathbf{k+q})}(E) \right) \\
&\overset{\mathbf{k'}=-(\mathbf{k+q})}{=} \sum_{\mathbf{k'}} \left(\widehat{G}^{(0)}_{-(\mathbf{k'+q})}(E) \widehat{G}_{\mathbf{k'}\downarrow}(E) + \widehat{G}_{-(\mathbf{k'+q})\uparrow}(E) \widehat{G}^{(0)}_{\mathbf{k'}}(E) \right) \\
&\overset{\mathbf{k'}=\mathbf{k}}{=} \sum_{\mathbf{k}} \left(\widehat{G}^{(0)}_{-(\mathbf{k+q})}(E) \widehat{G}_{\mathbf{k}\downarrow}(E) + \widehat{G}_{-(\mathbf{k+q})\uparrow}(E) \widehat{G}^{(0)}_{\mathbf{k}}(E) \right) \\
&= \sum_{\mathbf{k}} \left(\widehat{G}^{(0)}_{\mathbf{k+q}}(E) \widehat{G}_{\mathbf{k}\downarrow}(E) + \widehat{G}_{\mathbf{k+q}\uparrow}(E) \widehat{G}^{(0)}_{\mathbf{k}}(E) \right) \\
&= \sum_{\mathbf{k}} \left(\widehat{G}_{\mathbf{k+q}\uparrow}(E) \widehat{G}^{(0)}_{\mathbf{k}}(E) + \widehat{G}^{(0)}_{\mathbf{k+q}}(E) \widehat{G}_{\mathbf{k}\downarrow}(E) \right) \\
&= \sum_{\mathbf{k}} \left(\widehat{G}^{(0)}_{\mathbf{k}}(E) \widehat{G}_{\mathbf{k+q}\uparrow}(E) + \widehat{G}_{\mathbf{k}\downarrow}(E) \widehat{G}^{(0)}_{\mathbf{k+q}}(E) \right) \\
&= \sum_{\mathbf{k}} \widehat{A}^{\downarrow\uparrow}_{\mathbf{k},\mathbf{k+q}}(E)
\end{aligned} \tag{4.34}$$

i.e.

$$D^{\uparrow\downarrow}_{\mathbf{q}} = D^{\downarrow\uparrow}_{\mathbf{q}}$$

where we have made use of the fact of **k**- independent self-energy and

$$\widehat{\epsilon}(\mathbf{k+q}) = \widehat{\epsilon}(-(\mathbf{k+q})) \tag{4.35}$$

$$\sum_{\mathbf{k}} \widehat{G}_{\mathbf{k+q}\uparrow}(E) \widehat{G}^{(0)}_{\mathbf{k}}(E) = \sum_{\mathbf{k}} \widehat{G}^{(0)}_{\mathbf{k}}(E) \widehat{G}_{\mathbf{k+q}\uparrow}(E) \tag{4.36}$$

and

$$\sum_{\mathbf{k}} \widehat{G}^{(0)}_{\mathbf{k+q}}(E) \widehat{G}_{\mathbf{k}\downarrow}(E) = \sum_{\mathbf{k}} \widehat{G}_{\mathbf{k}\downarrow}(E) \widehat{G}^{(0)}_{\mathbf{k+q}}(E) \tag{4.37}$$

On the similar lines one can prove that

$$\sum_{\mathbf{k}} \left(\widehat{A}^{\uparrow\downarrow}_{\mathbf{k},\mathbf{k+q}}(E) + \widehat{A}^{\downarrow\uparrow}_{\mathbf{k},\mathbf{k+q}}(E) \right) = \sum_{\mathbf{k}} \left(\widehat{A}^{\uparrow\uparrow}_{\mathbf{k},\mathbf{k+q}}(E) + \widehat{A}^{\downarrow\downarrow}_{\mathbf{k},\mathbf{k+q}}(E) \right) \tag{4.38}$$

or

$$2 \sum_{\mathbf{k}} \widehat{A}^{\uparrow\downarrow}_{\mathbf{k},\mathbf{k+q}}(E) = \sum_{\mathbf{k}} \left(\widehat{A}^{\uparrow\uparrow}_{\mathbf{k},\mathbf{k+q}}(E) + \widehat{A}^{\downarrow\downarrow}_{\mathbf{k},\mathbf{k+q}}(E) \right) \tag{4.39}$$

i.e.

$$2 D^{\downarrow\uparrow}_{\mathbf{q}} = D^{\uparrow\uparrow}_{\mathbf{q}} + D^{\downarrow\downarrow}_{\mathbf{q}} \tag{4.40}$$

Thus, we get an effective isotropic Heisenberg spin Hamiltonian

$$H_f = -\sum_{ij}^{n.n} J^{\text{eff}}_{ij} \left[\frac{1}{2} \left(S^-_i S^+_j + S^+_i S^-_j \right) + S^z_i S^z_j \right] \tag{4.41}$$

Now in order to deterimine the f spin magnetization we follow along the lines of Callen [109] that results in

$$\langle S^z\rangle = \frac{\Big(S-\varphi\Big)\Big(1+\varphi\Big)^{2S+1} + \Big(S+1+\varphi\Big)\varphi^{2S+1}}{\Big(1+\varphi\Big)^{2S+1} - \varphi^{2S+1}} \tag{4.42}$$

where $\varphi(S)$ can be interpreted as average magnon number

$$\varphi(S) = \frac{1}{N}\sum_{\mathbf{q}} \frac{1}{e^{E(\mathbf{q})/k_BT}-1} \tag{4.43}$$

depending on S via magnon energies $E(\mathbf{q})$ which in turn can be obtained using the spin Green function as given below which were first proposed by Callen [109] as follows

$$P^{(a)}_{lm}(E) = \langle\langle S^+_l; e^{aS^z_m}\, S^-_m\rangle\rangle_E \tag{4.44}$$

with "a" as a parameter. The equation of motion for such a Green function is evaluated by applying the Hamiltonian as given in Eq. (4.41).

$$\begin{aligned} EP^{(a)}_{lm}(E) &= \delta_{lm}\langle A_a\rangle \\ -\sum_j J^{\text{eff}}_{lj}\langle\langle S^z_l S^+_j; e^{aS^z_m}\, S^-_m\rangle\rangle_E &- \sum_i J^{\text{eff}}_{il}\langle\langle S^z_l S^+_i; e^{aS^z_m}\, S^-_m\rangle\rangle_E \\ +\sum_j J^{\text{eff}}_{lj}\langle\langle S^z_j S^+_l; e^{aS^z_m}\, S^-_m\rangle\rangle_E &+ \sum_i J^{\text{eff}}_{il}\langle\langle S^z_i S^+_l; e^{aS^z_m}\, S^-_m\rangle\rangle_E \end{aligned} \tag{4.45}$$

where

$$\langle A_a\rangle = \langle\Big[S^+_l, e^{aS^z_m}\, S^-_m\Big]_-\rangle \tag{4.46}$$

Within the so-called Tyablikov approximation [110] (or random phase approximation) one finds that

$$\langle\langle S^z_i S^\pm_l; e^{aS^z_m}\, S^\mp_m\rangle\rangle_E \approx \langle S^z_i\rangle\langle\langle S^\pm_l; e^{aS^z_m}\, S^\mp_m\rangle\rangle_E \tag{4.47}$$

On substituting Eq. (4.47) in Eq. (4.45) and taking its Fourier transform we finally get

$$P^{(a)}_{\mathbf{q}} = \frac{\langle A_a\rangle}{E - E(\mathbf{q}) + i0^+} \tag{4.48}$$

where the dressed magnon energies are given by

$$E(\mathbf{q}) = 2\langle S^z\rangle\Big[J^{\text{eff}}(0) - J^{\text{eff}}(\mathbf{q})\Big] \tag{4.49}$$

with $J^{\text{eff}}(0) = J^{\text{eff}}(\mathbf{q}=0)$ and $i0^+$ is a small imaginary part. It is observed that the $\langle S^z\rangle$ appears in electronic self-energy which is used to calculate the exchange integrals. These exchange integrals along with $\langle S^z\rangle$ enter the magnon energies which in turn also appear in $\langle S^z\rangle$. Thus we have found a closed system of equations that can be solved self consistently for all quantities of interest, in particular those which tell us about the mutual influence of electronic and

magnetic properties of the exchange coupled system of itinerant electrons and localized f spins.

One of the central quantities in magnetic system is the Curie temperature, T_c, which can be ascribed as the temperature for which $\langle S^z \rangle \rightarrow 0$. On expanding Eq. (4.42) in $\frac{1}{\varphi(S)}$ we get

$$\langle S^z \rangle = \frac{S(S+1)}{3\varphi(S)} + O\left(\frac{1}{(\varphi(S))^2}\right) \tag{4.50}$$

For $\langle S^z \rangle \rightarrow 0$ we have

$$e^{E(\mathbf{q})/k_B T} \simeq 1 + \frac{E(\mathbf{q})}{k_B T} \tag{4.51}$$

Using Eqs. (4.43), (4.49), (4.50) and (4.51) we obtain

$$\boxed{T_c = \frac{2S(S+1)}{3k_B}\left[\frac{1}{N}\sum_{\mathbf{q}}\left(\frac{1}{J^{\text{eff}}(0) - J^{\text{eff}}(\mathbf{q})}\right)_{T_c}\right]^{-1}} \tag{4.52}$$

One can determine T_c within a self consistent cycle as shown in Figure 4.2 and which can be understood as follows. The single particle energies $\widehat{\epsilon}(\mathbf{k})$, intra-atomic exchange J, quantum spin number S and bandwidth W act as an input parameters in order to evaluate the free propagator, self-energy and full propagator as explained in Chapter 2. Then for a particular band occupation, n, and an initial temperature T_c^{ini}, the Fermi edge, μ which yields the correct value of n, is determined self consistently. Thus fixing upon the Fermi edge one evaluates the temperature dependent exchange integrals which gives the T_c^{fin} through Eq. (4.52). If the obtained temperature, T_c^{fin} is within convergent limit i.e., $\mid T_c^{ini} - T_c^{fin} \mid < \varepsilon$, then it is the resulting T_c for particular J and n. In case of multi- band model, the T_c additionally depends on the hybridization.

In the following section, we try to implement the algorithm as given in Figure 4.2 in order to obtain and analyse the dependence of T_c on various parameters of the model.

4.3 Numerical Results

In this section we would first like to highlight the numerical details in order to calculate the Curie temperature. The starting point are the effective exchange integrals which are as given below:

$$\begin{aligned} J^{\text{eff}}(\mathbf{q}) &= -\frac{J^2}{8}\sum_{\sigma} D_{\mathbf{q}}^{\sigma\sigma} \\ &= -\frac{J^2}{8}\left[-\frac{1}{\pi} Im \int_{-\infty}^{\infty} dE f_-(E) \frac{1}{N}\sum_{\mathbf{k}\sigma} \widehat{A}^{\sigma\sigma}_{\mathbf{k},\mathbf{k}+\mathbf{q}}(E)\right] \end{aligned} \tag{4.53}$$

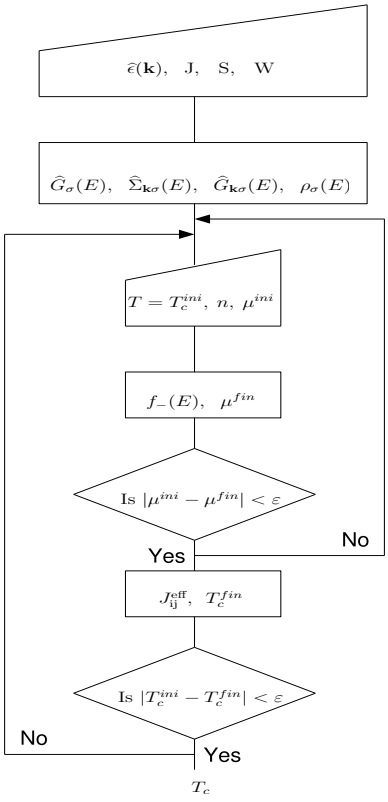

Figure 4.2: Flowchart exhibiting the self consistent determination of Curie temperature, T_c. The terminologies are as explained in the text.

Using Eq. (4.22) and Eq. (4.36) we get

$$\widehat{A}^{\sigma\sigma}_{\mathbf{k},\mathbf{k+q}}(E) = 2\Big(\widehat{G}^{(0)}_{\mathbf{k}}(E)\widehat{G}^{\sigma}_{\mathbf{k+q}}(E)\Big) \tag{4.54}$$

On substituting Eq. (4.54) in Eq. (4.53) and taking the Fourier transform we obtain

$$\begin{aligned} J^{\text{eff}}(\mathbf{q}) &= \frac{J^2}{4\pi}\left[Im\int_{-\infty}^{\infty} dE f_-(E)\frac{1}{N}\sum_{ij\sigma}\widehat{G}^{(0)}_{ij}(E)\widehat{G}^{\sigma}_{ij}(E)e^{i\mathbf{q}\cdot\Big(\mathbf{R}_i-\mathbf{R}_j\Big)}\right] \\ &= \sum_{ij}\left[\frac{J^2}{4\pi}Im\int_{-\infty}^{\infty} dE f_-(E)\frac{1}{N}\sum_{\sigma}\widehat{G}^{(0)}_{ij}(E)\widehat{G}^{\sigma}_{ij}(E)\right]e^{i\mathbf{q}\cdot\Big(\mathbf{R}_i-\mathbf{R}_j\Big)} \\ &= \sum_{ij} J_{ij}e^{i\mathbf{q}\cdot\Big(\mathbf{R}_i-\mathbf{R}_j\Big)} \\ &= \sum_{n,\Delta n} J_{n,\Delta n}e^{i\mathbf{q}\cdot\mathbf{R}_{n,\Delta n}} \end{aligned} \tag{4.55}$$

where

$$\boxed{J_{n,\Delta n} = \frac{J^2}{4\pi}Im\int_{-\infty}^{\infty} dE f_-(E)\frac{1}{N}\sum_{\sigma}\widehat{G}^{(0)}_{n,\Delta n}(E)\widehat{G}^{\sigma}_{n,\Delta n}(E)} \tag{4.56}$$

In the above equation, "n" denotes the n^{th} nearest neighbour shell of radius $\mathbf{R}_n$ spanning Δn number of nearest neighbours to the central atom as shown in Figure 4.3 for the case of 2-D cubic lattice and only upto third shell. In general, it can be extended up to any finite number of shells until convergence for the exchange integrals is reached. This will be explained later on with a more concrete example.

In case of single band, Eq. (4.56) reduces to

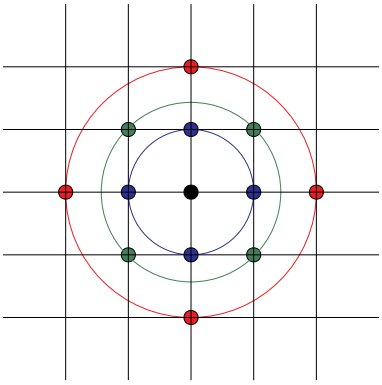

Figure 4.3: The shell model in 2-D cubic lattice with small black filled circle depicting the central atom. The blue, green and red colored circular lines represent the first, second and third nearest neighbouring shell respectively spanning the small filled circles as the corresponding number neighbouring atoms to the central one.

$$J_{n,\Delta n} = \frac{J^2}{4\pi} Im \int_{-\infty}^{\infty} dE f_-(E) \frac{1}{N} \sum_{\sigma} G^{(0)}_{n,\Delta n}(E) G^{\sigma}_{n,\Delta n}(E) \tag{4.57}$$

with

$$\begin{aligned} G^{(0)}_{n,\Delta n}(E) &= \frac{1}{N} \sum_{\mathbf{k}} e^{i\mathbf{k}\cdot\mathbf{R}_{n,\Delta n}} G^{(0)}_{\mathbf{k}}(E) \\ &= \frac{1}{N} \sum_{\mathbf{k}} e^{i\mathbf{k}\cdot\mathbf{R}_{n,\Delta n}} \int_{-\infty}^{\infty} dx \delta(x - \epsilon(\mathbf{k})) G^{(0)}_{x}(E) \\ &= \int_{-\infty}^{\infty} dx \left(\frac{1}{N} \sum_{\mathbf{k}} e^{i\mathbf{k}\cdot\mathbf{R}_{n,\Delta n}} \delta(x - \epsilon(\mathbf{k})) \right) G^{(0)}_{x}(E) \\ &= \int_{-\infty}^{\infty} dx \rho_n(x) G^{(0)}_{x}(E) \end{aligned} \tag{4.58}$$

where we have transformed the $\mathbf{k}$-summation into energy integration using

$$G^{(0)}_{x}(E) = \frac{1}{E - x + i0^+} \tag{4.59}$$

while

$$\boxed{\rho_n(x) = \frac{1}{N} \sum_{\mathbf{k}} e^{i\mathbf{k}\cdot\mathbf{R}_{n,\Delta n}} \delta(x - \epsilon(\mathbf{k}))} \tag{4.60}$$

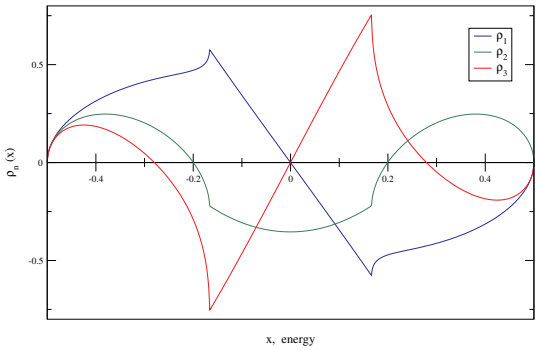

Figure 4.4: The modified density of states of first, second and third shell as shown in blue, green and red respectively.

being the "modified density of states" of the n^{th} shell. The results for first three shells are as shown in Figure 4.4 for 3-D simple cubic lattice with dispersion, $\epsilon(\mathbf{k}) = -\frac{1}{6}(cos(k_x a) + cos(k_y a) + cos(k_z a))$.

Similarly one finds that

$$G^{\sigma}_{n,\Delta n}(E) = \int_{-\infty}^{\infty} dx \rho_n(x) G^{\sigma}_x(E) \tag{4.61}$$

where

$$G^{\sigma}_x(E) = \frac{1}{E - x - \Sigma_\sigma + i0^+} \tag{4.62}$$

and Σ_σ being the electronic self-energy.

Let us now try to understand Eq. (4.56) for a two band model (α and β = 1,2) in order to generalize it by method of induction to an "n" band system. We need to evaluate the following

$$\widehat{G}^{(0)}_{n,\Delta n}(E) = \frac{1}{N} \sum_{\mathbf{k}} e^{i\mathbf{k}\cdot\mathbf{R}_{n,\Delta n}} \widehat{G}^{(0)}_{\mathbf{k}}(E) \tag{4.63}$$

where $\widehat{G}^{(0)}_{\mathbf{k}}(E)$ is a 2 x 2 matrix given as

$$\begin{aligned} \widehat{G}^{(0)}_{\mathbf{k}}(E) &= \left[E\widehat{I} - \widehat{\epsilon}(\mathbf{k})\right]^{-1} \\ &= \begin{bmatrix} E - \epsilon^{11}(\mathbf{k}) & -\epsilon^{12}(\mathbf{k}) \\ -\epsilon^{21}(\mathbf{k}) & E - \epsilon^{22}(\mathbf{k}) \end{bmatrix}^{-1} \\ &= \begin{bmatrix} E - \epsilon^{22}(\mathbf{k}) & \epsilon^{12}(\mathbf{k}) \\ \epsilon^{21}(\mathbf{k}) & E - \epsilon^{11}(\mathbf{k}) \end{bmatrix} \frac{1}{D} \end{aligned} \tag{4.64}$$

with

$$D = \Big(E - \epsilon^{22}(\mathbf{k})\Big)\Big(E - \epsilon^{11}(\mathbf{k})\Big) - \Big(\epsilon^{12}(\mathbf{k})\Big)\Big(\epsilon^{21}(\mathbf{k})\Big) \tag{4.65}$$

Considering $\epsilon^{11}(\mathbf{k}) = -\frac{1}{6}(cos(k_x a)+cos(k_y a)+cos(k_z a))$, $\epsilon^{12}(\mathbf{k}) = \epsilon^{21}(\mathbf{k}) = V$ (local hybridization, LH) or $\epsilon^{12}(\mathbf{k}) = \epsilon^{21}(\mathbf{k}) = V\epsilon^{11}(\mathbf{k})$ (non-local hybridization, NLH) and $\epsilon^{22}(\mathbf{k}) = E_0 + \epsilon^{11}(\mathbf{k})$ we finally get,

$$\widehat{G}^{(0)}_{\mathbf{k}}(E) = \begin{bmatrix} E - E_0 - \epsilon^{11}(\mathbf{k}) & V\epsilon^{11}(\mathbf{k}) \\ V\epsilon^{11}(\mathbf{k}) & E - \epsilon^{11}(\mathbf{k}) \end{bmatrix} \frac{1}{D'} \tag{4.66}$$

where

$$D' = \Big(E - E_0 - \epsilon^{11}(\mathbf{k})\Big)\Big(E - \epsilon^{11}(\mathbf{k})\Big) - V^2 \tag{4.67}$$

for local hybridization and

$$D' = \Big(E - E_0 - \epsilon^{11}(\mathbf{k})\Big)\Big(E - \epsilon^{11}(\mathbf{k})\Big) - V^2\Big(\epsilon^{11}(\mathbf{k})\Big)\Big(\epsilon^{11}(\mathbf{k})\Big) \tag{4.68}$$

for non-local hybridization.

On substituting Eq. (4.66) in Eq. (4.63) we need to carry out the **k**-summation. Since we have considered only one particular type of dispersion relation (nearest neighbour simple cubic) and hence the **k**-summation for each of the matrix element can be transformed into energy integration in the similar way as we did for the case of single band i.e. Eq.(4.58). And analogously, we can evaluate the matrix elements of the Green function $\widehat{G}^{\sigma}_{n,\Delta n}(E)$.

On optimizing the numerical factor [11], we evaluate the Curie temperature, i.e. Eq. (4.52), for various configurations of model parameters. We also try to reproduce the single band result for different values of band occupation as was previously obtained but using another electronic self-energy [111]. This will give us some confidence on the working of the algorithm.

Figure 4.5 shows the dependence of T_c on the strength of intra-atomic ex-

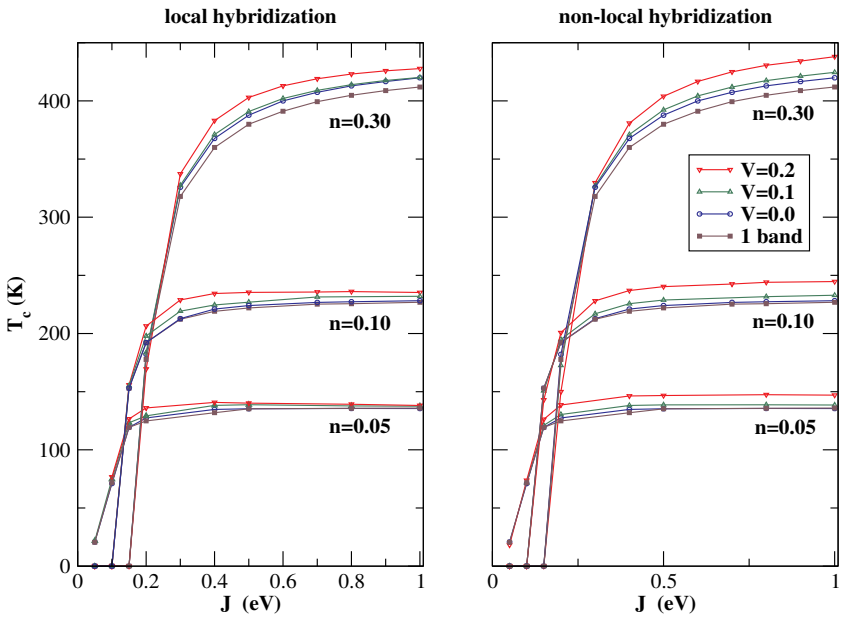

Figure 4.5: The dependence of Curie temperature (T_c) on intra-atomic exchange (J) for different values of band occupation. The exhibited results are for single and two band KLM with local (left panel) and non-local hybridization (right panel) on a simple cubic lattice.

change, J, for single and two band KLM. The left panel describes the results with local hybridization (LH) while the right panel for non-local hybridization

[11] for details please refer to Appendix E

(NLH) on a simple cubic lattice. The bandwidths of both the bands are taken to be 1.0 eV. The calculations are carried out for different values of band occupation, n, and hybridization, V.

Though both the graphs look quite similar but there are marked differences especially in the limit of strong coupling and low band occupation. The general behavior is that initially the T_c rises sharply with increasing J. For weak coupling, the usual RKKY mechanisms is observed predicting a J^2 dependence for T_c. However for higher band occupation, J is observed to exceed a critical value in order to allow ferromagnetism. Furthermore, with increasing J the critical temperature is observed to be deviating more and more from the RKKY behavior and finally reaches a saturation. The calculations done within single band model are comparable with previous calculations [111] obtained using a different self-energy.

As shown in Figure 4.5, the results for T_c in case of two unhybridized bands (V=0.0) are in comparison with that of the one band situation for low band occupation due to similar low energy paramagnetic density of states at the Fermi edge. And with increasing band occupation the results in both the situation (local and non-local hybridization) differ drastically. The values of Curie temperatures are found to be higher and increasing with increasing hybridization strength and band occupation for two hybridized bands as compared to the unhybridized or one band model. It can be understood as follows.

Figure 4.6 shows the low energy window of the paramagnetic density of

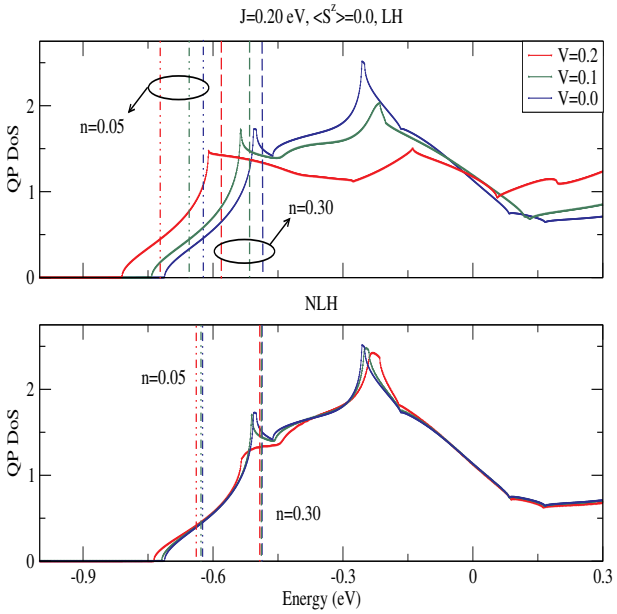

Figure 4.6: Lower edge of paramagnetic density of states of two band KLM with LH (upper panel) and NLH (lower panel) on a sc lattice for J=0.20 eV. The curves and vertical lines in yellow, orange and red are for V=0.0, 0.1 and 0.2 respectively. The vertical lines denotes the Fermi edge with dotted-broken and broken lines for a band occupation, n, of 0.05 and 0.30 respectively.

states of two band KLM with local and non-local hybridization shown in up-

per and lower panel respectively. The calculation is performed for a sc lattice and for J=0.20 eV. The curves and vertical lines in yellow, orange and red are for V=0.0, 0.1 and 0.2. The vertical lines signifies the Fermi edge with dotted-broken and broken lines for a band occupation of 0.05 and 0.30 respectively. The lines within the circle represent the Fermi edge for different values of hybridization but for the same value of band occupation. For low band occupation, the density of states at the Fermi edge are slightly different for different values of hybridization. But with increasing band occupation, the density of states at the Fermi edge changes abruptly for local as well as non-local hybridization.

Though for high band occupation the values of T_c in case of two hybridized

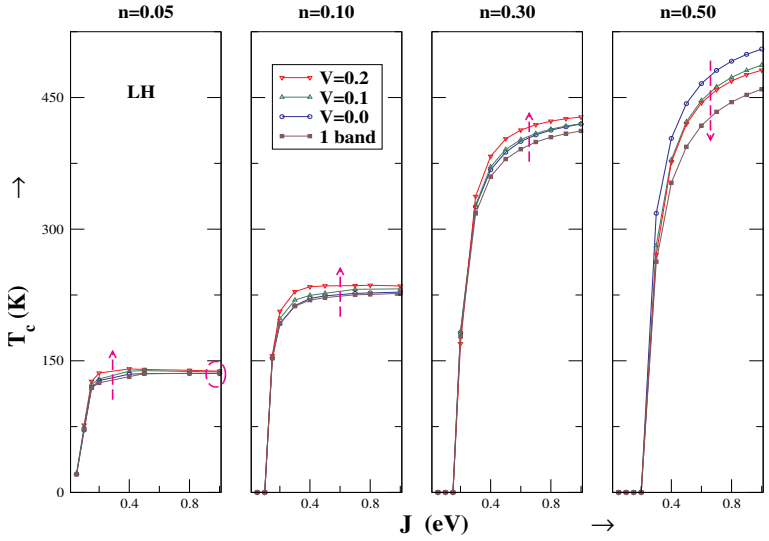

Figure 4.7: The same as in Figure 4.5 but only for LH and an additional result for band occupation of n=0.50.

bands are higher as compared to unhybridized or one band situation but for low band occupation and strong coupling limit, an interesting feature is observed as shown in Figure 4.7. Since this behavior is only noted for two locally hybridized bands so we do not consider the case of non-local hybridization. It is observed that in the limit of strong coupling the T_c starts decreasing for two hybridized band system as compared to two unhybridized band model. In this regime the short range order due to strong intra-atomic exchange and local hybridization decreases the kinetic energy leading to localization of the carrier. This results in decrease of the paramagnetic density of states at the Fermi edge thereby reducing the T_c to the value of the one band case which is encircled in the left-most panel in Figure 4.7. But on increasing the band occupation (moving to the right panels) we observe that the T_c increases with increase in hybridization and even in the limit of strong coupling due to the presence of more delocalized electrons. It can be again understood within the picture of the density of states.

Figure 4.8 shows the low energy spectrum of paramagnetic density of states for two locally hybridized band KLM on a simple cubic lattice for J=0.80 eV.

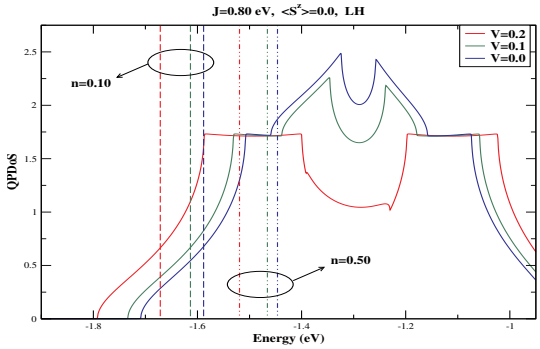

Figure 4.8: Lower edge of paramagnetic density of states for two locally hybridized band KLM on a sc lattice for J=0.80 eV. The curves and vertical lines in yellow, orange and red are for V=0.0, 0.1 and 0.2 respectively. The vertical lines denote the Fermi edge with dotted-broken and broken lines for a band occupation, n, of 0.10 and 0.50 respectively.

The curves and vertical lines in yellow, orange and red are for V=0.0, 0.1 and 0.2. The vertical lines denote the Fermi edge with dotted-broken and broken lines for a band occupation of 0.10 and 0.50 respectively. As observed for n=0.10 that the density of states at the Fermi edge are slightly different giving rise to marginal difference in T_c with increase in hybridization. But with increasing band occupation ($n = 0.30$), the density of states at the Fermi edge differ drastically giving rise to quite different Curie temperatures.

In the strong coupling limit we also observe that the density of states

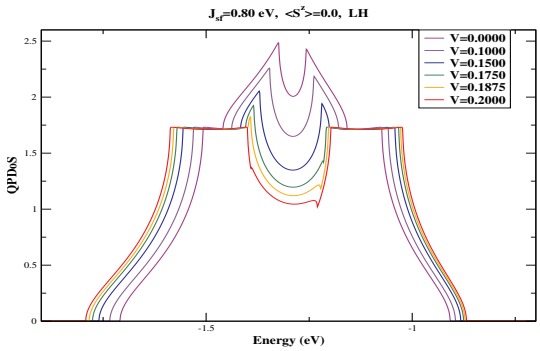

Figure 4.9: Lower edge of paramagnetic density of states for two locally hybridized band KLM on a sc lattice for J=0.80 eV and for different values of hybridization.

tend to seperate out with increasing value of hybridization as shown in Figure 4.8. But the change from V=0.1 to V=0.2 is quite sudden. In order to have a close look at it, we plot the paramagnetic density of states for J=0.80 eV and intermediate values of hybridization from V=0.1 to V=0.2 as shown in Figure 4.9. It is noted that there is an increase in bandwidth with increasing hybridization.

Another interesting feature is observed for band occupation of n=0.50. It is seen that the trend of higher and increasing value of T_c for two locally

hybridized band model is reversed as shown in the right most panel of Figure 4.7. As the Fermi edge keeps on moving to higher energies with an increase in band occupation, the paramagnetic density of states at the Fermi edge keeps on changing. This results in an observed change in the T_c. A similar pattern of decrease in the value of Curie temperature with increase in band occupation and strength of hybridization is also observed in case of non-local hybridization. The explanation lies similar to what we have explained earlier in case of local hybridization.

One the other hand, since the T_c is directly related to exchange integrals

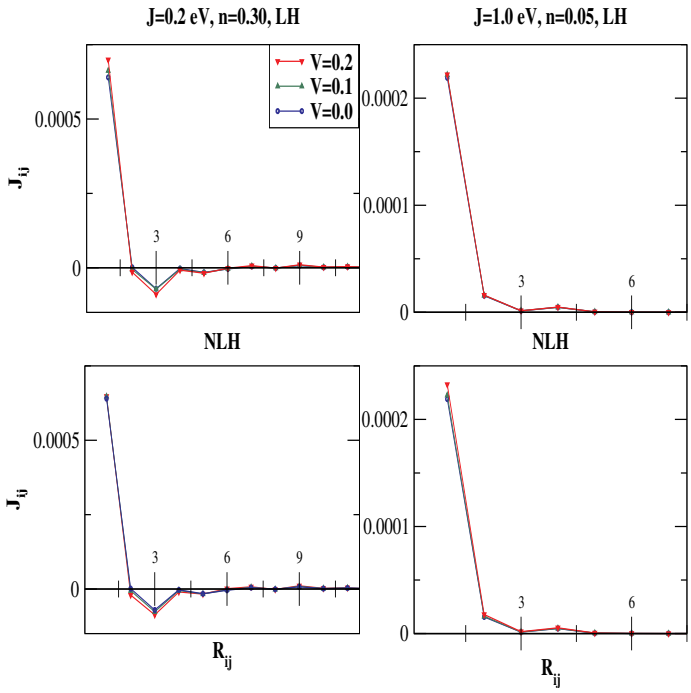

Figure 4.10: The indirect exchange integrals shown as a function of number of shells for local (upper panel) and non-local hybridization (lower panel). The shown results are for two different values of intra-atomic exchange and band occupation but for three different values of hybridization.

(Eq. 4.56), it is also interesting to notice the behavior of these exchange integrals for different values of n, J and V and for local as well as non-local hybridization. Figure 4.10 shows the dependence of indirect exchange integrals on two different parameter configuration of J, n and for three different values of hybridization. We observe the long- range RKKY kind of oscillations for weak coupling in case of local and non-local hybridization. The exchange integrals remain finite up to first twelve shells. In case of strong coupling, the local short range order is more strong. In that case, the exchange integrals gets converged very quickly within a few shells.

In summary, we find that the T_c as a function of intra-atomic exchange for a two band KLM is qualitatively the same for local as well as non-local hybridization between both the bands except for the limit of low band occupation and strong coupling. And in the latter case, the T_c is oscillating in its

dependence on the band occupation due to oscillating behavior of the effective exchange integrals.

Such an analysis can be very useful in order to understand the physical properties of real materials described within the multi- band models like the manganites which are designated within the strong coupling behavior or even the rare-earth metals which are described within the weak coupling regime. It would be equally encouraging to carry out the similar investigation for two different bandwidths of both the bands since the correlation effects scale as $\frac{J}{W}$ where W being the bandwidth [112].

In the following section, we would like to apply the multi- band modified RKKY theory in order to understand the basic mechanism behind the observed ferromagnetism in GdN.

4.4 Ferromagnetism in GdN

There are many puzzles on the mechanism of exchange interaction in GdN as in case of its electronic ground state. Initially, there had also been a dispute regarding the magnetic properties of GdN with earlier reports describing it to be an antiferromagnetic [113, 81] material while other studies indicated it to be a ferromagnet [114, 115]. But after such controversial discourse, it has been accepted that GdN is a ferromagnetic [71, 83, 116] material with experimental reported values of the Curie temperature in the range 58 - 90 K [114, 115, 117, 118, 119, 120, 121, 122, 123, 124, 125, 126, 116, 71, 83]. Phenomenologically GdN seem to behave like the ferromagnetic EuO since they have similar values of T_c [12] and magnetic moments [126]. But however, careful analysis indicates that essential distinction exist in the exchange mechanism between the two compounds.

There are mainly three mechanisms for the magnetic exchange interactions between atoms in the rare earth compounds. The first is due to the second-order perturbation of the intra-atomic *d-f* exchange interaction giving the RKKY interaction. The second is due to the third order perturbation theory of the *d-f* exchange interaction and the *d-f* mixing. The nearest neighbor exchange interaction J_1 in Eu chalcogenides is due to this mechanism. The third is due to the fourth order perturbation of the *d-f* or *p-f* mixings, where *p* are the anion states. The second and third mechanisms are important when the $4f$ level is near the Fermi edge, although they may be ignored when its level is sufficiently below the Fermi energy level. The first mechanism does not depend on the $4f$ level energy. Particularly, this should be the mechanism when the $4f$ level is sufficiently below and above the Fermi edge as found in case of GdN.

This means that the mechanism seems to be quite different in both EuO and GdN but then arises a question as to *why both of them have similar values of* T_c *?*. In order to resolve this issue, let us reconsider the nearest neighbor exchange interaction in Eu chalcogenides as briefly explained in the previous paragraph

[12] The T_c of pure EuO is $\sim$ 69 K.

and try to understand how different will it be in case of GdN. This exchange interaction is dominated by an indirect interaction arising from the virtual excitation of a $4f$ (lying inside the semiconducting gap for EuO) to a $5d$ state, which then overlaps the neighboring Eu and leads to a f-f interaction through the d-f exchange. This d-f exchange essentially measures the spin splitting of the d bands induced by their intra-atomic exchange interaction with the f state. One may visualize the effect as arising from the hopping of f electron to a neighboring site d orbital where it is subject to a spin exchange interaction, J_{df}. In the language of perturbation theory it means that the d orbital gets mixed into f band in an amount $\frac{t_{df}}{(\epsilon_d - \epsilon_f)}$ where t_{df} is the hopping integral and $(\epsilon_d - \epsilon_f)$ is the energy difference between the bottom of the d band and the localized f level. The corresponding contribution to the exchange interaction between the nearest neighbor f sites is inversely proportional to $(\epsilon_d - \epsilon_f)$.

Obviously since $(\epsilon_d - \epsilon_f)$ splitting is much larger in GdN than EuO (as the $4f$ level lie several eV below the Fermi edge in GdN as compared to EuO where it is near the Fermi edge), one would expect a smaller J_1. As a result there are a multide of questions which arise as follows:

- Is there an additional indirect mechanism ? *either the first or third mechanism as explained earlier.*
- If first (RKKY) is believed to be the one then where does the carrier comes from ?
- Are they due to non stochiometry ? *which is often reported experimentally but never measured quantitatively.*
- Does it mean that if it is possible to prepare non-stochiometric GdN then it shall have very low T_c ? *i.e. only second mechanism would prevail.*

In order to explain the additional mechanism, Kasuya and Li [126, 127] tried to sort a way out of this complex problem by developing the fourth order perturbation theory i.e. by choosing the third mechanism. The basic idea is the following. The exchange interaction in GdN can be explained by the cross process between the d-f mixing and d-f exchange interaction to form the $4f^8$ configuration, in which the added $4f$ electron should have the opposite sign direction to that of the $4f^7$ configuration. The lowest order process is of the fourth order, for example the $p(\mathrm{N}) \rightarrow 4f^8 \rightarrow 5d(\mathrm{NNGd}) \rightarrow$ d-f exchange $\rightarrow$ $p(\mathrm{N})$ and its reverse process. Let $(\epsilon_p - \epsilon_d)$ be the energy difference between the bottom of the d band and the top of the p band. Since the exchange interaction depends on inverse of $(\epsilon_p - \epsilon_d)$ and so it is evaluated to be large in GdN since the value of $(\epsilon_p - \epsilon_d)$ is small as compared to that in case of EuO.

But we take another route (*le tour de* RKKY), i.e. the first mechanism as explained earlier and which was also considered by Kuznietz [124]. It is well known that the RKKY mechanism is very sensitive to carrier concentration. Depending on the value of carrier concentration the RKKY oscillation can lie in the ferromagnetic or anti-ferromagnetic lobes. Different preparation methods lead to GdN samples with different carrier concentrations. This could be

the reason why GdN was reported to be an anti-ferromagnet at low fields with Neel temperature, T_N, of 40 K [113, 81].

Regarding the carrier concentration, it is experimentally reported that at the room temperature GdN carries a concentration between 10^{18} and 10^{21} [81, 71]. Though both nitrogen vacancies and oxygen donors have been proposed as a source of free carriers *but no conclusive identification relating the carrier concentration to any of these defects has been achieved.* Above the Curie temperature, it is an indirect small gap semiconductor displaying a thermally activated conductivity : activation energies varying between 1 and 10 meV have been observed [71, 83]. The authors from Ref. [128] have raised an open question *whether the activation energy corresponds to a particular defect level or whether it is the activation energy for hopping conductivity in a degenerate impurity band.*

In order to answer this question, we use our multi- band modified RKKY theory for realistic values of input parameters obtained from the previous chapter in order to evaluate the exchange integrals (Eq. 4.56) and thereby calculate T_c (Eq. 4.52) within a self-consistent scheme (Figure 4.2) for certain low values of carrier concentrations.

Figure 4.11 exhibits the dependence of T_c on carrier concentration for

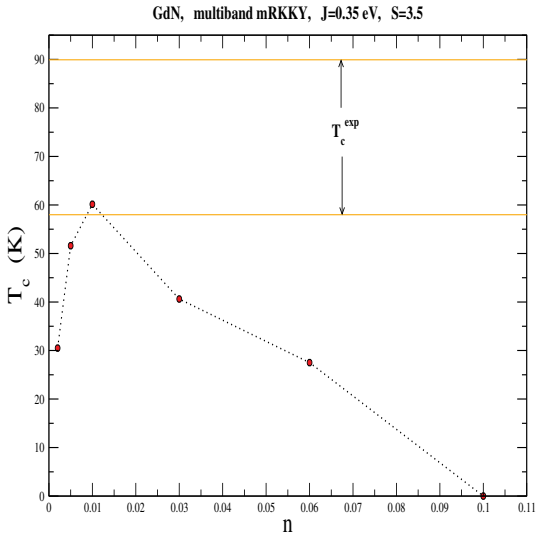

Figure 4.11: The dependence of Curie temperature on band occupation as calculated within modified RKKY theory for J=0.35 eV and S=3.5. The reported experimental range is within 58 - 90 K as shown by two horizontal lines.

GdN with the experimentally reported range depicted by horizontal lines. We obtain highest value of T_c=60.14 K for a carrier concentration,n=0.01 while for concentration of 0.1 the T_c drops down to 0 and this behavior is quite similar to that of substitution of Eu atoms by trivalent rare earth elements (Gd) in compounds of Eu chalcogenides [129].

But since our theoretical model doesn't take into consideration of any impurity level and rather determines the Fermi edge self-consistently for each carrier concentration, so we fall upon the question : *whether do the donor impurities really act as a source of carrier concentration ?*. On looking from the experimental perspective, one would obtain a positive answer to this question since as mentioned before different methods of sample preparation produces different amount of carriers thereby getting a certain range of T_c (58 - 90 K) which is what eventually is observed experimentally.

But in order to confirm the role of carriers and explain one of the anomaly

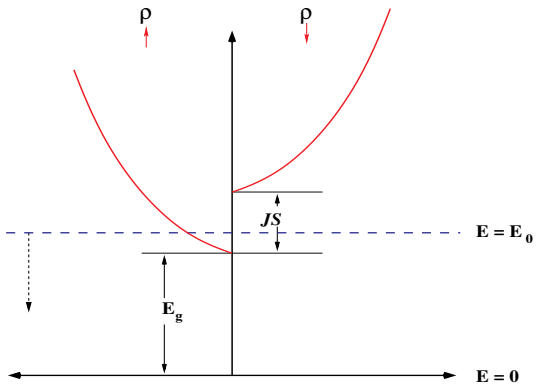

Figure 4.12: A schematic depicting the spin splitting (within mean field) of the density of states below the Curie temperature along with a movable impurity level, $E = E_0$.

in the low temperature behavior of resistivity [83, 130], we regard a very simple model as shown in Figure 4.12. We consider the spin splitting (within the mean field picture having energy difference of the order $\sim$ JS) of the density of states below the Curie temperature and an impurity level which can be shifted in or out of the spin-up bands. Since the impurity concentration in case of intrinsic semiconductor is proportional to the $e^{-\frac{\Delta E}{k_B T}}$, we also consider the resistivity to be proportional to $e^{-\frac{\Delta E}{k_B T}}$,

$$\boxed{\rho = \rho(0)\ e^{-\frac{\Delta E}{k_B T}}} \tag{4.69}$$

where the activation energy, ΔE, is given by

$$\boxed{\Delta E = E_0 - E_g - \frac{JS}{2}\left(1 - \frac{\langle S^z \rangle}{S}\right)} \tag{4.70}$$

The reason to assume such a form of activation enegy can be understood as follows. We try to model a ferromagnetic semiconductor [83] with a finite gap $E_g \gg k_B T$ and described within Kondo lattice model. It governs the temperature dependence via the magnetization ($\langle S^z \rangle$) which we consider within molecular field theory. Below the ferromagnetic transition temperature, T_c, the resistivity will depend on the scattering of carriers due to their interaction

with localized moments. These carriers arise as a result of thermal activation from the impurity level (E_0) in to lower conduction band edge. Above the transition temperature, the resistivity follows the normal thermally activated energy behavior and falls off exponentially with further increase in the temperature.

Now using the same parameters as we have used in case of GdN, i.e. J=0.35, S=$\frac{7}{2}$, E_g=0.30 eV [65] and $T_c = 69$ K [83], we try to evaluate Eq. (4.70) for different values of E_0 and $\rho(0)$. The result is as shown in Figure 4.13. The

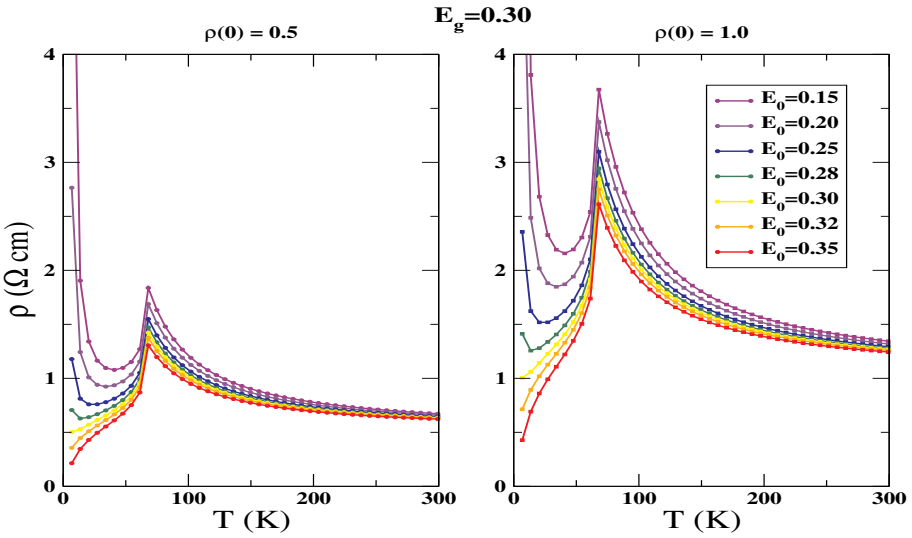

Figure 4.13: Temperature dependent resistivity showing metal-to-insulator transition for $\rho(0) = 0.5$ (left panel) and $\rho(0) = 1.0$ (right panel). Each graph shows the variation of the impurity level, E_0, moving away from inside to outside of the spin-up density of states.

left panel is for $\rho(0)$=0.50 while the right is for $\rho(0)$=1.0. This simple model shows such an important effect of metal-to-insulator transition at low temperature on moving the level E_0 away from the spin-up density of states as shown in Figure 4.12. On increasing $\rho(0)$ we just observe an increase in the value of the peak at $T = T_c$.

Figure 4.14 shows the temperature dependent resitivity with left panel being the experimental result [83] and the right panel being the theoretical fit for certain value of $\rho(0)$ and E_0. The movement of the level within a range of only several meV from the lower conduction band edge exhibits that the experimentally observed resistivity is an artifact of an impurity level i.e. the one which usually corresponds to donor impurities lying close to the lowest conduction band edge.

This explains not only the source of carriers which are eventually responsible for electron mediated ferromagnetism and thus enhancing the effective exchange integrals thereby raising the T_c but also the anomaly at the low temperature behavior of resistivity. Our result also indicate that if non-stochiometric GdN is prepared then it will have a low T_c. This result has to be experimentally verified.

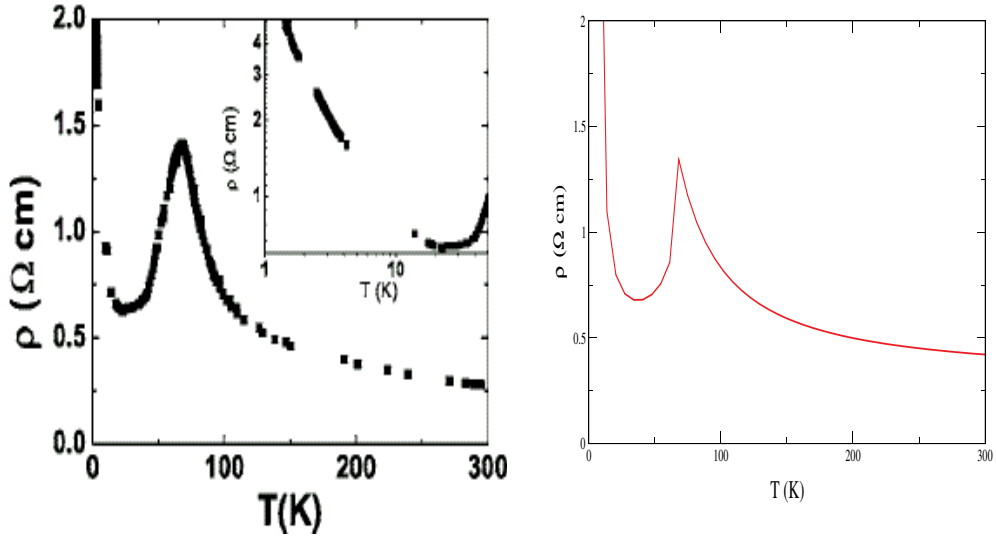

Figure 4.14: Temperature dependent resistivity with left panel showing the experimental result [83] while the theoretical fit is shown on right panel.

But it has motivated us enough so as to include the impurity level within our Kondo lattice model and thus calculate the T_c within a self-consistent scheme by just varying that level in and out of the lower conduction band edge. [131].

Chapter 5

Summary & Outlook

This is not the end. It is not even the beginning of the end. But it is, perhaps, the end of the beginning.

- Sir Winston Churchill.

In this dissertation, the electronic and magnetic properties of the multi-band Kondo lattice model are studied by performing a model calculation followed by its application to real materials like ferromagnetic semiconductors which can be well described within the model under consideration. The generalization of the system is always cross- checked by comparing the results with that of the single band variation and also to other limiting cases of the model. This allows us to systematically study the effect of various parameters of the system and the nature of its physical origin. The electronic and magnetic subsystems are treated within certain approximations and an attempt is made in order to understand the complex many- body physics described by the model.

In Chapter 2, we describe the Kondo problem which is followed by its lattice variation namely the ferromagnetic Kondo lattice model or simply the Kondo lattice model (as is used throughout the text). It is governed by the ferromagnetic intra- atomic exchange between the localized moments and itinerant electrons situated at each site on a periodic lattice. The kinetic energy of the system is characterized by the electrons hopping within a nearest neighbor tight binding description and single band per atom while the potential energy being due to the intra- atomic exchange interaction. In order to solve this model we utilize the Green function theory and equation of motion method. This chapter deals only with the electronic properties of the model i.e. calculating the spectral densities and density of states of the electronic sub- system. The electronic self- energy required for calculating the physical properties for the single band KLM is taken from the earlier proposed ansatz, namely the "interpolating self- energy approach" (ISA). It satisfies various limiting cases of single band KLM like the ferromagnetic saturation, atomic limit, high energy expansion and suitable for low carrier concentration. The spin sub- system is treated within the molecular field theory and the magnetization, being responsible for the temperature dependence, enters as a parameter via the Brillouin function. The strength of intra- atomic exchange and quantum spin are the

other parameters of the model. We study the correlation effects and give physical insights on the observed phenomena.

We extend our theory to the multi- band situation and thereby propose a multi- band self- energy ansatz which is proved to satisfy one of the limiting case of multi- band KLM, i.e. the ferromagnetically saturated semiconductor. In the multi- band model we have an additional parameter i.e. strength of hybridization apart from the parameters as used in the single band situation. We consider two locally hybridized bands per atom, i.e. strength of hybridization is constant, and its dependence on the correlation effect is highlighted. The interesting aspects which comes out of the model study is that it behaves similar to the single band in the limit of strong coupling (intra- atomic exchange).

Chapter 3 deals with an application of the earlier developed many body theory which is combined with the single particle ground state energies so as to study the temperature dependent correlation effects in real materials. The substances under consideration are one each from a rare earth monochalcogenide (Europium Sulphide, EuS) and monopnictide (Gadolinium Nitride, GdN) due to their similar rock- salt and strongly correlated electronic structure. They also have an identical ${}^8\mathrm{S}_{\frac{7}{2}}$ $4f$ shell configuration entailing zero orbital angular momentum.

The first principles calculations are performed within the TB- LMTO program which not only provides the ground state electron energies in the matrix form but also gives the strength of the intra- atomic exchange which is extracted assuming the Stoner theory of ferromagnetism. The obtained single particle energies and intra- atomic exchange enter as an input in the multi-band self energy ansatz which is used in calculating the physical properties of interest like the quasi- particle spectral density and quasi- particle density of states.

We first consider the $3p$ valence bands of EuS. Due to small value of intra-atomic exchange, the temperature dependent correlation effects are found to be rather weak. Only the middle part of energy spectrum in the quasi- particle bandstructure shows some finite lifetime effects. We further consider its $5d$ conduction band which has been calculated earlier by not only using a different self- energy scheme but also by a different way of treating the $5d$ bands. Our simple method of direct use of the kinetic energy matrix circumvents the problem of the somewhat ambiguous decomposition of the conduction band into single non- degenerate sub- bands. Taking this into consideration we find that our results are more pronounced as compared to the previous calculations on the $5d$ conduction bands of EuS. And especially in the high energy region our calculations clearly indicate the presence of strong correlation effects.

Our next step in the analysis of EuS was to combine both the conduction as well as valence bands in order to present for the first time a complete scenario of the temperature dependent quasi- particle bandstructure of any compound.

Finally we consider the similar study of $5d$ conduction bands of one of the rare earth monopnictides, namely GdN. The reason to carry out the familiar analysis for GdN was because this complex compound is not yet fully understood unlike the europium monochalcogenides. Moreover there are some

distinct dissimilarities in the electronic correlation between them which is ascribed to different relative energy position of the $4f$ levels.

We obtain very strong temperature dependent electronic correlation effects in the $5d$ conduction bands of GdN as clearly visible in its quasi- particle bandstructure. We further calculate the red- shift of the lower conduction band edge and find it to be 0.34 eV which is in excellent agreement with that of the very recent experimentally reported value of 0.40 eV. The other theoretical work which uses a different computational and analytical approach for self- energy find the value to be 0.483 eV.

In Chapter 4, we develop the multi- band modified RKKY theory. It concerns with averaging out the electronic charge degrees of freedom thereby mapping the multi- band Kondo lattice model onto an effective spin- spin Heisenberg- like exchange model. The exchange integrals are temperature dependent due to the fact that they depend on the electronic self- energy which in turn is governed by the temperature dependence of magnetization. Thus, both the electronic and magnetic sub- systems are calculated within a self consistent approach.

As a result, we obtain the T_c as a function of intra- atomic exchange J, band occupation n and strength of hybridization V between the bands of a multi- band KLM. We consider only two band model system and find the outcome to be qualitatively the same for local as well as non- local hybridization between both the bands except for the limit of low carrier concentration and strong coupling. And in the latter case, the T_c is oscillating in its dependence on the continous increase in band occupation due to oscillating behavior of the effective exchange integrals.

In order to apply the multi- band modified RKKY theory which might be helpful in explaining the basic mechanism of ferromagnetism in GdN, we first compare it with EuO which has a similar strongly correlated electronic structure and the value of T_c. But the mechanism appears to be different in both the compounds due to the different positioning of the $4f$ level. In order to explain the value of T_c in comparison with EuO, we assume an additional RKKY like mechanism and thereby make use of our multi- band modified RKKY theory. For the realistic input parameters in the theory like the single particle ground state energies, intra- atomic exchange and quantum spin of GdN, we use the same as obtained in Chapter 3. This helps us to evaluate the dependence of T_c on carrier concentration.

We find a sharp rise of T_c for very low carrier concentration which basically highlight their role in stabilizing the T_c. But one could ask whether where do the carriers come from ? In order to further prove their existence and also to understand an anomaly in the low temperature behavior of resistivity, we consider the following toy model. Let us assume spin- split bands below the Curie temperature showing parabolic low energy behavior (as found in case of the bottom of $5d$ conduction bands of GdN) and an impurity level depicting the donor states. These impurities are also mentioned in the experimental works but there has been no concrete description regarding their nature. On assuming a particular form of activation energy (which is proportional to the

logarithm of carrier concentration) we observe a distinct metal- to- insulator transition at low temperature. This effect is a consequence of moving the impurity level away from the lower band edge of the spin- up density of states. It helps to clarify three important facts as observed experimentally. First it indicates the presence of impurities existing at the bottom of the conduction band, secondly it explains the anomalous behavior of the temperature dependent resistivity as observed at the low temperatures and lastly it provides the reason for the experimentally reported wide range of T_c.

Thus the carrier- mediated mechanism (RKKY) is responsible for observed experimental Curie temperature. And according to our theory, non- stochiometric GdN will have a very low value of T_c. This result has to be experimentally verified or has to be evaluated theoretically within a self- consistent cycle which forms the outlook of this thesis.

Appendix A

Green Function Theory

Following is the definition of a double- time retarded Green function (propagator) for any two time- dependent operators, $A(t)$ and $B(t')$:

$$\begin{aligned} G^{(r)}(t,t') &= \langle\langle A(t); B(t')\rangle\rangle^{(r)} \\ &= -i\Theta(t-t')\langle[A(t), B(t')]_{-\eta}\rangle \end{aligned} \tag{A.1}$$

with

$$[A(t), B(t')]_{-\eta} = A(t)B(t') - \eta B(t')A(t) \tag{A.2}$$

where we have used the following terminologies : (r) means retarded ($t > t'$), Θ(t-t$'$) is the well- known Heaviside step function while η = - for Fermions (satisfying canonical anti- commutation relations [CAR]) and η = + for Bosons (satisfying canonical commutation relations [CCR]).

The Green function $G^{(r)}(t,t')$ obeys a differential equation via the so- called equation of motion method producing higher order Green functions which contain more operators as compared to $G^{(r)}(t,t')$. These higher order Green functions when solved within equation of motion method produces even higher order Green functions. This means that one has to deal with an infinite hierarchy of coupled differential equations. In practice, one usually breaks it by making some approximation (decoupling procedure) in the lowest order of the first equation, and simply dropping all the other equations in the chain.

In the following, we set up the equations of motion of the retarded Green function while the same analysis for other types of Green functions (advanced, casual) can be found in Ref [108]. We differentiate the definitions, Eq.(A.1) and Eq.(A.2), with respect to t and make use of the following equation for any general operator, $A(t)$;

$$i\hbar\frac{d}{dt}A(t) = [A(t), H]_{-} \tag{A.3}$$

Then we obtain

$$\begin{aligned} i\frac{d}{dt}G^{(r)}(t,t') &= \frac{d}{dt}\Theta(t-t')\langle[A(t), B(t')]_{-\eta}\rangle \\ &\quad + \langle\langle i\frac{d}{dt}A(t); B(t')\rangle\rangle^{(r)} \end{aligned} \tag{A.4}$$

i.e.

$$i\frac{d}{dt}\langle\langle A(t);B(t')\rangle\rangle^{(r)} = \delta(t-t')\langle[A(t),B(t')]_{-\eta}\rangle + \langle\langle[A(t),H]_{-};B(t')\rangle\rangle^{(r)} \tag{A.5}$$

where we have assumed $\hbar = 1$ and it has remained so throughout the thesis. We have also made use of the following relation between the discontinuous Heaviside function and delta function,

$$\Theta(t) = \int_{-\infty}^{t}\delta(t)dt \tag{A.6}$$

The commutator $[A(t),H]_{-}$ on the right will give Green functions which generally contain more operators than the left. The equation of motion of these higher order Green function is;

$$i\frac{d}{dt}\langle\langle[A(t),H]_{-};B(t')\rangle\rangle^{(r)} = \delta(t-t')\langle[[A(t),H]_{-},B(t')]_{-\eta}\rangle + \langle\langle[[A(t),H]_{-},H]_{-};B(t')\rangle\rangle^{(r)} \tag{A.7}$$

Generally, the last term has again a higher order than the term on the left and has a new equation of motion and so on. Finally, one obtains an infinite chain of equations of the Green functions as discussed before and thus, one is forced upon using some kind of an approximation. But before doing so it is useful to calculate the Fourier transform of $\langle\langle A(t);B(t')\rangle\rangle^{(r)}$,

$$\langle\langle A;B\rangle\rangle_{E}^{(r)} = \int_{-\infty}^{+\infty} d(t-t')\ \langle\langle A(t);B(t')\rangle\rangle^{(r)}\ e^{iE(t-t')} \tag{A.8}$$

because then we obtain ordinary equations instead of differential equations i.e.

$$E\langle\langle A;B\rangle\rangle_{E}^{(r)} = \langle[A,B]_{-\eta}\rangle + \langle\langle[A,H]_{-};B\rangle\rangle_{E}^{(r)} \tag{A.9}$$

The simplest approximation of the Green function is obtained if one can convert the term $\langle\langle[A,H]_{-};B\rangle\rangle_{E}^{(r)}$ to the form $F\,\langle\langle A;B\rangle\rangle_{E}^{(r)}$. Then it is possible to solve Eq.(A.9) with respect to $\langle\langle A;B\rangle\rangle_{E}^{(r)}$:

$$G^{(r)}(E) = \langle\langle A;B\rangle\rangle_{E}^{(r)} = \frac{\langle[A,B]_{-\eta}\rangle}{(E-F(E))} \tag{A.10}$$

Thus in the simplest approximation, $G^{(r)}(E)$ has one pole, i.e. $E-F(E)=0$ while in higher approximation one can expect more involved singularities (branch points, cut, etc...). It can be shown with the help of methods of contour integration that $G^{(r)}(E)$ can be analytically continued in the complex energy plane.

Now if we consider $A = c_{i\sigma}$ and $B = c_{j\sigma}^{\dagger}$, where are $c_{i\sigma}$ and $c_{j\sigma}^{\dagger}$ are annihilation and creation operators of an electron respectively, then we can define the corresponding single particle or one electron Green function:

$$G_{ij\sigma}^{(r)}(E) = \langle\langle c_{i\sigma};c_{j\sigma}^{\dagger}\rangle\rangle_{E}^{(r)} \tag{A.11}$$

and its Fourier transform:

$$G_{\mathbf{k}\sigma}^{(r)}(E) = \frac{1}{N}\sum_{ij}G_{ij\sigma}^{(r)}(E)\ e^{-i\mathbf{k}\cdot(\mathrm{R}_i-\mathrm{R}_j)} \tag{A.12}$$

Appendix B

CAR algebra and Fourier transforms

In this thesis, we make use of the following canonical anti- commutation relations (CAR) algebra :

$$[c_{i\alpha\sigma}, c_{j\beta\sigma'}]_+ = [c^\dagger_{i\alpha\sigma}, c^\dagger_{j\beta\sigma'}]_+ = 0 \tag{B.1}$$

$$[c_{i\alpha\sigma}, c^\dagger_{j\beta\sigma'}]_+ = \delta_{ij}\delta_{\alpha\beta}\delta_{\sigma\sigma'} \tag{B.2}$$

$$[c_{i\alpha\sigma}, n^\dagger_{j\beta\sigma'}]_- = \delta_{ij}\delta_{\alpha\beta}\delta_{\sigma\sigma'}c_{i\alpha\sigma} \tag{B.3}$$

where

$$n_{j\beta\sigma'} = c^\dagger_{j\beta\sigma'}c_{j\beta\sigma'} \tag{B.4}$$

and the spin operators which satisfy the following commutation relations :

$$[S^\sigma_i, S^z_j]_- = -z_\sigma\delta_{ij}S^\sigma_i \tag{B.5}$$

$$[S^\sigma_i, S^{-\sigma}_j]_- = 2z_\sigma\delta_{ij}S^z_i \tag{B.6}$$

Now if we consider H_{kin} and H_{int} as defined in Eq. 2.18 and Eq. 2.19, then upon using the above relations one obtains;

$$\begin{aligned}
[c_{l\mu\sigma}, H_{kin}]_- &= \sum_{ij\alpha\beta\sigma'} T^{\alpha\beta}_{ij}[c_{l\mu\sigma}, c^\dagger_{i\alpha\sigma'}c_{j\beta\sigma'}]_- \\
&= \sum_{ij\alpha\beta\sigma'} T^{\alpha\beta}_{ij}(c_{l\mu\sigma}c^\dagger_{i\alpha\sigma'}c_{j\beta\sigma'} - c^\dagger_{i\alpha\sigma'}c_{j\beta\sigma'}c_{l\mu\sigma}) \\
&= \sum_{ij\alpha\beta\sigma'} T^{\alpha\beta}_{ij}\delta_{il}\delta_{\alpha\mu}\delta_{\sigma\sigma'}c_{j\beta\sigma'} \\
&= \sum_{j\beta} T^{\mu\beta}_{lj}c_{j\beta\sigma}
\end{aligned} \tag{B.7}$$

$$
\begin{aligned}
[c_{l\mu\sigma}, H_{int}]_- &= -\frac{J}{2}\sum_{i\alpha\sigma'}\Big(z_{\sigma'}S_i^z[c_{l\mu\sigma}, n_{i\alpha\sigma'}]_- + S_i^{\sigma'}[c_{l\mu\sigma}, c_{i\alpha\sigma'}^\dagger c_{i\alpha\sigma'}]_-\Big) \\
&= -\frac{J}{2}\sum_{i\alpha\sigma'}\Big(z_{\sigma'}S_i^z\delta_{il}\delta_{\alpha\mu}\delta_{\sigma\sigma'}c_{l\mu\sigma} \\
&+ S_i^{\sigma'}[c_{l\mu\sigma}c_{i\alpha-\sigma'}^\dagger c_{i\alpha\sigma'} - c_{i\alpha-\sigma'}^\dagger c_{i\alpha\sigma'}c_{l\mu\sigma}]\Big) \\
&= -\frac{J}{2}\sum_{i\alpha\sigma'}\Big(S_i^z\delta_{il}\delta_{\alpha\mu}\delta_{\sigma\sigma'}c_{l\mu\sigma} + S_i^{\sigma'}\delta_{il}\delta_{\alpha\mu}\delta_{-\sigma'\sigma}c_{i\alpha\sigma'}\Big) \\
&= -\frac{J}{2}\Big(z_\sigma S_l^z c_{l\mu\sigma} + S_l^{-\sigma}c_{l\mu-\sigma}\Big) \qquad \text{(B.8)}
\end{aligned}
$$

$$
[S_k^+ c_{l\mu\uparrow}, H_{kin}]_- = S_k^+[c_{l\mu\uparrow}, H_{kin}]_- = S_k^+\sum_{j\beta}T_{lj}^{\mu\beta}c_{j\beta\uparrow} \qquad \text{(B.9)}
$$

$$
\begin{aligned}
[S_k^+ c_{l\mu\uparrow}, H_{int}]_- &= S_k^+[c_{l\mu\uparrow}, H_{int}]_- + [S_k^+, H_{int}]_-\, c_{l\mu\uparrow} \\
&= -\frac{J}{2}\Bigg[S_k^+\Big(S_l^z c_{l\mu\uparrow} + S_l^- c_{l\mu\downarrow}\Big) \\
&+ \Big(\sum_{i\alpha\sigma} z_\sigma[S_k^+, S_i^z]_- n_{i\alpha\sigma} - [S_k^+, S_i^\sigma]_- c_{i\alpha-\sigma}^\dagger c_{i\alpha\sigma}\Big)c_{l\mu\uparrow}\Bigg] \\
&= -\frac{J}{2}\Bigg[S_k^+\Big(S_l^z c_{l\mu\uparrow} + S_l^- c_{l\mu\downarrow}\Big) \\
&+ \Big(\sum_{i\alpha}\Big(\sum_\sigma z_\sigma(-\delta_{ik}S_k^+)n_{i\alpha\sigma}\Big) - 2\delta_{ik}S_k^z c_{i\alpha\uparrow}^\dagger c_{i\alpha\downarrow}\Big)c_{l\mu\uparrow}\Bigg] \\
&= -\frac{J}{2}\Bigg[S_k^+\Big(S_l^z c_{l\mu\uparrow} + S_l^- c_{l\mu\downarrow}\Big) \\
&- \Big(\sum_\alpha\Big(\sum_\sigma z_\sigma S_k^+ n_{k\alpha\sigma}\Big) + 2S_k^z c_{k\alpha\uparrow}^\dagger c_{k\alpha\downarrow}\Big)c_{l\mu\uparrow}\Bigg] \qquad \text{(B.10)}
\end{aligned}
$$

Now let us consider the following :

$$
\frac{1}{N}\sum_{lm} e^{-i\mathbf{k}\cdot\Big(\mathbf{R}_i - \mathbf{R}_j\Big)}T_{lm}^{\mu\nu} = \epsilon^{\mu\nu}(\mathbf{k}) \qquad \text{(B.11)}
$$

$$
\frac{1}{N}\sum_{lm} e^{-i\mathbf{k}\cdot\Big(\mathbf{R}_l - \mathbf{R}_m\Big)}G_{lm\sigma}^{\mu\nu}(E) = G_{\mathbf{k}\sigma}^{\mu\nu}(E) \qquad \text{(B.12)}
$$

and

$$
\frac{1}{N^{\frac{3}{2}}}\sum_{klm} e^{-i\Big(\mathbf{q}\cdot\mathbf{R}_k + \Big(\mathbf{k}-\mathbf{q}\Big)\cdot\mathbf{R}_l - \mathbf{k}\cdot\mathbf{R}_m\Big)}A_{klm\sigma}^{\mu\nu}(E) = A_{\mathbf{k},\mathbf{k}-\mathbf{q},\mathbf{q}\sigma}^{\mu\nu}(E) \qquad \text{(B.13)}
$$

where $A_{klm\sigma}^{\mu\nu}(E) = \Gamma_{klm\sigma}^{\mu\nu}(E),\ \ F_{klm\sigma}^{\mu\nu}(E)$.

With the help of above equations, the Fourier transforms appearing in

chapter 2 can be evaluated as given below :

1) $$\frac{1}{N}\sum_{lm} e^{-i\mathbf{k}\cdot\left(\mathbf{R}_l-\mathbf{R}_m\right)}\sum_{j\beta} T_{lj}^{\mu\beta} G_{jm\sigma}^{\beta\nu}(E)$$

$$= \frac{1}{N}\sum_{lmj\beta} e^{-i\mathbf{k}\cdot\left(\mathbf{R}_l-\mathbf{R}_m\right)}\left(\frac{1}{N}\sum_{\mathbf{k}'}\epsilon^{\mu\beta}(\mathbf{k}')e^{i\mathbf{k}'\cdot\left(\mathbf{R}_l-\mathbf{R}_j\right)}\right)G_{jm\sigma}^{\beta\nu}(E)$$

$$= \frac{1}{N}\sum_{mj\beta}\sum_{\mathbf{k}'} e^{-i\left(\mathbf{k}'\cdot\mathbf{R}_j-\mathbf{k}\cdot\mathbf{R}_m\right)}\epsilon^{\mu\beta}(\mathbf{k}')\underbrace{\frac{1}{N}\sum_{l} e^{i\left(\mathbf{k}'-\mathbf{k}\right)\cdot\mathbf{R}_l}}_{\delta_{\mathbf{k}',\mathbf{k}}} G_{jm\sigma}^{\beta\nu}(E)$$

$$= \sum_{\beta}\epsilon^{\mu\beta}(\mathbf{k})\frac{1}{N}\sum_{mj} e^{-i\mathbf{k}\cdot\left(\mathbf{R}_j-\mathbf{R}_m\right)}G_{jm\sigma}^{\beta\nu}(E)$$

$$= \sum_{\beta}\epsilon^{\mu\beta}(\mathbf{k})G_{\mathbf{k}\sigma}^{\beta\nu}(E) \qquad \text{(B.14)}$$

2) $$\frac{1}{N^{\frac{3}{2}}}\sum_{klm} e^{-i\left(\mathbf{q}\cdot\mathbf{R}_k+(\mathbf{k}-\mathbf{q})\cdot\mathbf{R}_l-\mathbf{k}\cdot\mathbf{R}_m\right)}\sum_{p\gamma} T_{lp}^{\mu\gamma} F_{kpm\downarrow}^{\gamma\nu}(E)$$

$$= \frac{1}{N^{\frac{3}{2}}}\sum_{klpm\gamma} e^{-i\left(\mathbf{q}\cdot\mathbf{R}_k+(\mathbf{k}-\mathbf{q})\cdot\mathbf{R}_l-\mathbf{k}\cdot\mathbf{R}_m\right)}\left(\frac{1}{N}\sum_{\mathbf{k}'}\epsilon^{\mu\gamma}(\mathbf{k}')e^{i\mathbf{k}'\cdot\left(\mathbf{R}_l-\mathbf{R}_p\right)}\right)F_{kpm\downarrow}^{\gamma\nu}(E)$$

$$= \frac{1}{N^{\frac{3}{2}}}\sum_{kpm\gamma}\sum_{\mathbf{k}'} e^{-i\left(\mathbf{q}\cdot\mathbf{R}_k+(\mathbf{k}-\mathbf{q})\cdot\mathbf{R}_p-\mathbf{k}\cdot\mathbf{R}_m\right)}\epsilon^{\mu\gamma}(\mathbf{k}')\underbrace{\frac{1}{N}\sum_{l} e^{i\left[\mathbf{k}'-\left(\mathbf{k}-\mathbf{q}\right)\right]\cdot\mathbf{R}_l}}_{\delta_{\mathbf{k}',\mathbf{k}-\mathbf{q}}} F_{kpm\downarrow}^{\gamma\nu}(E)$$

$$= \sum_{\gamma}\epsilon^{\mu\gamma}(\mathbf{k})\frac{1}{N^{\frac{3}{2}}}\sum_{kpm} e^{-i\left(\mathbf{q}\cdot\mathbf{R}_k+(\mathbf{k}-\mathbf{q})\cdot\mathbf{R}_p-\mathbf{k}\cdot\mathbf{R}_m\right)}F_{kpm\downarrow}^{\gamma\nu}(E)$$

$$= \sum_{\gamma}\epsilon^{\mu\gamma}(\mathbf{k})F_{\mathbf{k},\mathbf{k}-\mathbf{q},\mathbf{q}\downarrow}^{\gamma\nu}(E) \qquad \text{(B.15)}$$

3) $$\frac{1}{N^{\frac{3}{2}}}\sum_{klm} e^{-i\left(\mathbf{q}\cdot\mathbf{R}_k+(\mathbf{k}-\mathbf{q})\cdot\mathbf{R}_l-\mathbf{k}\cdot\mathbf{R}_m\right)}\delta_{kl}F_{klm\downarrow}^{\mu\nu}(E)$$

$$= \frac{1}{N^{\frac{3}{2}}}\sum_{klm} e^{-i\left(\mathbf{q}\cdot\mathbf{R}_k+(\mathbf{k}-\mathbf{q})\cdot\mathbf{R}_l-\mathbf{k}\cdot\mathbf{R}_m\right)}\left(\frac{1}{N}\sum_{\mathbf{k}'} e^{i\mathbf{k}'\cdot\left(\mathbf{R}_k-\mathbf{R}_l\right)}\right)F_{klm\downarrow}^{\mu\nu}(E)$$

$$= \frac{1}{N}\sum_{\mathbf{k}'}\frac{1}{N^{\frac{3}{2}}}\sum_{klm} e^{-i\left[\left(\mathbf{q}-\mathbf{k}'\right)\cdot\mathbf{R}_k+\left[\mathbf{k}-\left(\mathbf{q}-\mathbf{k}'\right)\right]\cdot\mathbf{R}_l-\mathbf{k}\cdot\mathbf{R}_m\right]}F_{klm\downarrow}^{\mu\nu}(E)$$

$$= \frac{1}{N}\sum_{\mathbf{k}'}\frac{1}{N^{\frac{3}{2}}}\sum_{klm} e^{-i\left(\mathbf{t}\cdot\mathbf{R}_k+(\mathbf{k}-\mathbf{t})\cdot\mathbf{R}_l-\mathbf{k}\cdot\mathbf{R}_m\right)}F_{klm\downarrow}^{\mu\nu}(E) \quad \left[\text{taking}\left(\mathbf{q}-\mathbf{k}'\right)\rightarrow\mathbf{t}\right]$$

$$= \frac{1}{N}\sum_{\mathbf{t}} F^{\mu\nu}_{\mathbf{k,k\text{-}t,t}\downarrow}(E) \tag{B.16}$$

4) $\frac{1}{N^{\frac{3}{2}}}\sum_{klm} e^{-i\left(\mathbf{q}\cdot\mathbf{R}_k+(\mathbf{k}\text{-}\mathbf{q})\cdot\mathbf{R}_l-\mathbf{k}\cdot\mathbf{R}_m\right)}\delta_{kl}G^{\mu\nu}_{lm\downarrow}(E)$

$$= \frac{1}{N^{\frac{3}{2}}}\sum_{klm} e^{-i\left(\mathbf{q}\cdot\mathbf{R}_k+(\mathbf{k}\text{-}\mathbf{q})\cdot\mathbf{R}_l-\mathbf{k}\cdot\mathbf{R}_m\right)}\left(\frac{1}{N}\sum_{\mathbf{k}'} e^{i\mathbf{k}'\cdot\left(\mathbf{R}_k-\mathbf{R}_l\right)}\right)G^{\mu\nu}_{lm\downarrow}(E)$$

$$= \frac{1}{N}\sum_{\mathbf{k}'}\frac{1}{N^{\frac{3}{2}}}\sum_{klm} e^{-i\left[\left(\mathbf{q}-\mathbf{k}'\right)\cdot\mathbf{R}_k+\left[\mathbf{k}-\left(\mathbf{q}-\mathbf{k}'\right)\right]\cdot\mathbf{R}_l-\mathbf{k}\cdot\mathbf{R}_m\right]}G^{\mu\nu}_{lm\downarrow}(E)$$

$$= \sum_{\mathbf{k}'}\frac{1}{N^{\frac{3}{2}}}\sum_{lm} e^{-i\left[\left[\mathbf{k}-\left(\mathbf{q}-\mathbf{k}'\right)\right]\cdot\mathbf{R}_l-\mathbf{k}\cdot\mathbf{R}_m\right]}\left(\frac{1}{N}\sum_{k} e^{-i\left[\left(\mathbf{q}-\mathbf{k}'\right)\cdot\mathbf{R}_k\right]}\right)G^{\mu\nu}_{lm\downarrow}(E)$$

$$= \sum_{\mathbf{k}'}\frac{1}{N^{\frac{3}{2}}}\sum_{lm} e^{-i\left[\left[\mathbf{k}-\left(\mathbf{q}-\mathbf{k}'\right)\right]\cdot\mathbf{R}_l-\mathbf{k}\cdot\mathbf{R}_m\right]}\underbrace{\left(\frac{1}{N}\sum_{k} e^{-i\left[\left(\mathbf{q}-\mathbf{k}'\right)\cdot\mathbf{R}_k\right]}\right)}_{\delta_{\mathbf{q},\mathbf{k}'}}G^{\mu\nu}_{lm\downarrow}(E)$$

$$= \frac{1}{N^{\frac{3}{2}}}\sum_{lm} e^{-i\mathbf{k}\cdot\left(\mathbf{R}_l-\mathbf{R}_m\right)}G^{\mu\nu}_{lm\downarrow}(E)$$

$$= \frac{1}{N^{\frac{1}{2}}}\left(\frac{1}{N}\sum_{lm} e^{-i\mathbf{k}\cdot\left(\mathbf{R}_l-\mathbf{R}_m\right)}G^{\mu\nu}_{lm\downarrow}(E))\right)$$

$$= \frac{1}{N^{\frac{1}{2}}}G^{\mu\nu}_{\mathbf{k}\downarrow}(E) \tag{B.17}$$

Appendix C

Density Functional Theory

The goal of density functional theory (DFT) as introduced by Hohenberg and Kohn [50] is to find the exact ground state density and total energy of a system of N interacting electrons in an external potential which is achieved using the following two theorems due to them :

First theorem: The external potential $v(\mathbf{r})$ is a unique functional of the ground state density $\mathrm{n}(\mathbf{r})$ of a many-electron system, apart from a trivial additive constant.
An immediate consequence is that the ground state expectation value of any observable $\widehat{O}$ is a unique functional of the exact ground state electron density,

$$\langle\Psi|\widehat{O}|\Psi\rangle = O[\mathrm{n}] \tag{C.1}$$

Second theorem: The ground state energy assumes its minimum value for the correct $\mathrm{n}(\mathbf{r})$, if the admissible functions are restricted by the condition,

$$N[\mathrm{n}] = \int \mathrm{n}(\mathbf{r})d\mathbf{r} = N \tag{C.2}$$

The proof of the above theorems can be found in the original paper [50]. Although the Hohenberg-Kohn theorems are extremely powerful, they do not offer a way of computing the ground state energies of an interacting system in practice. About one year after the Hohenberg- Kohn's seminal DFT paper, Kohn and Sham [51] devised a simple method for carrying out DFT calculations that retains its exact nature. Their formulation centred on mapping the full interacting system with the real potential onto a fictitious non- interacting system whereby the electrons move within an effective "Kohn- Sham" single-particle potential $v_{KS}(\mathbf{r})$. The Kohn- Sham potential,$v_{KS}(\mathbf{r})$ is constructed to ensure that the ground state density of the non- interacting fictitious system equals the ground state density of the interacting system. This method is still exact and greatly facilitates the calculation. The Kohn- Sham potential constitutes of an external potential, a Hartree potential and an exchange-correlation potential and within an approximate scheme for the exchange- correlation potential one can calculate the ground state single particle energies of such a mapped non- interacting system as briefly explained below :

Consider a Hamiltonian, $\widehat{H} = \widehat{T} + \widehat{U} + \widehat{V}$, of a stationary (time- independent) system of N interacting electron where $\widehat{T}$ is the kinetic energy, $\widehat{U}$ being

the potential energy due to electron-electron interaction and $\widehat{V}$ as the static external potential.

Within Hohenberg-Kohn's first theorem, for $\widehat{O}$ being the hamiltonian $\widehat{H}$, the ground state total energy functional $H[\mathrm{n}] = E_v[\mathrm{n}]$ is of the form

$$\begin{aligned} E_v[\mathrm{n}] &= \underbrace{\langle\Psi|\widehat{T}+\widehat{U}|\Psi\rangle}_{F_{HK}[\mathrm{n}]} + \langle\Psi|\widehat{V}|\Psi\rangle \\ &= F_{HK}[\mathrm{n}] + \int \mathrm{n}(\mathbf{r})v(\mathbf{r})d\mathbf{r} \end{aligned} \tag{C.3}$$

where the electron density is obtained from the many- body wavefunction, which is usually the ground state wavefunction of the above Hamiltonian.

Now let us consider the variational problem presented in the second Hohenberg-Kohn theorem that the ground state energy of a many- electron system can be obtained by minimising the energy functional, subject to the constraint that the number of electrons N is conserved, which leads to

$$\delta\left[F[\mathrm{n}(\mathbf{r})] + \int \mathrm{n}(\mathbf{r})v(\mathbf{r})d\mathbf{r} - \mu\left(\int \mathrm{n}(\mathbf{r})d\mathbf{r} - N\right)\right] = 0 \tag{C.4}$$

and the corresponding Euler equation is given by,

$$\mu = \frac{\delta F[\mathrm{n}(\mathbf{r})]}{\delta \mathrm{n}(\mathbf{r})} + v(\mathbf{r}) \tag{C.5}$$

where μ is the Lagrange multiplier associated with the constraint of constant N. The idea of Kohn and Sham was to set up a system where the interacting single particle Hamiltonian could be determined exactly as this was a major problem in Thomas-Fermi [49] theory. This was achieved by invoking a non-interacting system of electrons. The corresponding groundstate wavefunction Ψ_{KS} for this type of system is given exactly by a determinant of single- particle orbitals $\psi_i(\mathbf{r}_i)$,

$$\Psi_{KS} = \frac{1}{\sqrt{N!}}\ \det[\psi_1(\mathbf{r}_1)\psi_2(\mathbf{r}_2)\ldots\psi_N(\mathbf{r}_N)]$$

The universal functional $F[\mathrm{n}(\mathbf{r})]$ was then partitioned into three terms,

$$F[\mathrm{n}(\mathbf{r})] = T_s[\mathrm{n}(\mathbf{r})] + E_H[\mathrm{n}(\mathbf{r})] + E_{XC}[\mathrm{n}(\mathbf{r})] \tag{C.6}$$

where $T_s[\mathrm{n}(\mathbf{r})]$ is the kinetic energy of a non- interacting electron gas of density $\mathrm{n}(\mathbf{r})$ and $E_H[\mathrm{n}(\mathbf{r})]$ is the classical electrostatic (Hartree) energy of the electrons which are known exactly while $E_{XC}[\mathrm{n}(\mathbf{r})]$ is the exchange- correlation energy, being discussed in the section 1.1, which contains the difference between the exact and non- interacting kinetic energies plus the non-classical contribution to the electron-electron interactions of which the exchange energy is a part. The first two terms in Eq. (C.6) constitute the majority of the energy while the third being a small unknown quantity, except in case of strongly correlated electron systems. Therefore any discussion of the validity of the above equations has to focus on how well we can approximate the density of an interacting

system with that of a non- interacting system.

In the Kohn-Sham prescription, the Euler equation now becomes

$$\mu = \frac{\delta T_s[\mathrm{n}(\mathbf{r})]}{\delta \mathrm{n}(\mathbf{r})} + v_{KS}(\mathbf{r}) \tag{C.7}$$

where the Kohn-Sham potential $v_{KS}(\mathbf{r})$ is given by

$$v_{KS}(\mathbf{r}) = v(\mathbf{r}) + v_H(\mathbf{r}) + v_{XC}(\mathbf{r}) \tag{C.8}$$

The ground state density is obtained in practice by solving the N one-electron Schrödinger equations,

$$\left[T_s[\mathrm{n}(\mathbf{r})] + v_{KS}(\mathbf{r})\right]\psi_i(\mathbf{r}) = \varepsilon_i \psi_i(\mathbf{r}) \tag{C.9}$$

where ε_i are Lagrange multipliers corresponding to the orthonormality of the N single-particle states $\psi_i(\mathbf{r})$, and the density is constructed from,

$$\mathrm{n}(\mathbf{r}) = \sum_{i=1}^{N} |\psi_i(\mathbf{r})|^2 \tag{C.10}$$

Although exact in principle, Kohn-Sham theory is approximate in practice because of the unknown exchange-correlation functional $E_{XC}[\mathrm{n}(\mathbf{r})]$. An implicit definition of $E_{XC}[\mathrm{n}(\mathbf{r})]$ can be given as,

$$E_{XC}[\mathrm{n}(\mathbf{r})] = T[\mathrm{n}(\mathbf{r})] - T_s[\mathrm{n}(\mathbf{r})] + E_{ee}[\mathrm{n}(\mathbf{r})] - E_H[\mathrm{n}(\mathbf{r})] \tag{C.11}$$

where $T[\mathrm{n}(\mathbf{r})]$ and $E_{ee}[\mathrm{n}(\mathbf{r})]$ are the exact kinetic and electron-electron interaction energies respectively.

It can be shown [51] that all functionals can be written in the following general form,

$$E_{XC}[\mathrm{n}(\mathbf{r})] = \int \mathrm{n}(\mathbf{r})\varepsilon_{XC}(\mathbf{r})d\mathbf{r} \tag{C.12}$$

where $\varepsilon_{XC}(\mathbf{r})$ is the exchange-correlation energy per particle, or energy density for short. Functionals can be characterised by the way in which the density surrounding each electron is sampled in order to construct $\varepsilon_{XC}(\mathbf{r})$.

The type of functional which we used in our calculations is the oldest, simplest and probably the most important functional, the local density approximation (LDA). In the following text, we present a very brief description of it.

The LDA was proposed by Kohn and Sham [51]. It consists of locally approximating the true exchange-correlation energy of a system by the exchange-correlation energy associated with a homogeneous electron gas of the same density. The LDA is only dependent on the local density, and the total energy is commonly written as,

$$E_{XC}^{LDA}[\mathrm{n}(\mathbf{r})] = \int \mathrm{n}(\mathbf{r})\varepsilon_{XC}^{hom}[\mathrm{n}(\mathbf{r})]d\mathbf{r} \tag{C.13}$$

where $\varepsilon_{XC}^{hom}[\mathrm{n}(\mathbf{r})]$ is the exchange-correlation energy density corresponding to a homogeneous electron gas of density $\mathrm{n}(\mathbf{r})$. The energy can be decomposed

into exchange, $E_X[\mathrm{n}(\mathbf{r})]$, and correlation, $E_C[\mathrm{n}(\mathbf{r})]$, contributions. The latter is determined from an interpolation formula that connects the known limiting form of $\varepsilon_C^{hom}[\mathrm{n}(\mathbf{r})]$ in the high and low density limits.

Despite its simplicity, the LDA works well for bulk systems and has been widely used in solid state calculations for many years. However, its success is limited and does not transfer to systems with strongly inhomogeneous charge densities e.g., calculated atomic ionization energies are greatly in error, its tendency to overbind is particularly severe for molecules.

Some of the other approximations which are also in use are as listed below,

1. Local Spin Density Approximation (LSDA) which is a straightforward generalization of the LDA to include electron spin :

$$E_{XC}^{LSDA}[\mathrm{n}_\uparrow(\mathbf{r}), \mathrm{n}_\downarrow(\mathbf{r})] = \int \mathrm{n}(\mathbf{r})\varepsilon_{XC}^{hom}[\mathrm{n}_\uparrow(\mathbf{r}), \mathrm{n}_\downarrow(\mathbf{r})]d\mathbf{r} \tag{C.14}$$

2. Generalized Gradient Approximations (GGA) which takes into account the gradient of the density at the same co-ordinate:

$$E_{XC}^{GGA}[\mathrm{n}_\uparrow(\mathbf{r}), \mathrm{n}_\downarrow(\mathbf{r})] = \int \mathrm{n}(\mathbf{r})\varepsilon_{XC}^{hom}[\mathrm{n}_\uparrow(\mathbf{r}), \mathrm{n}_\downarrow(\mathbf{r}), \nabla\mathrm{n}_\uparrow(\mathbf{r})\nabla\mathrm{n}_\downarrow(\mathbf{r})]d\mathbf{r} \tag{C.15}$$

3. Self-Interaction Correction (SIC) [132] is a correction to the single particle energies formed due to any of the above mentioned approximations,

$$E_{XC}^{SIC} = E_{XC}^{approx}[\mathrm{n}_\uparrow(\mathbf{r}), \mathrm{n}_\downarrow(\mathbf{r})] - \sum_{\alpha\sigma}\delta_{\alpha\sigma} \tag{C.16}$$

where

$$\delta_{\alpha\sigma} = U[\mathrm{n}_{\alpha\sigma}] + E_{XC}^{approx}[\mathrm{n}_{\alpha\sigma}, 0] \tag{C.17}$$

is the self-interaction of orbital $\alpha\sigma$.

During the last 40 years or so there has been a lot of development in extending or generalizing DFT. Accordingly, the field of theoretical material science has progressed rapidly by making use of DFT. Due to the vastness of the subject, we don't include it in our thesis and interested audience is directed towards already existing excellent books [133, 134, 135] and reviews [136, 137] for further reading.

Appendix D

Photoemission Spectroscopy

An electron which is bound in an atom, molecule or solid is fully characterized by quantum numbers such as those for energy, momentum or angular momentum. Among many techniques which probe such quantum numbers, photoelectron spectroscopy (PES) is distinct in being universal and direct. From the discovery of the photoelectric effect in the early days of the 20th century, photoemission spectroscopy has developed into an invaluable experimental method for the study of electron excitations in bulk solids and surfaces. PES and its inverse counterpart (IPES) have been instrumental for our current understanding of elementary excitation processes in condensed matter and for deciphering the electronic structure of many materials. The success of PES and IPES owes much to the interpretation of the photoelectron spectra in terms of single particle excitations or quasi-particles in the language of many-body theory. An excellent review in this respect is given by Onida [138] while in the following text we present a brief introduction of the much involved subject.

In PES, electrons are ejected from a sample upon irradiation with visible or ultraviolet light (UPS) or with x-rays (XPS), as schematically shown in Figure D.1a). The energy of the bound electron states ϵ_{i} can be calculated from the photon energy $\mathrm{h}\nu$ and the kinetic energy $\mathrm{E_{kin}}$ of the photoelectrons that reach the detector as follows,

$$\epsilon_{\mathrm{i}} = \mathrm{h}\nu - \mathrm{E_{kin}} \tag{D.1}$$

The above equation defines the binding energy of the electron in the solid. In other words, if one considers the photoelectrons to be completely decoupled from the sample then due to energy and momentum conservation law one can deduce the change in total energy of the sample, which is interpreted as the energy level of the "hole" i.e. the level that was formerly occupied by the photoelectron. Hence as a first approach one can state that photoemission measures the density of occupied states.

By inverting the photoemission process, as schematically sketched in Figure D.1b), the unoccupied states can be probed. An incident electron with energy, $\epsilon_i = \mathrm{E_{kin}}$ is scattered in the sample which eventually will undergo a radiative transition into a lower-lying unoccupied state, emitting a photon that carries the transition energy $\mathrm{h}\nu$. The energy of the final, unoccupied state can

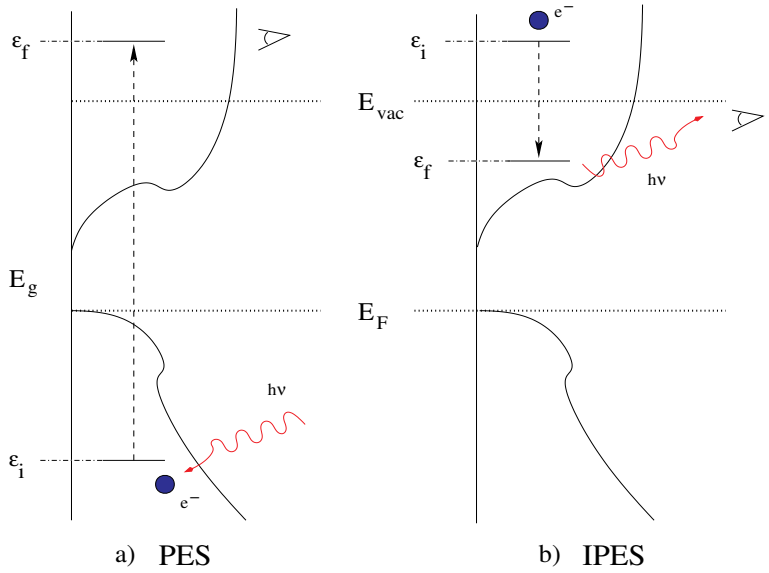

Figure D.1: Schematic of the PES and IPES process. In PES (left) an electron (e^-) is excited from an occupied valence state into the continuum starting above the vacuum level E_{vac} by an incoming photon (red wavy arrow) of energy $h\nu$. In IPES (right), an injected electron with kinetic energy $\epsilon_i = E_{kin}$ undergoes a radiative transition to an unoccupied state emitting a photon in the process. Herer, E_F is the Fermi energy of the system.

be deduced from the measured photon energy using the following relation,

$$\epsilon_f = E_{kin} - h\nu \tag{D.2}$$

This technique is commonly referred to as IPES or bremsstrahlung isochromat spectroscopy (BIS). The experimental observable in PES is the photocurrent. The structures in the photoemission spectrum can be associated with features in the density of states (DOS), i.e. if the imaginary part of the single particle Green function is known,

$$S_{\mathbf{k}}(E) = -\frac{1}{\pi} Im G_{\mathbf{k}}(E) \tag{D.3}$$

then the photocurrent is the integral of the spectral function, $A_{\mathbf{k}}$. In Eq. (D.3), we have used the single particle Green function as defined in section 2.2:

$$G_{\mathbf{k}}(E) = [(E + i0^+) - \epsilon(\mathbf{k}) - \Sigma_{\mathbf{k}}(E)]^{-1} \tag{D.4}$$

The interpretation of photoemission spectra as a density of occupied states is linked to the picture of independent electrons which occupy some well defined energy level in the system. But it is clear that electrons are not independent and while leaving the sample they will lead the remaining electrons to relax. This relaxation energy and other quantum mechanical contributions must be taken into account if energy differences are to be calculated correctly. In other words, in photoemission the single electron energy levels are renormalized by

the presence of the other electrons. One can then still retain the picture of single particle energy levels, but these particles are quasielectrons and quasi-holes, i.e. they contain the effects of all the other particles and are in general known as quasi-particles [139] as introduced in section 2.2.

Thus in theory, the many body Hamiltonian can be transformed into single particle Hamiltonian with a non-interacting part and another term which contains all the electron-electron interaction. The latter can be assigned with the self-energy of the particle which is complex in general due to Dyson's equation :

$$\Sigma_{\mathbf{k}}(E) = G_{\mathbf{k}}^{(0)-1}(E) - G_{\mathbf{k}}^{-1}(E) \tag{D.5}$$

where the non-interacting (free) single electron Green function is given as:

$$G_{\mathbf{k}}^{(0)}(E) = [(E + i0^{+}) - \epsilon(\mathbf{k})]^{-1} \tag{D.6}$$

In theory of Fermi liquids [140], the real part of this complex self-energy is associated with the energy of the quasi-particle excitation and the imaginary part with its inverse lifetime.

Further, by varying the angle of incidence [angle-resolved photoelectron spectroscopy (ARPES) [141, 142] and **k**-resolved inverse photoelectron spectroscopy (KRIPES) [143]], dispersion relations of the excited states can be obtained.

In the above consideration, the analysis is just based upon the energy and momentum of the photoelectron but in general it is also possible to measure the spin-resolved photoemission for ferromagnets.

Appendix E

Technical Aspects

In the following we mention a few technical points of importance which are used in order to optimize the numerical parameters in our results as obtained in chapter 4. As it is known from the literature that conventional RKKY (cRKKY) exhibits a long range order so we need a large number of shells (see Figure 4.3) for the exchange integrals i.e. Eq. (4.56) to get converged within certain limit. So, one of the other important aspect remains the strength of the small imaginary part.

In Figure E.1, the exchange integrals for the case of single band model

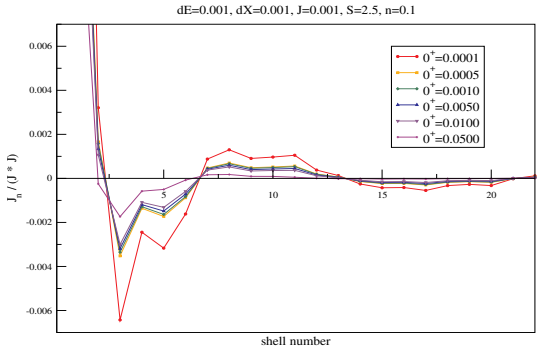

Figure E.1: The exchange integrals for single band KLM at T=0 K for n=0.1 in the low-J limit and different values of the small imaginary part. The sizes of the inner and outer energy intervals used for integration are 0.001 eV.

are plotted for S=$\frac{5}{2}$, n=0.1 in the low-J limit at T=0 K and different values of the small imaginary part. The energy intervals, outer dE and inner dx, used in Eq. (4.56), (4.58) and (4.61) are 0.001 eV each. We observe that for a certain range of interval of 0^+ ($0.0005 < 0^+ < 0.01$) the exchange integrals are quantitatively the same while in the other regions the oscillations either increase ($0^+ > 0.01$) or decrease ($0^+ < 0.0005$). This will amount in a slight change of values in the Curie temperaures and this sensitivity has to be taken care of while comparing results with different calculations.

In Figure E.2, we have repeated the calculations as shown in Figure E.1 but for more number of energy points i.e. smaller values of the outer and inner energy intervals as compared to the previous one. It is observed that the

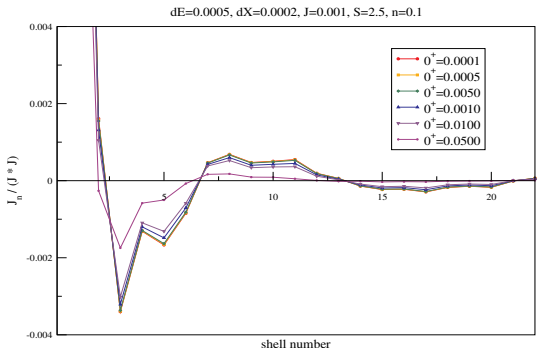

Figure E.2: The same as in Figure E.1 but for inner and outer energy intervals of 0.0002 and 0.0005 eV respectively.

exchange integrals remain sensitive to the higher values ($0^+ > 0.01$) of small imaginary part while least susceptible to smaller values of 0^+ which is quite expected and can be understood as follows. The smaller the value of 0^+, the less is full width half maximum of the delta peak which is due to 0^+. And now, if the energy interval is decreased or equivalently the number of energy points are increased then more delta peaks are taken into account giving approximate value of integration which is quite closer to the actual value. On the other hand increase in energy interval or rather decrease in the number of energy points leaves out a lot of delta peaks which results in the not so accurate integration. All this analysis helps us to optimize the value of small imaginary part while using the adaptive routines [13] for performing energy integrations.

[13] We use the *dqag* 1-D quadrature available within SLATEC libraries from NETLIB.

Acknowledgement

This work would not have been possible without the help of a lot of people and here, I take an opportunity to express my gratitude towards them.

It would have been unmanageable to successfully finish this work without the support of my supervisor, Prof. Wolfgang Nolting. I would like to thank him for giving me an opportunity to work in his group and for providing interesting projects, especially the problem regarding Gadolinium Nitride. His help has been instrumental in guiding me right from the beginning until the end of this work. I would like to appreciate his careful reading and comments on the initial version of this thesis and ofcourse for translating the abstract in to German language. At various stages of this work, his valuable suggestions were like a strong field acting on my poly- directional thoughts and allowing them to point in the right direction.

I am also grateful to the Humboldt University at Berlin for the financial support throughout this work.

I would like to thank our group secretary, Frau Marion Goetsch fuer die Behandlung aller administrativen Probleme und fuer das Verbessern meiner deutsch Sprachkenntnisse[14].

Working at the TFK group was a great learning as well as an enjoyable experience. Dr. Wolf Mueller helped me with the TB- LMTO- ASA program and discussing all sorts of scientific, numerical and administrative problems with Dr. Tilmann Hickel, Dr. Carlos Santos, Dr. Peter Sinjukow, Jochen Kienert, Soeren Henning, Vadym Bryksa, Martin Stier and Niko Sandschneider helped me reach the end. Special thanks to Soeren and Vadym, "the Bryksa" for creating the lighter moments. Due to space constraint I might have not mentioned the names of some of the former and present colleagues of the group but ofcourse I do not underestimate the value of their contribution.

A valuable addition to my scientific knowledge was imparted by the guest scientists like Prof. Anupuru Ramakanth, Prof. Peter Dowben, Prof. Wladyslaw Borgiel, Prof. A. Dmietriev, Dr. Gangadhar Reddy, Dr. Tang and Prof. Avinash Singh. I would also like to thank Prof. Walter Lambrecht, Prof. C.-g.Duan and PD Dr. Eyert for sharing their work on GdN.

The support of the Indian diaspora never made me feel homesick. My roommates, Manu and Bansi, deserve a special recognition. Right from dawn, by waking up listening to "desi" radio, till dusk, by ending up eating the delicious food, their help in all terms is indescribable. The weekends and other social

[14]for handling all the administrative problems and for improving my german language skills

events were full of fun due to Aniket, Rashmi, Nimisha, Krishnan, Deepika, Rohan, Ram, Umesh, Titu, Sangeeta, Avik, Harsh, Kanchan, Sakshi, Dev, Anuya, Abhay n family, Satish, Jatin,...[15]. I thank them for setting up the mood for playing cards "all- the- nite" and these days getting in to poker fewer. I would also like to thank "lord" Krishna, Shekar, Prajna, Anindita, Sushil, Joanna, Ela, Matthias, Marcin, Arun, Pranav, Abhinav, Prasad, Anjali and Harshad for providing some cherishable moments during my stay in Germany.

One of my hobby of reading books led me to join a book club in Berlin and i would like to thank Geert, for introducing me to the club, while I am grateful to Irene, Cary, Violet, Conny and Hannelies for providing the right kind of an atmosphere.

I am obliged to all my friends in India who kept me motivated though being distant apart.

No words of gratitude can express the way I wish to thank my family members and I would like to dedicate this work to them. I wish to express my deepest appreciation to my parents : Madanlal Sharma and Bhagwati Sharma, my brother : Manoj Sharma, and his family, and my sister : Manisha Mudgal, and her family and my brother cum friend : Mohit for giving me their love and all the emotional support.

Last but not the least I would like to thank Dorothea for tolerating and supporting me at the last stages of this work.

Thank you all.

[15]and all those who do not find themselves in the list due to space limitations

Bibliography

[1] M. Born and R. Oppenheimer. Zur quantentheorie der molekeln. *Ann. Phys. (Leipzig)*, 389:457, 1927.

[2] D. Vollhardt. Elektronische korrelationen im festkörper: Vom modell zum material. http://www.physik.uni-augsburg.de/theo3/Talks/Berlin_Magnus-Haus_Jan07.pdf, 2007.

[3] M.N.Baibich, J.M.Broto, A.Fert, F.Nguyen Van Dau, F.Petroff, P.Eitenne, G.Creuzet, A.Friederich, and J.Chazelas. Giant magnetoresistance of (001)Fe/(001)Cr magnetic superlattices. *Phys. Rev. Lett.*, 61: 2472, 1988.

[4] P. Grünberg, R.Schreiber, Y.Pang, M.B.Brodsky, and H.Sowers. Layered magnetic structures: Evidence for antiferromagnetic coupling of Fe layers across Cr interlayers. *Phys. Rev. Lett.*, 57:2442, 1986.

[5] T.Dietl. Why ferromagnetic semiconductors? *Acta Phys. Pol. A*, 100: S139, 2001.

[6] B.T.Matthias, R.M.Bozorth, and J.H.Van Vleck. Ferromagnetic interaction in EuO. *Phys. Rev. Lett.*, 7:160, 1961.

[7] T.R.McGuire, B.E.Argyle, M.W.Shafer, and J.S.Smart. Ferromagnetism in divalent Europium salts. *Appl. Phys. Lett.*, 1:17, 1962.

[8] J.K.Furdyna. Diluted magnetic semiconductors. *J. Appl. Phys.*, 64:R29, 1988.

[9] T.Jungwirth, J.Sinova, J.Masek, J.Kucera, and A.H.MacDonald. Theory of ferromagnetic (III,Mn)V semiconductors. *Rev. Mod. Phys.*, 78:809, 2006.

[10] T.Jungwirth, K.Y.Wang, J.Masek, K.W.Edmonds, J.König, J.Sinova, M.Polini, N.A.Goncharuk, A.H.MacDonald, M.Sawicki, A.W.Rushforth, R.P.Campion, L.X.Zhao, C.T.Foxon, and B.L.Gallagher. Prospects for high temperature ferromagnetism in (Ga,Mn)As semiconductors. *Phys. Rev. B*, 72:165204, 2005.

[11] W.J. de Haas, J.de Boer, and G.J.van den Berg. The electrical resistance of gold, copper and lead at low temperatures. *Physica*, 1:1115, 1934.

[12] S.Vonsovskii. Electron theory of transition metals. *Zh. Eksperim. i Teor. Fiz. (Sov. Phys. JETP)*, 16:981, 1946.

[13] J.Kondo. Resistance minimum in dilute magnetic alloys. *Prog. Theor. Phys.*, 32:37, 1964.

[14] A.M.Tsvelick and P.B.Wiegmann. Exact results in the theory of magnetic alloys. *Adv. in Phys.*, 32:453, 1983.

[15] N.Andrei, K.Furuya, and J.H.Lowenstein. Solution of the Kondo problem. *Rev. Mod. Phys.*, 55:331, 1983.

[16] A.C.Hewson. *The Kondo Problem to Heavy Fermions*. Cambridge University Press, London, UK, 1997.

[17] Kondo effect - 40 years after the discovery. http://www.ipap.jp/jpsj/announcement/announce2004Dec.htm, 2004.

[18] P.W.Anderson. Localized magnetic states in metals. *Phys. Rev.*, 124:41, 1961.

[19] P. de Faget de Casteljau and J. Friedel. Étude de la résistivité et du pouvoir thermoélectrique des impuretés dissoutes dans les métaux nobles. *J. Phys. Radium*, 17:27, 1956.

[20] J.Bonca, P.Prelovsek, A.Ramsak, and S.Sarkar. *Open Problems in Strongly Correlated Electron Systems*. Springer, Berlin, Germany, 2001. NATO Science Series II: Mathematics, Physics and Chemistry.

[21] R.Jullien, J.Fields, and S.Doniach. Kondo lattice: Real-space renormalization-group approach. *Phys. Rev. Lett.*, 38:1500, 1977.

[22] W.Nolting. Theory of ferromagnetic semiconductors. *Phys. Status Solidi B*, 96:11, 1979.

[23] A.J.Millis, P.B.Littlewood, and B.I.Shraiman. Double exchange alone does not explain the resistivity of $La_{1-x}Sr_xMnO_3$. *Phys. Rev. Lett.*, 74: 5144, 1995.

[24] R.Schiller. *Correlation effects and temperature dependencies in thin ferromagnetic films - magnetism and electronic structure*. PhD thesis, Humboldt Universität zu Berlin, Germany, 2000. http://edoc.huberlin.de/dissertationen/schiller-roland-2000-11-01/PDF/Schiller.pdf.

[25] C.Santos, W.Nolting, and V.Eyert. Ferromagnetism and temperature-dependent electronic structure of hcp Gadolinium. *Phys. Rev. B*, 69: 214412, 2004.

[26] J.Kienert and W.Nolting. Curie temperature of Kondo lattice films with finite itinerant charge carrier density. *Phys. Rev. B*, 75:094401, 2007.

[27] G.Tang and W.Nolting. Carrier-induced ferromagnetism in diluted local-moment systems. *Phys. Rev. B*, 75:024426, 2007.

[28] A.Singh, S.K.Das, A.Sharma, and W.Nolting. Spin dynamics in the diluted ferromagnetic Kondo lattice model. *J. Phys.: Cond. Mat.*, 19: 236213, 2007.

[29] W.Nolting and M.Matlak. Complete analytical solution for the zero bandwidth s-f model. *Phys. Status Solidi B*, 123:155, 1984.

[30] W. Metzner and D. Vollhardt. Correlated lattice fermions in d=∞ dimensions. *Phys. Rev. Lett.*, 62:324, 1989.

[31] W.Nolting, S.Rex, and S.Mathi Jaya. Magnetism and electronic structure of a local moment ferromagnet. *J. Phys.: Cond. Mat.*, 9:1301, 1997.

[32] D.Meyer, C.Santos, and W.Nolting. Quantum effects in the quasiparticle structure of the ferromagnetic Kondo lattice model. *J. Phys.: Cond. Mat.*, 13:2531, 2001.

[33] A.Georges, G.Kotliar, W.Krauth, and M.J.Rozenberg. Dynamical mean-field theory of strongly correlated fermion systems and the limit of infinite dimensions. *Rev. Mod. Phys.*, 68:13, 1996.

[34] N.Matsumoto and F.Ohkawa. Kondo-lattice model in infinite dimensions. *Phys. Rev. B*, 51:4110, 1995.

[35] T.Hickel. *Theory of many-body effects in the Kondo-lattice model - projection-operator method*. PhD thesis, Humboldt Universität zu Berlin, Germany, 2005. http://edoc.hu-berlin.de/dissertationen/hickel-tilmann-2005-09-23/PDF/hickel.pdf.

[36] T.Hickel and W.Nolting. Proper weak-coupling approach to the periodic s-d(f) exchange model. *Phys. Rev. B*, 69:85110, 2004.

[37] W.Nolting, G.G.Reddy, A.Ramakanth, and D.Meyer. Low-density approach to the Kondo-lattice model. *Phys. Rev. B*, 64:155109, 2001.

[38] W.Nolting, G.G.Reddy, A.Ramakanth, D.Meyer, and J.Kienert. Self-energy approach to the correlated Kondo lattice model. *Phys. Rev. B*, 67:024426, 2003.

[39] R.J.Jelitto. The density of states of some simple excitations in solids. *J. Phys. Chem. Solids*, 30:609, 1969.

[40] B.Sriram Shastry and D.C.Mattis. Theory of the magnetic polaron. *Phys. Rev. B*, 24:5340, 1981.

[41] H.Nagao. Theoretical studies on many-band effects in superconductivity and magnetism. *Int. Journ. Quan. Chem.*, 100:867, 2004.

[42] K.Penc, H.Shiba, F.Mila, and T.Tsukagoshi. Ferromagnetism in multiband Hubbard models: From weak to strong Coulomb repulsion. *Phys. Rev. B*, 54:4056, 1996.

[43] Y.-Q.Wang, H.Q.Lin, and J.E.Gubernatis. Zero temperature numerical studies of multiband lattice models of strongly correlated electrons. *Commun. Comput. Phys.*, 1:575, 2006.

[44] A.Sharma and W.Nolting. Correlation effects in the valence bands of ferromagnetic semiconductor EuS. *Phys. Status Solidi B*, 243:641, 2006.

[45] P.Wachter. The optical electrical and magnetic properties of the Europium chalcogenides and the rare earth pnictides. *CRC Crit. Rev. Solid State Sciences*, 3:189, 1972.

[46] T.Kasuya. Energy spectra of magnetic semiconductors: Eu chalcogenides and NiO. *J. Appl. Phys.*, 41:1090, 1970.

[47] E.Kaldis and P.Wachter. The semiconductor-metal transition of the samarium mono-chalcogenides. *Solid State Comm.*, 11:907, 1972.

[48] P.Wachter. Electronic structure, magnetic exchange, and electrical transport properties of the magnetic compounds EuS, GdS and GdP. *Phys. Rep. (Rev. Sec. of Phys. Lett.)*, 44:159, 1978.

[49] L.H.Thomas. The calculation of atomic fields. *Proc. Camb. Phil. Soc.*, 23:542, 1927.

[50] P.Hohenberg and W.Kohn. Inhomogeneous electron gas. *Phys. Rev.*, 136:B864, 1964.

[51] W.Kohn and L.J.Sham. Self-consistent equations including exchange and correlation effects. *Phys. Rev.*, 140:A1133, 1965.

[52] K.Held, I.A.Nekrasov, N.Blümer, V.I.Anisimov, and D.Vollhardt. Realistic modeling of strongly correlated electron systems : An introduction to the lda+dmft approach. *Int. J. Mod. Phys. B*, 15:2611, 2001.

[53] G.Kotliar, S.Y.Savrasov, K.Haule, V.S.Oudovenko, O.Parcollet, and C.A.Marianetti. Electronic structure calculations with dynamical mean-field theory. *Rev. Mod. Phys.*, 78:865, 2006.

[54] L.Hedin. New method for calculating the one-particle Green's function with application to the electron-gas problem. *Phys. Rev.*, 139:A796, 1965.

[55] M.S.Hybertsen and S.G.Louie. First-principles theory of quasiparticles: Calculation of band gaps in semiconductors and insulators. *Phys. Rev. Lett.*, 55:1418, 1985.

[56] F.Aryasetiawan and O.Gunnarsson. The GW method. *Rep. Prog. Phys.*, 61:237, 1998.

[57] W.G.Aulbur, L.Jönsson, and J.W.Wilkins. *Solid State Physics*, volume 54, page 1. Academic Press, New York, USA, 2000.

[58] M.van Schilfgaarde, T.Kotani, and S.Faleev. Quasiparticle self-consistent GW theory. *Phys. Rev. Lett.*, 96:226402, 2006.

[59] W.Müller and W.Nolting. Temperature-dependent quasiparticle band structure of the ferromagnetic semiconductor EuS. *Phys. Rev. B*, 66: 085205, 2002.

[60] O.K.Andersen. The Tight Binding Linear Muffin-Tin Orbital Method. http://www.fkf.mpg.de/andersen/LMTODOC/LMTODOC.html, 2000.

[61] O.K.Andersen. Linear methods in band theory. *Phys. Rev. B*, 12:3060, 1975.

[62] H.L.Skriver. *The LMTO Method*. Springer, New York, USA, 1984.

[63] O.K.Andersen and O.Jepsen. Explicit, first-principles tight-binding theory. *Phys. Rev. Lett.*, 53:2571, 1984.

[64] A.Hasegawa and A.Yanase. Energy band structures of Gd-pnictides. *J. Phys. Soc. Japan*, 42:492, 1977.

[65] W.R.L.Lambrecht. Electronic structure and optical spectra of the semimetal ScAs and of the indirect-band-gap semiconductors ScN and GdN. *Phys. Rev. B*, 62:13538, 2000.

[66] D.B.Ghosh, M.De, and S.K.De. Electronic, magnetic, and optical properties of Gd monopnictides: An lda+u study. *Phys. Rev. B*, 72:45140, 2005.

[67] C.M.Aerts, P.Strange, M.Horne, W.M.Temmerman, Z.Szotek, and A.Svane. Half-metallic to insulating behavior of rare-earth nitrides. *Phys. Rev. B*, 69:45115, 2004.

[68] V.Eyert. Private communication, 2006.

[69] C.-g.Duan, R.F.Sabirianov, W.N.Mei, P.A.Dowben, S.S.Jaswal, and E.Y.Tsymbal. Electronic, magnetic and transport properties of rare-earth monopnictides. *J.Phys.: Cond. Mat.:*, 19:315220, 2007.

[70] A.G.Petukhov, W.R.L.Lambrecht, and B.Segall. Electronic structure of rare-earth pnictides. *Phys. Rev. B*, 53:4324, 1996.

[71] F.Leuenberger. *Elemental resolved magnetism of Gadoliniumnitride layers and GdN/Fe multilayers.* PhD thesis, Georg-August-Universität zu Göttingen, Germany, 2004. http://webdoc.sub.gwdg.de/diss/2004/leuenberger/leuenberger.pdf.

[72] W.Nolting, W.Borgiel, and G.Borstel. Coulomb correlation effects in the quasiparticle band structure of ferromagnetic rare-earth insulators. *Phys. Rev. B*, 37:7663, 1988.

[73] S.Rex, V.Eyert, and W.Nolting. Temperature-dependent quasiparticle bandstructure of ferromagnetic Gadolinium. *J. Mag. Mag. Mat.*, 192: 529, 1999.

[74] P.Wachter. *Handbook on the Physics and Chemistry of Rare Earth*, chapter 19. North Holland Publishing Company, Amsterdam, Netherland, 1979. Vol. 2.

[75] A.Mauger and C.Godart. The magnetic, optical, and transport properties of representatives of a class of magnetic semiconductors: The Europium chalcogenides. *Phys. Rep. (Rev. Sect. of Phys. Lett.)*, 141:51, 1986.

[76] P.Heller and G. Benedek. Nuclear resonance in EuS from 4.2k to the critical temperature region. *Phys. Rev. Lett.*, 14:71, 1965.

[77] C.Ren, J.Trbovic, R.L.Kallaher, J.G.Braden, J.S.Parker, S.von Molnár, and P.Xiong. Measurement of the spin polarization of the magnetic semiconductor EuS with zero-field and zeeman-split andreev reflection spectroscopy. *Phys. Rev. B*, 75:205208, 2007.

[78] D.E.Eastman and M.Kuznietz. Photoemission studies of f states and valence bands in several rare-earth and uranium compounds. *J. Appl. Phys.*, 42:1396, 1971.

[79] J.T.Janak and A.R.Williams. Giant internal magnetic pressure and compressibility anomalies. *Phys. Rev. B*, 14:4199, 1976.

[80] U.K.Poulsen, J.Koller, and O.K.Andersen. Magnetic and cohesive properties from canonical bands (for transition metals). *J. Phys. F : Met. Phys.*, 6:L241, 1976.

[81] P.Wachter and E.Kaldis. Magnetic interaction and carrier concentration in GdN and $GdN_{1-x}O_x$. *Solid State Comm.*, 34:241, 1980.

[82] J.Q.Xiao and C.L.Chien. Proximity effects in superconductor/insulating-ferromagnet NbN/GdN multilayers. *Phys. Rev. Lett.*, 76:1727, 1996.

[83] S.Granville, B.J.Ruck, F.Budde, A.Koo, D.J.Pringle, F.Kuchler, A.R.H.Preston, D.H.Housden, N.Lund, A.Bittar, G.V.M.Williams, and H.J.Trodahl. Semiconducting ground state of GdN thin films. *Phys. Rev. B*, 73:235335, 2006.

[84] S.A.Wolf, D.D.Awschalom, R.A.Buhrman, J.M.Daughton, S.von Molnár, M.L.Roukes, A.Y.Chtchelkanova, and D.M.Treger. Spintronics: A spin-based electronics vision for the future. *Science*, 294:1488, 2001.

[85] J.F.Gregg, I.Petej, E.Jouguelet, and C.Dennis. Spin electronics - a review. *J. Phys. D: Appl.Phys.*, 35:R121, 2002.

[86] A.N.Chantis, M.van Schilfgaarde, and T.Kotani. Quasiparticle self-consistent GW method applied to localized 4f electron systems. *Phys. Rev. B*, 76:165126, 2007.

[87] A.Sharma and W.Nolting. Temperature dependent electronic correlation effects in GdN. *J. Phys.: Cond. Mat.*, 18:7337, 2006.

[88] S.Bhattacharjee and S.M.Jaya. Influence of correlation and temperature on the electronic structure of bulk and thin film GdN. *Eur. J. Phys. B*, 49:305, 2006.

[89] W.Nolting, S.Mathi Jaya, and S.Rex. Magnetic polaron in ferro- and antiferromagnetic semiconductors. *Phys. Rev. B*, 54:14455, 1996.

[90] F.Leuenberger, A.Parge, W.Felsch, F.Baudelet, C.Giorgetti, E.Dartyge, and F.Wilhelm. X-ray magnetic circular dichroism at the Gd $L_{2,3}$ absorption edges in GdN layers: The influence of lattice expansion. *Phys. Rev. B*, 73:214430, 2006.

[91] H.J.Trodahl, A.R.H.Preston, J.Zhong, B.J.Ruck, N.M.Strickland, C.Mitra, and W.R.L.Lambrecht. Ferromagnetic redshift of the optical gap in GdN. *Phys. Rev. B*, 76:085211, 2007.

[92] D.C.Mattis. *The theory of magnetism.* Harper and Row, New York, USA, 1965. and references therein.

[93] W.Heisenberg. Zur theorie des ferromagnetismus. *Z.Physik*, 49:619, 1928.

[94] H.A.Kramers. Classical idea of electron spin. *Physica*, 1:191, 1934.

[95] P.W.Anderson. Antiferromagnetism. theory of superexchange interaction. *Phys. Rev.*, 79:350, 1950.

[96] C.Zener. Interaction between the d shells in the transition metals. *Phys. Rev.*, 81:440, 1951.

[97] M.A.Ruderman and C.Kittel. Indirect exchange coupling of nuclear magnetic moments by conduction electrons. *Phys. Rev.*, 96:99, 1954.

[98] T.Kasuya. A theory of metallic ferro- and antiferromagnetism on Zener's model. *Prog. Theor. Phys.*, 16:45, 1956.

[99] K.Yosida. Magnetic properties of Cu-Mn alloys. *Phys. Rev.*, 106:893, 1957.

[100] N.Bloembergen and T.J.Rowland. Nuclear spin exchange in solids: Tl^{203} and Tl^{205} magnetic resonance in Thallium and Thallic oxide. *Phys. Rev.*, 97:1679, 1955.

[101] Jr. W.J.Carr. Use of non-orthogonal wave functions in the treatment of solids, with applications to ferromagnetism. *Phys. Rev.*, 92:28, 1953.

[102] N.L.Huang and R.Orbach. Biquadratic superexchange. *Phys. Rev. Lett.*, 12:275, 1964.

[103] G.Bastard and C.Lewiner. Indirect-exchange interactions in zero-gap semiconductors. *Phys. Rev. B*, 20:4256, 1979.

[104] L.Liu. Indirect exchange interaction in semiconductors. *Solid State Comm.*, 35:187, 1980.

[105] S.Schwieger and W.Nolting. Long-range superexchange: An exchange interaction through empty bands. *Phys. Rev. B*, 65:205210, 2002.

[106] T.Dietl, A.Haury, and Y.M. d'Aubigné. Free carrier-induced ferromagnetism in structures of diluted magnetic semiconductors. *Phys. Rev. B*, 55:R3347, 1997.

[107] V.I.Litvinov and V.K.Dugaev. Ferromagnetism in magnetically doped III-V semiconductors. *Phys. Rev. Lett.*, 86:5593, 2001.

[108] D.N.Zubarev. Double- time green functions in statistical physics. *Usp. Fiz. Nauk*, 71:71, 1960.

[109] H.B.Callen. Green function theory of ferromagnetism. *Phys. Rev.*, 130: 890, 1963.

[110] N.N.Bogoliubov and S.V.Tyablikov. Retarded and advanced green functions in statistical physics. *Dokl. Akad. Nauk. SSSR*, 126:53, 1959.

[111] C.Santos and W.Nolting. Ferromagnetism in the Kondo-lattice model. *Phys. Rev. B*, 65:144419, 2002.

[112] A.Sharma and W.Nolting. Ferromagnetism in the multiband Kondo lattice model. *Phys. Rev. B*, 78:054402, 2008.

[113] R.A.Cutler and A.W.Lawson. Synthesis and magnetic behavior of GdN. *J. Appl. Phys.*, 46:2739, 1975.

[114] G.Busch, P.Junod, O.Vogt, and F.Hulliger. Ferro- and metamagnetism of rare earth compounds. *Phys. Lett.*, 6:79, 1963.

[115] E.L.Boyd and R.J.Gambino. Nuclear magnetic resonance of Gd^{155} and Gd^{157} in the cubic ferromagnet GdN. *Phys. Rev. Lett.*, 12:20, 1964.

[116] D.X.Li, Y.Haga, H.Shida, T.Suzuki, Y.S.Kwon, and G.Kido. Magnetic properties of stoichiometric Gd monopnictides. *J. Phys.: Cond. Mat.*, 9: 10777, 1997.

[117] D.P.Schumacher and W.E.Wallace. Magnetic characteristics of Gadolinium, Praseodymium, and Thulium Nitrides. *J. Appl. Phys.*, 36:984, 1965.

[118] P.Junod and F.Levy. Spontaneous magnetization of EuO and GdN. *Phys. Lett.*, 23:624, 1966.

[119] D.B.McWhan. Effect of pressure on the Curie temperature and volume of GdN. *J. Chem. Phys.*, 44:3528, 1966.

[120] G.Busch. Magnetic properties of rare-earth compounds. *J. Appl. Phys.*, 38:1386, 1967.

[121] P.Junod, A.Menth, and O.Vogt. Rare- earth monochalcogenides. *Phys. Kondens. Mat.*, 8:323, 1969.

[122] T.R.McGuire, R.J.Gambino, S.J.Pickart, and H.A.Alperin. Magnetic structure and exchange interactions in cubic Gadolinium compounds. *J. Appl. Phys.*, 40:1009, 1969.

[123] R.J.Gambino, T.R.McGuire, H.A.Alperin, and S.J.Pickart. Magnetic properties and structure of GdN and $GdN_{1-x}O_x$. *J. Appl. Phys.*, 41:933, 1970.

[124] M.Kuznietz. Effect of substitutional anions on the magnetic properties of the mononitrides of Uranium and Gadolinium. *J. Appl. Phys.*, 42: 1470, 1971.

[125] A.Narita and T.Kasuya. Magnetic exchange interactions and spin structures in some rare earth pnictides. *J. Mag. Mag. Mat.*, 52:373, 1985.

[126] T.Kasuya and D.X.Li. Mechanism of strong ferromagnetism in GdN. *J. Mag. Mag. Mat.*, 167:L1, 1997.

[127] T.Kasuya and D.X.Li. Anomalous exchange mechanism in Gd monopnictides. *Physica B*, 230-232:472, 1997.

[128] K.Khazen, H.J.von Bardeleben, J.L.Cantin, A.Bittar, S.Granville, H.J.Trodahl, and B.J.Ruck. Ferromagnetic resonance study of GdN thin films with bulk and extended lattice constants. *Phys. Rev. B*, 74:245330, 2006.

[129] F.Holtzberg, T.R.McGuire, S.Methfessel, and J.C.Suits. Effect of electron concentration on magnetic exchange interactions in rare earth chalcogenides. *Phys. Rev. Lett.*, 13:18, 1964.

[130] D.X.Li, Y.Haga, H.Shida, and T.Suzuki. Magnetic properties of ferromagnetic GdN. *Physica B*, 199 & 200:631, 1994.

[131] A.Sharma and W.Nolting. to be published, 2009.

[132] J.P.Perdew and A.Zunger. Self-interaction correction to density-functional approximations for many-electron systems. *Phys. Rev. B*, 23: 5048, 1981.

[133] R.M.Dreizler and E.K.U.Gross. *Density Functional Theory*. Springer-Verlag, Berlin, Germany, 1990.

[134] R.G.Parr and W.Yang. *Density-Functional Theory of Atoms and Molecules*. Oxford University Press, London, UK, 1989.

[135] V.Eyert. *The Augmented Spherical Wave Method: A Comprehensive Treatment*. Springer, Berlin, Germany, 2007.

[136] K.Capelle. A bird's-eye view of density-functional theory. *cond-mat*, 0211443, 2003.

[137] K.Burke et al. http://dft.rutgers.edu/kieron/beta, 2003.

[138] G.Onida, L.Reining, and A.Rubio. Electronic excitations: density-functional versus many-body Greens-function approaches. *Rev. Mod. Phys.*, 74:601, 2002.

[139] L.D.Landau. The theory of fermi liquid. *Sov. Phys. JETP*, 3:920, 1957.

[140] D.Pines and P.Nozieres. *Theory of Quantum Liquids: Normal Fermi Liquids*. Addison Wesley Publishing Company, Reading, MA, USA, 1989.

[141] F.J.Himpsel. Angle-resolved measurements of the photoemission of electrons in the study of solids. *Adv. in Phys.*, 32:1, 1983.

[142] L.Kevan. *Angle-Resolved Photoemission*. Elsevier, Amsterdam, Netherland, 1992.

[143] J.C.Fuggle and J.E.Inglesfield. *Unoccupied electronic states*. Springer-Verlag, Berlin, Germany, 1992.

List of Figures

Selbstaendigkeitserklaerung

Hiermit erklaere ich, die vorliegende Arbeit selbstaendig ohne unerlaubte Hilfe verfasst und nur die angegebene Literatur und die angegebenen Hilfsmittel Verwendet zu haben.

Berlin,den